EXPERIMENTAL AND NUMERICAL STUDIES ON VENOUS ULCERS

By

Wu Pan Zagorski

A DISSERTATION

Submitted to
Michigan State University
in partial fulfillment of the requirements
for the degree of

Engineering Mechanics – Doctor of Philosophy

2017

ABSTRACT

EXPERIMENTAL AND NUMERICAL STUDIES ON VENOUS ULCERS

By

Wu Pan Zagorski

Venous ulcers are the most common and severe skin wounds occurring in lower legs. They are painful, hard to heal and have a 78% chance of recurrence after two years, which leads to frequent visits to wound care clinics and results in huge financial burdens to the patients, family, and society. Contemporary treatments include compression stockings, drugs, and surgeries. However, these only treat the ulcers after they have occurred. Therefore, it is necessary to understand the pathology of ulcer formation, which will then allow us to predict the onset of an ulcer and implement preventive measures early.

The commonly accepted theory of venous ulcer pathology is that the ulcers are caused by chronic venous insufficiency (CVI) which is a resultant of calf muscle pump failure. CVI causes blood pooling in the lower leg, leads to inflammation, skin edema, tissue necrosis, and ultimately skin ulcers. However, various hypotheses existed between the stages of blood pooling and the ulceration.

Therefore, the goals of this research were to: i) determine the blood flow response to loading in lower legs between venous ulcers patients and a healthy population; ii) quantify the hemodynamic parameters that contribute to the differences in blood flow; iii) understand the progressive changes between inflammation and skin edema in the development of skin ulcers.

To address the first goal, a blood perfusion test was performed on the lower legs of ulcer patients and a healthy group. External normal, and combined normal and shear loads

were applied to the lower legs. The blood perfusion profiles were analyzed and results showed that the ulcerated legs were significantly different than healthy legs in response to load and reactive hyperemia. The legs that did not have open wounds but were from the same ulcer patient exhibited an intermediate trend between the wounded and healthy legs. This suggests a progressive change existed during ulcer development.

The second goal was achieved by the development of a Windkessel based circuit model. The model output was compared with the blood flow profiles from the perfusion tests. Patient-specific parameters were obtained and compared across the wounded, non-wounded, and healthy legs. Results indicated that significant differences existed in localized vessel resistance and compliance between wounded and healthy legs, suggesting a threshold of those parameters existed from each category. The results explained the differences in locally measured blood perfusion and indicated the potential of identifying populations at risk of developing venous ulcers.

Finally, the third goal was reached by the development of a skin Finite Element (FE) model with series of parametric studies. The influence of the glycosaminoglycans (GAGs) and sodium during inflammation on the skin edema and tissue damage were explored. Results showed that the increased GAGs and sodium content led to edema and an increased fluid pressure within the tissue. This explained the increased reactive hyperemia from wounded legs in the perfusion tests. Increased fluid pressure causes tissue ischemia and an increased tissue stress; both have been shown to cause tissue damage and wound formation. The FE model provides insights to the detailed pathological events that happen between inflammation, edema and skin ulceration.

To the dreams being forever chased

ACKNOWLEDGEMENTS

I am beyond thrilled to be able to come this far and have been incessantly grateful for all the people who helped me along this journey.

First of all, I would like to thank my advisor, Dr. Tamara Reid Bush, who opened the door for me and spared no effort to guide me in all aspects of academic and life in grad school. I would also like to thank my committee members, Dr. Sara Roccabianca, Dr. Seungik Baek, and Dr. Laura Bix for supporting and providing valuable insights for this research. Additionally, I want to thank Dr. Marc D. Basson for many inspirational suggestions from the clinical side of this study.

Special thanks for my colleagues at Biomechanical Design Research Laboratory, Josh Drost, Amy Lenz, Amber Cussen, Dr. Sam Leitkam, Dr. Abinand Manorama, Jessica Buschman, Kelly Patterson and the rest of the group for many insightful and fruitful discussions.

I would like to take this opportunity to also thank the late Dr. Jilong Xie who shaped me into a researcher from an undergrad, who believed in me, and encouraged and supported me to pursue my goal of research in the United States.

Thanks to all my friends who supported me through the darkest days and laughed with me over the brightest times.

Finally, I would like to thank my Pan and Zagorski families who always make me feel loved.

TABLE OF CONTENTS

LIST OF TABLES

LIST OF FIGURES

1 INTRODUCTION

Venous ulcers are skin wounds that often occur in lower extremities. These wounds are one of the most common types of leg ulcers, affecting nearly 2.5 million people in the US every year (Arnold et al. 1994; Brem et al. 2004; Cleveland Clinic 2015; Milic et al. 2009). Most patients who suffer from venous ulcers are elderly with limited mobility (Brem et al. 2004). However, it should be noted that venous ulcers differ from pressure ulcers (wounds commonly found on the bottom of the buttocks in individuals with limited mobility), in that venous ulcers are on the leg, and there is no external loading that drives their formation. Data also indicate that women over the age of 60 have a higher risk of developing venous ulcers in comparison to men (Margolis et al. 2002; Callam et al. 1987; Markova & Mostow 2012). Venous ulcers are chronic, hard to heal, and have high recurrence rates. A 2004 study showed that a healed ulcer had a 30% chance of reoccurring in the first year and a 78% chance after two years (Abbade & Lastoria 2006). Venous ulcers tend to be bilateral; in other words, once an ulcer has occurred in one leg, the other leg is likely develop an ulcer within three to five years (Abbade & Lastória 2005; Kunimoto et al. 2001). Treatment for venous ulcers costs over $25 billion dollars per year in the US (Lazarus et al. 2014). The frequent visits to the wound care clinic and the painful healing process as well as the decreased quality of life due to these ulcers results in emotional and psychosocial burdens on the patients and family (Howard et al. 2008; Lal 2015). Still, the etiology, precise pathogenesis, and physiology of ulcer formation are not well understood. Also, there are no early detection methods, resulting in the inability to predict ulcer formation (Valencia et al. 2001; Fonder et al. 2008; Beebe-Dimmer et al. 2005). Once diagnosed with a venous ulcer, a stocking or pressure bandaging treatment is often needed for the rest of the

individual's life. A need exists to better understand this disease so that preventive approaches can be implemented prior to wound formation.

Studies have indicated that venous ulcers are caused by chronic venous insufficiency (CVI), such as venous hypertension (Pascarella et al. 2005), or skin edema that results from calf muscle pump failure (Bergan et al. 2006; Reeder 2013). These factors lead to the inability of the veins to pump blood back to the heart. When blood is pooled to the lower extremities, it leads to subcutaneous tissue necrosis and propagates to the superficial skin level; this produces swelling and inflammation in the skin, causing the skin to break, eventually resulting in a venous ulcer. This process especially happens in the lower calf regions, above the ankles (Mlacak et al. 2005; Kunimoto et al. 2001). Patients with CVI usually start with venous varicose and deep venous thrombosis, leading to venous hypertension. However, after the stage of venous hypertension, theories differ on how the ulcers are formed (Abbade & Lastória 2005).

Currently, the most common treatment is the application of compression bandages or stockings to the wound area (Kolluri 2014). Other treatments include antibiotics, elevation and surgery, skin grafts, alternative therapeutic compressions, and drug therapies (Kunimoto et al. 2001; Johnson 2002; Shingler & Robertson 2013; Brem et al. 2004; Abbade & Lastória 2005; Collins & Seraj 2010). However, most of the treatments only address the symptom (ulcers), but not the underlying cause of the ulcerations. Therefore, current treatment needs to take ulcer formation and recurrence into consideration. Rather than just healing the open ulcers, there is a need for researchers and clinicians to identify the factors that indicate the onset of an ulcer prior to formation. Prevention of ulcer formation is the greater challenge (Callam et al. 1987).

Once ulcer onset can be predicted, preventative measures can be implemented before an ulcer forms leading to reduced medical costs and psychosocial burdens on the patients.

The goal of this research was to study the blood flow under various loadings, the hemodynamic response of blood flow, and the tissue fluid pressure and stress distribution during skin inflammation and edema. These were evaluated and compared for patients with venous ulcers and a healthy population.

The following chapters address these goals

Chapter 2: In this chapter, a literature review was conducted to identity gaps in knowledge about venous ulcers.

Chapter 3: In this chapter, an overview of the experimental tests conducted on patients with venous ulcers and a healthy population, and the results are provided. The blood perfusion data under normal, and combined normal and shear loads between patients with existing venous ulcers and a healthy sample were collected and analyzed. Eighteen participants with venous ulcers on their lower legs and twenty healthy participants were tested. External normal and shear loads were applied on the lateral surface of the calf while blood perfusion was monitored. Data were collected before loading, during loading, and after loading. The blood perfusion data were analyzed and compared between the groups.

Chapter 4: In this chapter, the development of a Windkessel based model was discussed. Differences in the hemodynamic characteristics between patients with venous ulcers and a healthy sample were compared with the model. Specifically, the blood perfusion regions associated with loading, the reactive hyperemia (spike in blood perfusion after release of loading), and the recovery of blood perfusion were analyzed. The output from this model was

then compared with the perfusion data obtained from previous chapter. An iteration process was conducted for the values of the resistors and capacitors until the model output matched the experimental data for each test participant.

Chapter 5 provides a detailed literature review specifically on the existing wound modeling methods and skin Finite Element models. This review gathered the information and prepared the establishment of the first computational model for investigating changes in skin tissue during the formation of venous ulcers.

Chapter 6: In this chapter, a Finite Element (FE) model to determine the bio-mechanical and bio-chemical driven changes in skin tissue due to the increased pressure and stress as a result of skin inflammation and edema. The skin was defined as a multi-layer model with different hyperelastic material properties for each layer. Two inflammation identifiers: Glycosaminoglycans (GAGs) and sodium were used as variables in the model to study their contribution in ulcer formation. The model simulated skin edema when the skin undergoes the inflammation process. The model predicted the parameters for skin edema, tissue ischemia and tissue damage. It explored the progressive changes in the skin tissue from blood pooling to venous ulcers formation.

The significance of this research presented in this dissertation was that it enabled us to better understand the quantifiable differences in the blood flow and vessel hemodynamic characteristics between venous ulcer patients and a healthy population. Additionally, it exposed the internal changes in vessel compliances and resistances, tissue pressures, and stresses when undergoing inflammation and edema, and provided a path for predicting the onset of venous ulcers. This work laid a solid foundation for understanding venous ulcer

pathophysiology which will lead to developing better preventive measures and clinical care in the future.

2 LITERATURE REVIEW

2.1 Venous Ulcers

A venous ulcer, which is also called stasis ulcer, varicose ulcer, gravitational ulcer or hypostatic ulcer, is the most common ulcer that occurs in the lower leg (Abbade & Lastória 2005). Venous ulcers make up 70%~90% of chronic lower leg ulcers and are caused mainly by chronic venous insufficiency (CVI) (Cleveland Clinic 2015; Snyder 2005). Venous ulcers usually occur among the older population, especially women over the age of 60; the gender gap tends to become smaller as age increases (Ontario 2011; Beebe-Dimmer et al. 2005; Sieggreen 2005; Margolis et al. 2002; Kolluri 2014; Valencia et al. 2001). Venous ulcers affect roughly 2.5 million of people every year in the US; 6 million people in Brazil; and approximately 14 million people in Europe. Also, ulcer prevalence tends to be higher in the western countries (Callam et al. 1987; Villavicencio 2013; Margolis et al. 2002; Abbade & Lastória 2005; Crane & Cheshire 2008; Carpentier et al. 2004; Salomé & Ferreira 2013; United Nations 2015). Researchers also believe that the reported statistics generally underestimate these numbers because they can be challenging to diagnose (Sieggreen 2005; Douglas & Simpson 1995; Abbade & Lastória 2005).

In the US, 25 billion dollars are spent on ulcer treatment and care every year (Lazarus et al. 2014). Also, the recurrence rate for venous ulcers is high. Studies indicate 33% of patients experience a reoccurrence after traditional compression treatment and 15% after surgical intervention (Howard et al. 2008). In addition, after an ulcer has healed the reoccurrence rate within two years is as high as 78% (Kolluri 2014) . Therefore, most ulcer patients often must revisit the clinic after a couple years for treatment of new wounds (Abbade & Lastória 2005; Pascarella & Shortell 2015; Yavuz et al. 2012; Kolluri 2014; Lamel & Kirsner 2013). Hence, it is

important to better understand parameters that lead to venous ulcer formation so that they can be prevented, rather than just treated after forming.

Many studies have proposed various theories of pathophysiology for the formation of venous ulcers, but there is no agreed upon mechanism that has been proven (Abbade & Lastória 2005). A commonly accepted theory for venous ulcer formation is that they are a direct consequence of CVI, which is usually caused by calf muscle pump failure. This occurs when the muscular pump on the calf does not function properly, and the blood flow back to the heart is impaired (Milic et al. 2009; Bergan et al. 2006; Burton 1991; Gonsalves 2003). Due to gravity, blood pools in the lower calf regions, causing inflammation, which can lead to tissue necrosis and skin ulceration (Ontario 2010; Collins & Seraj 2010).

Common risk factors for venous ulcers are age, obesity, immobility and a history of leg injuries (Carpentier et al. 2004; Beebe-Dimmer et al. 2005; Abbade & Lastória 2005). Leg ulcers can be caused by the insufficiency of the leg veins at the superficial, perforating, or deep levels; one such example is postphlebitic syndrome, which is a representative symptom that associates the deep vein thrombosis with venous ulceration (Valencia et al. 2001). In addition, edema, congenital absence of valves, diabetes, and congestive heart failure also contribute to the likelihood of developing venous ulcers (Lazarus et al. 2014).

The most standard and common treatments for venous ulcers are compression stockings or bandages (Milic et al. 2009) which date back to the time of the Pharaohs in ancient Egypt (Davies et al. 2009). Compression therapy is believed to improve the tissue blood flow and assist the calf muscle pump (Davies et al. 2009). However, compression therapy is difficult to use for many patients since they need to be trained by nurses or professionals for

appropriate usage. If patients cannot wear a compression stocking or bandage properly, the therapy will fail or could lead to additional skin wounds and damage (Nole et al. 2015; Johnson 2002; Kramer 1999). Compression stockings have a rating system; they are rated based on the pressure the stocking can apply. Higher rated pressure stockings are used for more severe ulcer situations to apply a higher level of pressure. However, patients with more severe ulcers often experience increased pain, making the higher rated compression stockings difficult for them to use (Carman 2009; Partsch 2013).

Other treatments of venous ulcers include Unna boots, antibiotics, electrical stimulation, skin grafts, and venous surgeries (where the goal of surgical intervention is to ablate the pathologic veins) (Thakral et al. 2015). However, several studies have shown that there is no significant difference between venous surgery and standard care treatment with regard to the healing and recurrence (de Carvalho 2015). In addition, regular surgical processes exclude the patients at high risk or patients with severe venous disease (Thakral et al. 2015), so they are only suitable for standard care treatments, which are the compression stockings.

Unfortunately, there are no current approaches to predict when an ulcer is about ready to form, so the current approach is to treat the ulcer after formation. The inability to predict the onset of a venous ulcers leads to multiple clinic visits, high care costs and long painful treatment processes for the patients (Nole et al. 2015; Zimmet 1999; Lazarus et al. 2014). If an approach could be developed to detect the underlying changes in the system prior to the formation of a wound, then preventive approaches could be applied, reducing the number of clinic visits and the pain experienced by patients, as well as the disruption to their daily lives.

The significance of the work proposed here is that the combined experimental and modeling approaches developed provide us with a better understanding of venous ulcers. This increased understanding will aid in the development of improved detection and preventative measures for this disease.

2.2 Blood perfusion

Perfusion is defined as blood delivered into the vascular bed through biological tissue (Miller-Keane & O'Toole 2003); it is an important index for studying the microcirculation in tissues. There are many methods for measuring the skin blood perfusion, such as magnetic resonance imaging (MRI), computed tomography (CT) scans, and laser Doppler (Fonder et al. 2008). Compared to MRI and CT, the laser Doppler perfusion monitoring method has a significant advantage of providing real-time, continuous measurements of the microvascular blood flow (Lausten et al. 1993). Additionally, the laser Doppler probe is non-invasive, and measurements can be taken by taping the device to the skin. In our study, laser Doppler flowmetry was used to measure the blood perfusion.

The laser Doppler perfusion technique and the non-invasive method to assess blood perfusion *in vivo* has been used to study blood microcirculation for over 30 years (Nilsson 1984). In the instrumentation of a laser Doppler Perfusion Monitor (LDPM), fiber optics are used to apply laser light to the skin. Once the laser light hits the moving blood cells, it will scatter and change frequency due to a Doppler shift. The laser light is then reflected and the signal is converted to a perfusion value (Nilsson 1984; Ahn et al. 1987; Leahy et al. 1999). In clinical usage, LDPM has the limitation of the readings being presented in an arbitrary unit, i.e., perfusion unit, which is proportional to the volumetric blood flow per unit weight of tissue

(such as ml/s/100g) (Morales et al. 2005a; Roustit & Cracowski 2012; Perimed 2001). However, even with this limitation, the LDPM is useful in comparing the differences in perfusion responses between patients and changes within a patient.

Figure 2-1 provides a typical LDPM output diagram. In our work, several parameters were studied: including the baseline perfusion, perfusion under loading (ischemia), reactive hyperemia after occlusion, and the recovery period (reperfusion), all shown on Figure 1.

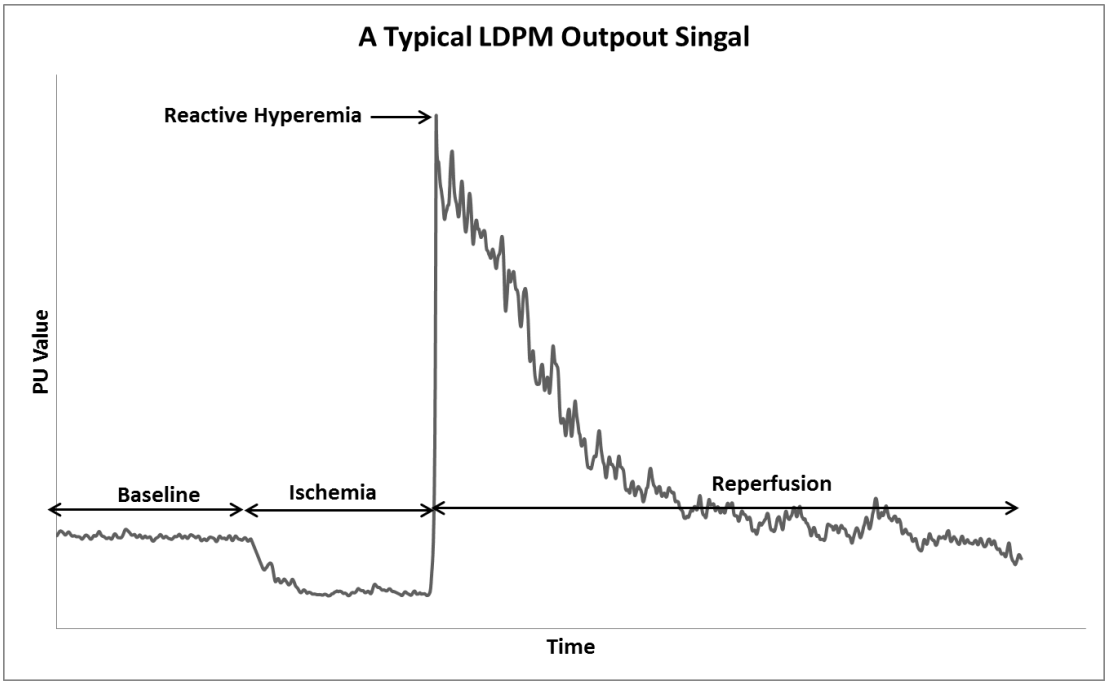

Figure 2-1: Typical LDPM output diagram. The baseline is when no load is applied; the ischemia is the blood perfusion decrease when the external load is applied; the reactive hyperemia is the spike in blood perfusion upon the removal of the load; the reperfusion is the recovery of the blood perfusion from the reactive hyperemia spike

The ischemia and following reactive hyperemia has been widely studied and has shown a relation to tissue injury, also known as reperfusion injury. When tissue is loaded, the reduced oxygen and nutrition supply leads to tissue necrosis, however, when the blood is restored in the tissue (during reperfusion), the excessive oxygen and nutritional supply is beyond the capacity of tissue self-regulation, resulting in cytotoxic tissue and future tissue injuries (Carden &

Granger 2000; Peirce et al. 2000; Tsuji et al. 2005). Reperfusion injury is one of the factors that has raised considerable interest recently in the formation of chronic skin ulcers (Coleridge Smith 2001; Park et al. 2009; Bergan et al. 2006).

In the work proposed here, the skin blood perfusion data obtained through experimental work via LDPM was used for comparison with a new model based on a Windkessel approach. This new model will allow us to better understand the underlying changes in ulcer formation and has the potential for use as a prediction tool for ulcers.

2.3 Modeling with a compartmental system

The compartmental system has been widely used in biomedical modeling studies, one of the most common approaches is the "Windkessel" model, which was first proposed by Otto Frank in 1899 (Sagawa et al. 1990). Windkessel, which means "air chamber" in German, is used to model the hemodynamic characteristic of human blood flow with a compartmental circuit system. In this system, voltage (V) represents the blood pressure, current (I) represents the blood flow, and resistors (R) and capacitors (C) represent the blood resistance and blood vessel capacitance respectively (Westerhof et al. 2009; Zheng & Mayhew 2009). This type of model has been used as the clinical index for aortic pressure and artery stiffness measurements, but few models have been developed for the venous or capillary systems (Abdolrazaghi et al. 2010; Segers et al. 1997).

In early 1990, a mathematical model in which the blood vessel was treated as a single tube was proposed and developed by Smye et al.. The goal of this simple model was to study reactive hyperemia. The model adopted the quasi-steady flow to represent blood flow in a vascular bed (Smye & Bloor 1990). The model was idealized by the assumption of a Newtonian

fluid and the tube was one-dimensional with velocity along the axial direction. The boundary condition included the pressure upstream when the cuff was released. This model gave a peak hyperemic flow of approximately 4-6 times the steady resting flow and suggested that the flow evolution was governed by a pressure gradient. Smye's model served as the initial model for future more sophisticated models.

In 2000, a simplified model for reactive hyperemia was introduced by Humeau et al.. This model emphasized simulating the effects that occurred during reactive hyperemia with a single blood vessel to study the change in blood velocity and vasodilation as well as vasoconstrictions (Humeau et al. 2000). Results showed that after occlusion, moving blood cells reached steady state rapidly in the microcirculation vessels and the vessel radii increased rapidly to compensate for deficiencies in the exchanges between the blood and tissue. De Mul et al. developed a mathematical model for the physiology of reactive hyperemia (de Mul et al. 2005). This simplified model was compared with experimental data obtained by testing subjects with peripheral arterial occlusive disease (PAOD), subjects with Diabetes Mellitus (DM), and healthy subjects with the application of a LDPM. Results indicated that this model was capable of differentiating the post occlusive reactive hyperemia (PORH) between PAOD, DM patients, and a healthy population.

Two years later, Van Vo and his group proposed a more sophisticated mathematical model to study the hemodynamic response based on the concept of De Mul's model. In Van Vo's model, a variable resistor and voltage diode were introduced into the model for hemodynamic changes induced by venous occlusion in the human forearm (Vo et al. 2007). Limitations of this model existed. The model could not directly be applied to arterial occlusions;

and due to the fixed capacitor, this model could not represent the high transmural pressure that leads to the change in venous compliance.

More recently, Solovyev adopted De Mul's model and incorporated it into an agent-based model (ABM) for pressure ulcer formation (Solovyev et al. 2013; de Mul et al. 2009).The agents used in the model were tissue cells, inflammatory cells, oxygen and inflammatory signals. The external pressure was output from the ABM and served as the input for De Mul's model. The output blood flow from De Mul's model was then used as the input for the ABM model. Solovyev, who proposed this hybrid model, suggested that the best-fit parameters of the resistor and capacitor values were different between pressure ulcer patients with and without spinal cord injuries.

Even though there are several models capable of modeling the reactive hyperemia and the recovery period; only Van Vo's approach was able to model the occlusion, the reactive hyperemia and reperfusion at the same time under certain conditions. Furthermore, no such model has been developed or applied to the study of venous ulcers. As part of this work, we have developed a unique model that incorporates the entire perfusion cycle with baseline flow, ischemia, reactive hyperemia and reperfusion. Our model also has the ability to represent different external loadings as well as patient-specific blood flow behavior. Our model is novel that it provides insight in understanding the difference in hemodynamic performance on the leg under external loadings between patients with venous ulcers and a healthy population.

2.4 Modeling for venous ulcers

2.4.1 Wound healing models

Mathematical and numerical models have been developed for the wound healing process. Wound healing is a complex and multi-factored problem and involves many bio-chemical and bio-mechanical processes. Due to this fact, many of the models on wound healing only take one or few aspects into consideration. The most common aspects addressed are epidermal healing, dermal extracellular matrix (ECM) repair, wound angiogenesis (formation and growth of new blood vessels) and wound contraction (Sherratt & Dallon 2002; Geris et al. 2010; Buganza Tepole & Kuhl 2013).

2.4.1.1 Wound angiogenesis and inflammation modeling

Inflammatory responses is an important aspect in modeling wound angiogenesis and wound healing for chronic skin wounds such as venous ulcers, especially for ischemic wounds (wound sites with limited nutrients, oxygen and circulation cells) (Geris et al. 2010; Bennett et al. 2003). In the modeling of inflammation and wound ischemia, many mathematical models incorporated bio-chemical agents into differential equations to simulate these processes (Geris et al. 2010; Gefen 2009). Schugart et al. developed mathematical models using a series of Partial Differential Equations to describe the wound angiogenesis in space and time. This model treated wound angiogenesis as oxygen parameters in the model and studied the optimal hyperbaric oxygen treatment for wound healing (Schugart et al. 2008). After Schugart's model, Xue et al. proposed a model that incorporated factors of inflammation and ischemia to study the wound closure time. The model simplified the open wound as a circular shaped region with three concentric layers defined as wounded, partially healed, and healthy tissue. In the model,

the wound boundary was set to be free moving and the ECM as a viscoelastic material property which was a growing factor in the model (Xue et al. 2009). The results of the model agreed with the experimental data and the statistical model by Roy et al. (Roy et al. 2009). Roy et al.'s experimental results showed that after four weeks of healing, ischemic wounds were less than half closed while non-ischemic wounds were completely closed. The experimental data also showed that ischemic wounds had chronic inflammation during the healing process. These findings provided a more comprehensive understanding for ischemic wound healing.

2.4.1.2 Wound contraction modeling

The modeling of wound contraction was first proposed by Murray et al. in late 1980s (Murray et al. 1988), in which a general model for tissue biomechanics was adapted for wounds. The results of this study suggested that a mechanical force primarily guided the tissue patterning and shape. Later, Vermolen and his group proposed a model that combined wound contraction, wound angiogenesis, and wound closure. In Vermolen's model, the geometry of skin was defined in two layers: the epidermis and dermis and the initial wound region penetrated both epidermis and dermis layers. This work modeled the contractile force exerted by tissue ECM. Results indicated that this contraction force not only affected the dermis, but also affected the tissue in the epidermis. For modeling wound angiogenesis, the model adopted a negative feedback mechanism to regulate the oxygen concentration and the capillary regeneration. Vermolen's model showed that the epidermal cells generated growth factors that led the wound to close from the edge towards the center of the wound, the healing also stratified in both epidermal and dermal layers. Vermolen's model has been successfully applied

to the study of healing wounds from pressure ulcers and burns (Vermolen et al. 2012; Vermolen & Javierre 2010; Vermolen & Rijn 2012; Vermolen & Javierre 2012).

2.4.2 Skin swelling and edema finite element models

2.4.2.1 Blood pooling and skin swelling

Many of the wound modeling studies focus on the healing process; however, there is a lack of research on wound formation and development. The etiology of venous ulcers have indicated that blood pooling in the lower leg leads to an inflammatory process, edema, and eventually venous ulcer development (Collins & Seraj 2010; Ontario 2010). A schematic process of the ulcer formation can be seen in Figure 2-2. When the blood pools in the vessels of the subcutaneous skin layer (hypodermis), the blood vessel wall will break resulting in fibrinogens, red blood cells and fluid leaking into the tissue (Burnand, Whimster, et al. 1982; Fahey 1998). The interstitial fluid accumulating in the tissue causes the a palpable swelling known as edema (Ely et al. 2006). The fibrinogens form a fibrin layer which restricts oxygen transportation and results in tissue necrosis and ulceration (Valencia et al. 2001; Burnand, Whimster, et al. 1982). When fibrin deposits, the fibrotic tissue will form along with inflammation, increase the risks for leg ulcerations (Falanga et al. 1987; Falanga 1993; Wahl 1997; Coleridge Smith 2001).

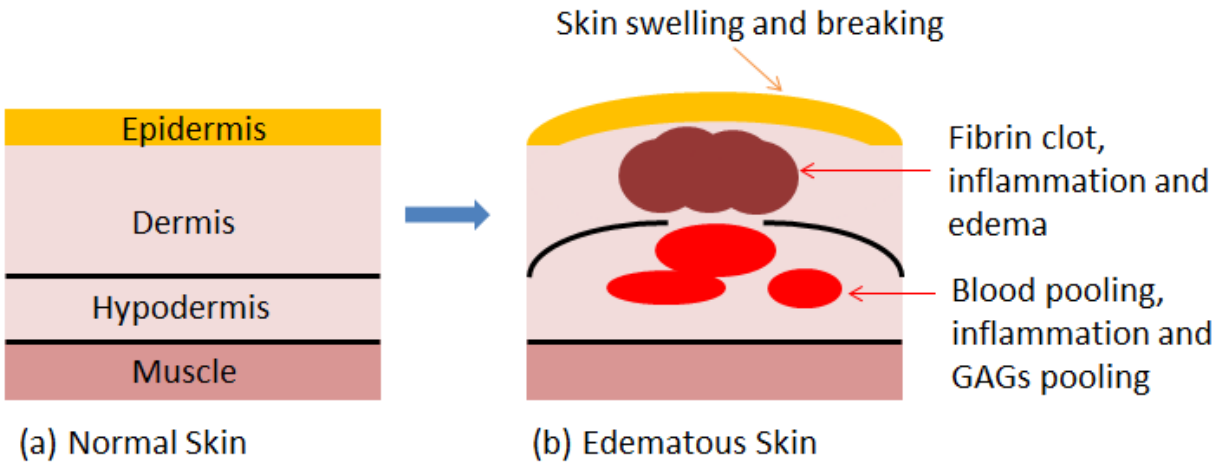

Figure 2-2: Schematic process of skin edema due to the blood pooling (a) normal skin; (b) skin with edema and swelling

During the inflammation, Glucosaminoglycans (GAGs) which are polyanionic molecules, are released in the body to regulate the inflammatory process (Lever et al. 2001). The GAGs possess negative charges that attract water into the tissue (House et al. 2009) and will cause an osmotic swelling pressure that lead to tissue property changes(House et al. 2009). The osmotic swelling and the accumulation of GAGs has been studied in cardiovascular research recently (Humphrey 2012; Lanir 2012). Roccabianca et al. has modeled and proven that the pooled GAGs will induce stress concentrations and increase swelling and osmotic pressure within the aortic wall. GAGS will perturb smooth muscle, disrupt ECM homeostasis and can lead to tearing or rupture of the aortic wall of thoracic aorta (Sara Roccabianca et al. 2014). Roccabianca's model provided an insight to the relation of GAGs pooling and tissue swelling for the aorta, but these principles also apply to the skin for wound formation. These literatures support the need for the inclusion of GAGs in the development of a model for wound formation. We incorporated GAGs into the Finite Element (FE) model developed in this study.

2.4.2.2 Skin Finite Element modeling

Skin is the largest organ of human body and has been modeled numerically in many theoretical and clinical studies (Jor et al. 2013). Several studies use Finite Element simulations to study various aspects of the skin. In these models, the skin was established as either two or three layers with no friction between layers. The thickness of each layer was obtained from histology and varied between different body regions or test subjects (Zöllner et al. 2013; Hendriks et al. 2003). Neo-Hookean was the most used material model in these skin simulations (Buganza Tepole & Kuhl 2013; Socci et al. 2007; Zöllner et al. 2013). More sophisticated models involved different parameters of the same material model for different skin layers (Sopher & Gefen 2011; Groves 2011), or different material models for different skin layers (Flynn & McCormack 2010).

Therefore, by adopting approaches similar to Roccabianca's work, we developed a FE model that studies the skin swelling and edema resulting from GAGs pooling in the inflammatory process and thus obtain a better understanding of how wounds can form. The model was capable of parametric studies for different sizes and distributions of the GAGs in the skin, and had the potential of determining the critical stresses for the skin with a specific focus on skin rupture and ulcer initiation.

3 SKIN PERFUSION RESPONSES UNDER NORMAL AND COMBINED LOADINGS: COMPARISONS BETWEEN LEGS WITH VENOUS STASIS ULCERS AND HEALTHY LEGS

(Wu Pan, Joshua P Drost, Marc D Basson, Tamara Reid Bush., 2015. Skin perfusion responses under normal and cominbed loadings: Comparions between legs with benous stasis ulcers and healthy legs. Clinical Biomechanics, 30(10), pp.1218-1224)

3.1 Introduction

Venous ulcers, also known as stasis ulcers, are skin wounds that occur most commonly on the lower leg. These wounds are due to chronic venous insufficiency and are the most common ulceration in the lower extremities, affecting almost 2.5 million patients every year in the United States (Brem et al. 2004; Arnold et al. 1994; Milic et al. 2009). Gravity makes the lower legs the most vulnerable to venous blood reflux for patients with insufficient venous function (Kramer 1999; Villavicencio 2013; Partsch 2013; Sieggreen 2005). Pooled blood in the lower legs induces high intravascular pressure, leakage of plasma proteins and fluid into the surrounding tissues, which causes increased interstitial pressure, tissue breakdown, and ulcer formation (Collins & Seraj 2010; Burton 1991). Poor perfusion related to arterial insufficiency is a common cause of poorly healing leg (Valencia et al. 2001; Douglas & Simpson 1995). However, circulatory problems may be arterial or venous. Patients with venous insufficiency (including those with venous vascular dysfunction, venous thrombosis, and large "perforators" that connect the deep and superficial venous system) are at high risk for what are called venous stasis ulcers, which are also difficult to heal. Demographically, these patients are frequently elderly, diabetic, inactive, or have a history of leg trauma (Valencia et al. 2001; Margolis et al. 2002; Kolluri 2014; Markova & Mostow 2012). Although the genetics are unclear, there is some propensity of the disease to cluster in families (Suehiro et al. 2014; Ontario 2011).

Treatment for venous ulcers in current clinical practice tends to focus more on treating the ulcer than on prevention or avoiding recurrence (Alvarez et al. 1998; Ghatnekar et al. 2011; Omar et al. 2004; Poblete & Elias 2009; Thomas 2013). Stasis ulcers, however, have high recurrence rates; 33% percent recur after traditional compression treatment and 15% after

surgical intervention (Howard et al. 2008). Such recurrences result in multiple visits to wound clinics or hospitals, substantial costs for the patient and/or health care system, and frustration and stress for patients (Ma et al. 2014; George et al. 2014; Lamel & Kirsner 2013). Many employed patients must take time off from work for leg elevation or wound care, creating an additional financial burden. In addition, since venous disease is often bilateral, patients with venous ulcers on one leg are likely to develop ulcers on the other leg within 3 to 5 years if no preventive measures are taken (Abbade & Lastória 2005; Kunimoto et al. 2001). Patients with healed ulcers may be advised to wear compression stockings, but the discomfort these engender leads to poor compliance. Interestingly, a recent meta-analysis found insufficient evidence to support the prophylactic efficacy of such compression stockings (Shingler & Robertson 2013).

Ablative venous surgical procedures may be more effective in preventing recurrence (Ontario 2011), but it is difficult to decide which patients require such therapy. Indeed, at least in the United States, most insurers will not pay for venous ablative procedures unless patients have failed medical therapy for their acute ulceration over a prolonged period; this creates a large subgroup of patients who recur frequently even though they are healed each time with aggressive nonsurgical therapy. Thus, more information is needed on how to decrease the recurrence rate and reduce the burden of venous ulcer disease (Langemo 1999; Palfreyman & Stone 2014). One approach would be the identification of physical characteristics of the patient's leg that might predict venous ulceration and/or recurrence.

Prolonged external loads on the skin impair blood circulation and can cause ulceration. Although much attention has been paid to pressure from normal loads (perpendicular to the

skin) (Bliss & Schofield 1996; Reeder 2013; Lewis & Towne 2011; Kramer 1999), increasing attention has been paid to the influence of shear loads (loads parallel to the skin) and their relationship to decreased blood flow and ulcer formation (Manorama et al. 2010; Manorama et al. 2013). Additionally, the high blood flow during reperfusion after the loads are removed leads to ischemia-hyperemia injury, which may contribute to venous ulceration (Liao et al. 2013; Loerakker et al. 2011; Morales et al. 2005b; Rendell & Wells 1998; Capp et al. 2004).

Despite the importance of loading, little is known about how responses to loading in healthy legs compare to the responses of legs with wounds. In particular, the possibility that blood flow response may differ with respect to different loading conditions between ulcerated skin and healthy skin is important, as legs are subjected to both normal loading (perpendicular to the skin) and shear loading in common daily postures. In this study, differences in lower leg skin perfusion responses to various types of loading were investigated among patients with venous ulcers and healthy individuals. Understanding differences in skin blood flow during ischemia and between patients with venous ulcers compared to healthy individuals will lay a foundation for establishing a tissue injury model for ulcer formation and has the potential to provide preventive indicators and measures for venous ulcer treatment.

3.2 Methods

3.2.1 Equipment

Load was applied using a custom built device. The device included a six axis load cell (MC3A, AMTI, USA) mounted on its side in a vertical frame (Figure 3-1) that was calibrated prior to each use. The load cell was constrained to two degrees of freedom in this study, allowing

force to be measured in the X and Z directions. The normal loading was applied on the lateral portion of the calf; approximately 25 cm above the ankle with the force vector directed medially (X direction) (Figure 3-1). The load cell also was free to move vertically (Z), allowing for shear load application to the skin. For participants with existing leg wounds, loads were applied at least 24.5 mm away from the wound to avoid any potential deleterious effect on the wound itself. Thus, in some cases, the load application was adjusted superiorly or inferiorly slightly to accommodate the wound the contralateral leg would be tested at the corresponding same height. Since the blood perfusion was measured in capillary level and this slight adjustment would not affect the homogeneity of the blood flow(Jakobsson & Nilsson 1993; Mayrovitz & Larsen 1994).

To mimic loading that participants would see in everyday living, the loads applied were subject specific. The magnitude of normal loading equaled 75% of the subject's lower leg weight which was 4.5% of the subject's whole body weight (Chaffin & Andersson 1991); shear loading, in the combined loading condition, was 50% of the applied normal loading. The forces used were clinically relevant because they are comparable to those that the leg might experience intermittently during normal living, such as crossing one's legs or resting one's leg on a couch or ottoman while sitting (Kohnle 2000; Douglas & Simpson 1995; Bush & R. P. Hubbard 2007; Goossens et al. 1997).

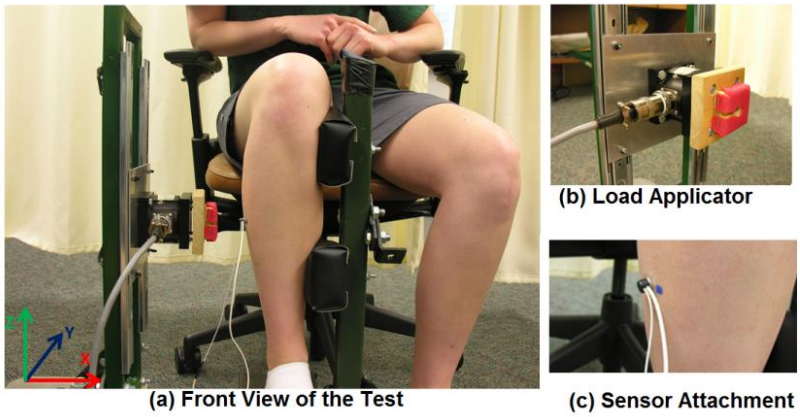

Figure 3-1: Perfusion test apparatus with a healthy participant. (a) Front view of the apparatus with the perfusion sensor and load applicator located to the right of subject's right leg. (b) Load applicator with customized slot cut to fit in the laser Doppler perfusion sensor. (c) Sensor attached to the skin of a healthy lower leg is surface-mounted and non-invasive

A Laser Doppler Perfusion Monitor (PF 5010 LDPM Unit, Perimed, Sweden) was used to monitor and record the blood perfusion of the skin during the entire test period(Nilsson 1984). The Laser Doppler sensor was attached to the leg via a hypoallergenic adhesive such that the customized device surrounded the sensor; loading was then applied around the region of the sensor. The laser Doppler system is non-invasive; it is mounted to the surface of the skin, no penetration occurs. Temperature consistency was maintained through the heated sensor, which was set at 37 °C.

Both the load cell and the perfusion monitor have been proved of their validity and reliability for presented testing protocol(Bartlett et al. 2014; Chen & Bates 2000; Manorama et al. 2010).

3.2.2 Test procedure

Two groups of test participants were recruited for this research. Eighteen individuals were included in the wounded group if they were over the age of 18 years, had stasis ulcers on at least one leg, were able to sit for at least one hour and had no mental health issues. Additionally, twenty healthy participants were included in the healthy group if they were over the age of 18, indicated they did not have a history of vascular disease, stasis ulcers or diabetic ulcers. Patients with wounds were recruited via fliers posted in the Sparrow Hospital wound and hyperbaric clinic; healthy volunteers were recruited via fliers posted on the university campus. Protocols were approved by both Sparrow Hospital's Institutional Review Board and the Biomedical and Health Institutional Review Board of Michigan State University. Healthy subjects were asked to complete an additional health questionnaire to confirm that they did not have disease history of vascular disease, diabetic ulcers or stasis ulcers. Measurements on these two groups of subjects thus produced three sets of data, reflecting measurements on wounded legs, non-wounded legs from patients with wounds, and healthy legs. From the population with wounds, this resulted in evaluations of 20 legs with wounds and 15 legs without wounds (some patients had bilateral wounds).

The following physical measurements of the lower leg were recorded: width (anterior-posterior) and thickness (medial-lateral) of the calf at the same level as the attachment of the perfusion sensor; leg length from ankle to knee; and the distance from the ankle to the perfusion sensor. For participants with leg wounds, additional measurements were recorded for the circumference; width and thickness of the calf at the same level as the wound and the

vertical distance from the wound to the perfusion sensor; the distance from wound to the lateral malleolus at the ankle; and the weight of each subject.

All testing was completed in one session that ranged between one and two hours. Each perfusion test consisted of 5 phases: baseline, normal loading, recovery from normal loading, combined normal and shear loading, and recovery from combined loading. Baseline data were collected before loading. Once baseline perfusion values were recorded, loads were applied to participants' calves. In the normal loading phase; load was applied medially to the lateral surface of the calf. In the combined loading phase, the same normal load was applied as in the normal loading phase, while simultaneously applying a shear load superiorly. The two recovery phases were defined as the period of time from the release of the load until the blood perfusion reached baseline or maximum 10 minutes. Loading order was altered between subjects. Odd numbered subjects had the normal load applied first, while even numbered subjects had the combined loading as their first load application.

3.2.3 Analytical methods and data interpretation

A sample blood perfusion curve is provided in Figure 3-2, from which seven parameters were extracted. A_0 represented the time period during the baseline assessment (no loading); B_1 and B_2 represented the duration where loading was applied and the perfusion values decreased; C_1 and C_2 were the peak perfusion values measured from zero after removal of each load, which represented the post occlusive reactive hyperemia (PORH) level; and A_1 and A_2 were the last 10% of data in the recovery phase. The average perfusion values of regions defined by A_0, B_1, B_2 are denoted as $\overline{A_0}$, $\overline{B_1}$, $\overline{B_2}$ respectively, and averages of $A_1$and A_2 are denoted as $\overline{A_1}$, $\overline{A_2}$ respectively. Together with C_1 and C_2, these represent the seven parameters

in the data analysis. Perfusion was measured in a Perfusion Unit (PU) which is defined as relative number and velocity of blood cells in the tissue (PERIMED 2001).

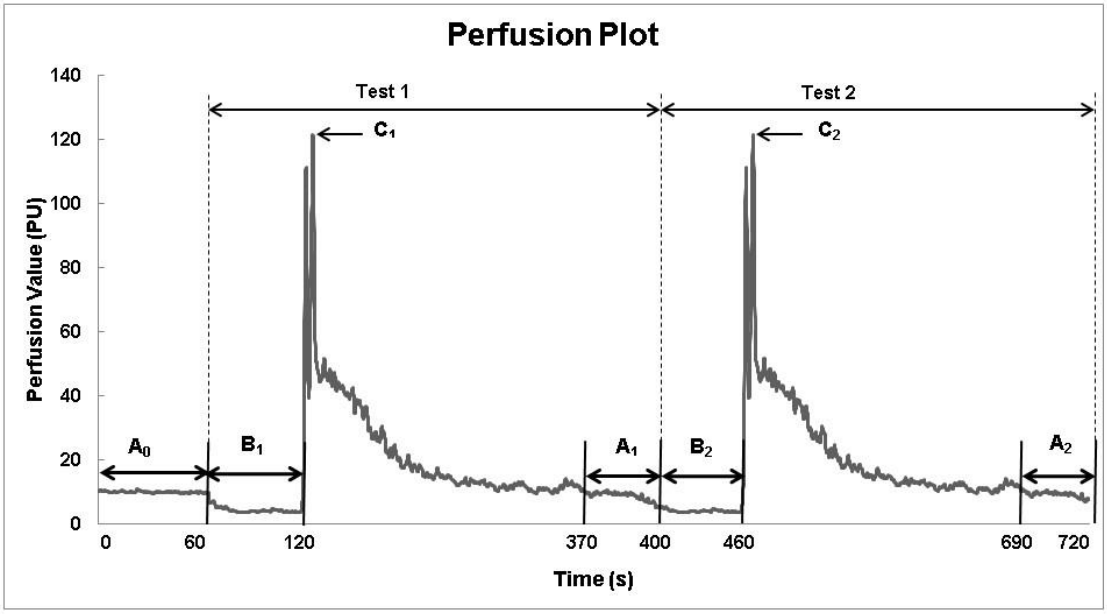

Figure 3-2: Blood perfusion curve with parameters identified: A0 is the original pre-loading baseline region; A1 is the last 10% during recovery after load 1; A2 is the last 10% during recovery after load 2; B1 is the region where load 1 occurred; B2 is the region where load 2 occurred; C1: is the hyperemia after load 1 is released (ARHV); C2 is hyperemia after load 2 is released (ARHV). The Relative Reactive Hyperemia Magnitude (RRHM) is defined as C_1-$\overline{B_1}$ after load 1 and C_2-$\overline{B_2}$ is the RRHM after load 2

Data were investigated and summarized during the following events: perfusion during loading, Post Occlusive Reactive Hyperemia (PORH), and recovery. Perfusion values during loading, $\overline{B_1}$ and $\overline{B_2}$, were compared to determine the influence of the shear loading on the change of blood flow. The decreases in perfusion values caused by loadings were determined by subtracting the difference between the blood perfusion values prior to loading and the blood perfusion values in the subsequent loading phases. This was described as the differences between $\overline{B_1}$ and $\overline{A_0}$, and the differences between $\overline{B_2}$ and $\overline{A_1}$.

The spikes in perfusion after the release in load were also evaluated. C_1 and C_2 represented the PORH values (denoted as the *Absolute Reactive Hyperemia Value*, ARHV). To

account for the maximum value of blood reperfusion after loads were removed, C_1-$\overline{B_1}$ and C_2-$\overline{B_2}$ were also compared. These values represented the relative hyperemia value of PORH and account for the differences between the perfusion level due to the loading and the peak perfusion value due to reactive hyperemia (denoted as the *Relative Reactive Hyperemia Magnitude*, RRHM)

The recovery level was analyzed in two ways: the first took into consideration the loading order and the second did not. Considering loading order, recovery level was defined as (3-1):

$$\boldsymbol{RL_1 = \frac{C_i - \overline{A_i}}{C_i - \overline{A_{i-1}}} \quad i = 1, 2} \qquad (3\text{-}1)$$

Here RL is the abbreviation for Recovery Level. In this way, recovery level always compared blood flow restoration after loading to before loading.

Since some participants did not fully recover to initial baseline from the PORH, but rather achieved only 90% of recovery, it was also important to compare the recovery level with respect to the final perfusion values before the second loading was applied. Therefore, the recovery level independent of loading order was calculated as (3-2):

$$\boldsymbol{RL_2 = \frac{C_i - \overline{A_i}}{C_i - \overline{A_0}} \quad i = 1, 2} \qquad (3\text{-}2)$$

By similar concept, RL_2 was considered as blood flow restoration after loading compared to the blood flow during the baseline phase.

3.2.4 Statistical method

Statistical analysis and comparisons were performed. Paired t-tests were conducted within the healthy subjects to determine if differences existed between the left legs and right legs of the same subjects. All data met the requirements for usage of a t-test. Next, a Kruskal-

Wallis test followed by Dunn's post-hoc test (Glantz 1997; Zar 1999) was conducted to compare the three sample groups: wounded legs, non-wounded legs and healthy legs during different loading conditions (MATLAB, R2013a). Finally effect sizes were calculated between the groups by Cohen's method (Cohen 1988).

3.3 Results

3.3.1 Participants

Eighteen individuals with wounds on at least one lower leg and twenty healthy individuals with no vascular issues participated in the testing. One leg of one participant could not be tested due to the number and locations of the wounds on that leg, the test apparatus was not able to be placed on the leg without covering a wound. Thus, a total of seventy five legs were evaluated. The group with leg wounds included eleven male and seven female participants. Their average age was 71 years (SD 12.2) with an average mass of 106.4kg (SD 50.2). The average BMI for wound patients was 32.9 (SD 13.5) Ten male and ten female participants comprised the healthy subject group with an average age of 29 years (SD 19.6) and average mass of 83.9kg (SD 20.5). The average BMI for this group was 27.0 (SD 5.0) Although gender distribution was similar between the two groups, those with ulcers tended to be older and more obese, consistent with the known epidemiology of this disease (Abbade & Lastória 2005).

Each leg of each participant was tested except for the one leg with widespread wounds that prohibited testing. From the population with wounds, this resulted in evaluations of 20 legs with wounds and 15 legs without wounds (since some patients had bilateral wounds).

Three groups were then defined for comparison: legs with existing wounds (here and after defined as “Wounded”); legs without wounds but from participants with wounds (here and after denoted as “Non-Wounded”); and legs from healthy participants (here and after called “Healthy”). Since we found no statistical difference between paired measurements in left legs and right legs in any of the groups, we have pooled left and right leg data in the analysis that follows.

3.3.2 Post Occlusive Reactive Hyperemia

The PORH was investigated in two aspects: the absolute reactive hyperemia value (ARHV) and the relative reactive hyperemia magnitude (RRHM), as described in the previous section.

Figure 3-3 shows that wounded legs had highest hyperemia, followed by non-wounded legs; the healthy legs had the lowest hyperemia values for both the ARHV and the RRHM. Kruskal-Wallis test followed by a Dunn’s post-hoc test demonstrated significant differences between wounded and healthy legs for both ARHV ($p=0.029$ for normal loading; $p=0.029$ for combined loading) and RRHM ($p=0.0255$ for normal loading; $p=0.0014$ for combined loading) (Figure 3-3).

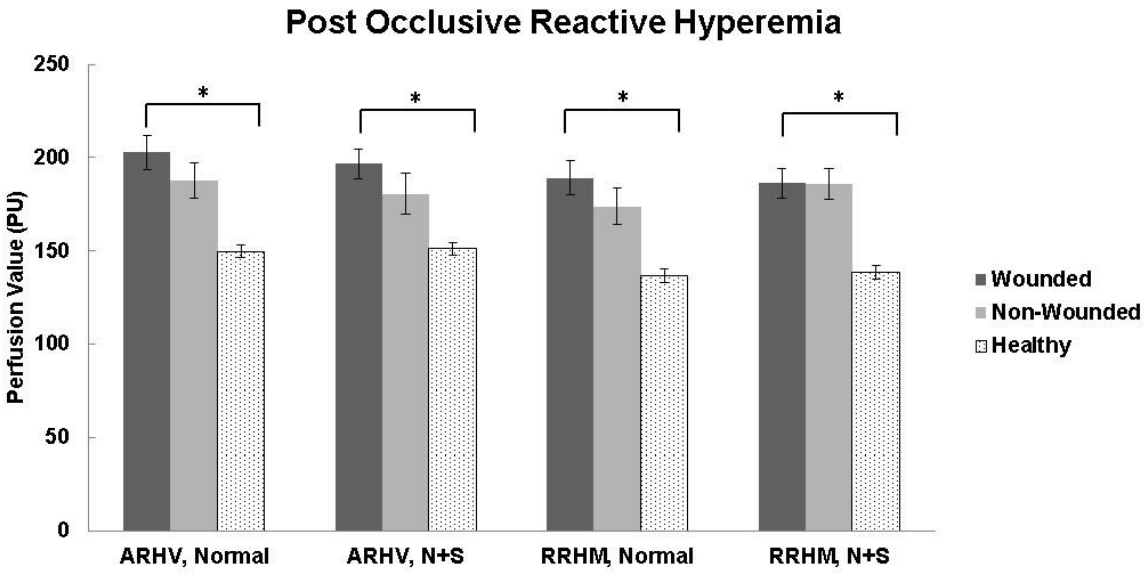

Figure 3-3:Post Occlusive Reactive Hyperemia (PORH) perfusion values for the Absolute Reactive Hyperemia Values (ARHV) and Relative Reactive Hyperemia Magnitudes (RRHM) after normal loading and combined normal and shear (N+S) loading. (* indicates significant differences, ($p<0.05$))

3.3.3 Perfusion

3.3.3.1 Perfusion during baseline and loading

Averages of blood perfusion values were calculated during three loading conditions: baseline, normal loading, and combined normal and shear loading, results are listed in Figure 3-4.

Wounded legs had the highest perfusion values during baseline; healthy legs had the lowest baseline perfusion values. Statistically significant differences occurred between wounded legs and healthy legs during baseline study (Figure 3-4, $p=0.002$).

When comparing the healthy to wounded to non-wounded legs under normal loading, the average perfusion values were the lowest for the healthy group, the highest for the non-wounded group and an intermediate for the wounded group. However, significant differences were not found between the three groups.

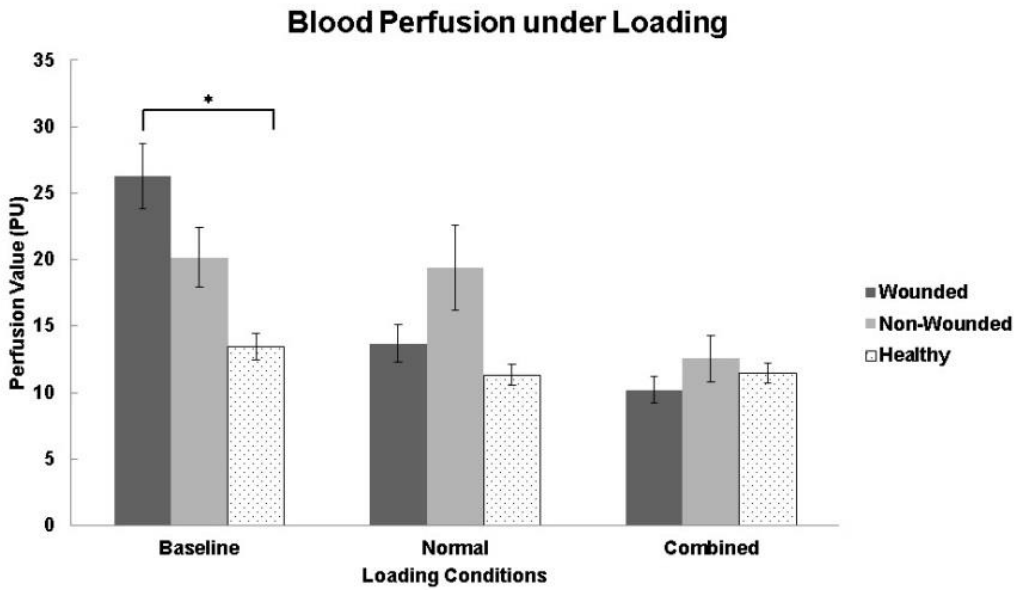

Figure 3-4: Blood perfusion values during baseline, normal, and combined normal and shear loading. (* indicates significant differences, (p<0.05))

For combined loading, the lowest perfusion values were found in the wounded group, followed by the healthy group and then the non-wounded group. It should be noted, that the combined loading introduced the largest decrease in perfusion for all three samples. No significant differences were found between the three groups for the perfusion values produced from combined loads.

3.3.3.2 Perfusion *decrease* due to the application of the loads applied to the skin

Two different approaches were used to evaluate the perfusion changes. The first examined the difference with regard to the initial baseline data set ($\overline{A_0} - \overline{B_i}$ i=1, 2); while the second treated the period immediately prior to the trial as the "new baseline" and compared perfusion data to this value ($\overline{A_{i-1}} - \overline{B_i}$ i=1,2). Perfusion values of wounded legs decreased the most when loading was applied regardless of the approach used for comparison. Each approach

yielded significant and similar differences between the wounded and healthy legs. (Figure 3-5, p=0.020 for $\overline{A_0} - \overline{B_i}$ under normal loading; p=0.025 for $\overline{A_0} - \overline{B_i}$ under combined loading; p = 0.186 for $\overline{A_{i-1}} - \overline{B_i}$ under normal loading; p=0.0017for $\overline{A_{i-1}} - \overline{B_i}$ under combined loading). The other comparisons (wounded vs. non-wounded, and wounded vs. healthy) did not yield significant differences for either approach.

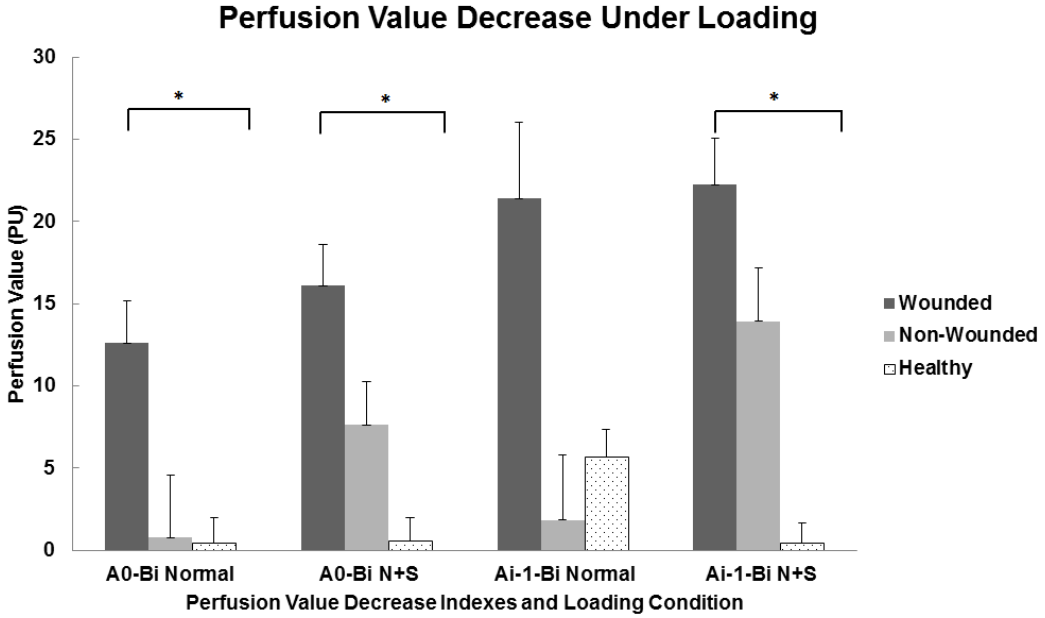

Figure 3-5: Decrease in perfusion due to loading. A0-Bi is the perfusion value decrease during loading compared to the initial baseline, Ai-1-Bi is perfusion value decrease during loading compared to the perfusion value prior to loading. Normal refers to normal loading and N+S refers to combined normal and shear loading. (* indicates significant differences, (p<0.05))

3.3.4 Recovery percentage

As described in section 3.3, recovery level was calculated via two approaches according to Eq. (3-1) and (3-2). Based on the first approach, the wounded legs had averages of 94% and 96% recovery after normal and combined loading, respectively; non-wounded legs had an

average recovery of 97% and 92%; healthy legs had 98% recovery in both normal and combined loading. Based on the second approach (Eq. 3-2), wounded legs had an average recovery of 96% and 100% from the normal and combined loading; non-wounded legs had average recovery of 98% and 100%; healthy legs had 100% and 96% recovery. These data indicated that the duration of the recovery phase was sufficient for the participants to recover at a 90% level or higher after loads were removed.

3.3.5 Effect size

Effect sizes indicate the strength of a relationship. Small to medium effect sizes (range 0.1~0.3) (Cohen 1992; Nakagawa & Cuthill 2007) were observed between wounded legs and non-wounded legs for reactive hyperemia after both normal and combined loadings, and for blood perfusion values during baseline, normal and combined loading. Small to medium effect sizes also occurred between non-wounded legs and healthy legs for blood perfusion decrease due to the loadings. Medium effect sizes (range 0.3~0.5) were found in comparison between non-wounded legs and healthy legs for blood perfusion values during baseline and loadings. In addition, medium effect sizes were also shown between wounded legs and non-wounded legs for blood perfusion decrease under normal and combined loadings.

This finding suggested that statistically significant differences might be expected for higher sample sizes for comparison of reactive hyperemia between wounded and non-wounded legs as well as for the comparison of perfusion values during baseline and loadings between non-wounded legs and healthy legs.

3.4 Discussion

This initial study investigated the different blood flow responses to normal loading and combined normal and shear loading between patients with existing venous ulcers on their legs and healthy individuals. Legs with venous ulcers exhibited the highest values of post occlusive reactive hyperemia (PORH), followed by legs without ulcers but from participants with venous ulcers on the other leg; healthy legs had the lowest values of PORH. This contrasts with the other common cause of lower extremity ulceration, which is inadequate arterial perfusion(Valencia et al. 2001; Douglas & Simpson 1995). One might have predicted from the phenomenon of ischemic ulceration that venous ulcer patients might exhibit insufficient blood circulation and restoration after external loading, perhaps from tissue edema, and that this might in turn cause ulceration or interfere with healing. However, both basal perfusion and post-occlusive hyperemic perfusion were higher in the legs with venous ulcers than in non-wounded legs or healthy legs. As vasodilation and hyperemia may accompany inflammation; these phenomena may reflect the inflammatory physiology of the tissues near the venous ulcers. The etiology of such inflammation is unclear. The chronic wound might itself induce inflammation in the surrounding nearby skin, but such a wound seems less likely to induce systemic changes sufficient to induce hyperemia of the contralateral (unwounded) leg. Some have postulated that local iron overload from hemosiderin deposition could generate free radicals and modulate inflammation (Zamboni et al. 2006). Increased interstitial tissue pressure can itself activate inflammatory cells. Increased extracellular pressure stimulates macrophage phagocytosis and cytokine release as well as the release of cytokines from dendritic cells (Shiratsuchi & Basson 2004; Shiratsuch & Basson 2005; Craig et al. 2009). Interestingly,

chronically increased extracellular pressure also inhibits epithelial wound healing in the gut mucosa (Kovalenko et al. 2012).

Previous research has shown that shear loading plays an important role for reducing the local blood flow of the skin of the forearm (Manorama et al. 2013) . In the present study, a different body region was investigated and different populations were compared. Both normal and shear loadings reduced blood flow. Legs with venous ulcers had the largest decrease in blood flow in response to either normal or combined normal and shear loadings. Non-wounded legs and healthy legs exhibited relatively similar blood flow decreases in response to normal loading. However, in response to combined loading, the blood flow of non-wounded legs in patients with contralateral venous stasis disease decreased more than that of healthy legs. This emphasizes the need to consider *both* normal and shear loading in future investigations of the biology of this disease.

The statistical evaluations indicated that wounded legs are different than healthy legs blood perfusion changes under loading and for reactive hyperemia. Furthermore, the effect size calculations suggest that statistically significant differences are likely to be observed between wounded legs and non-wounded legs, and non-wounded legs and healthy legs for larger sample sizes. The finding that the wounded leg yields different responses from the healthy leg, coupled with the fact that the contralateral unwounded legs exhibit intermediate responses raises the possibility that a measurable progression occurs as movement from a healthy to a non-healthy to a stasis ulcer formation occurs. This is noteworthy because patients with venous stasis ulcers in one leg may be at a statistically higher risk of developing venous stasis ulcers in the contralateral leg (Erickson et al. 1995) . Clinically, this suggests the possibility that this approach

might be useful for identifying at-risk legs and then preventing venous stasis ulceration by patient education and the use of prophylactic compression stockings. Clearly much more work needs to be done to validate this further hypothesis, but it represents a challenging and potentially fruitful area for further study. In addition, longitudinal studies with larger numbers of patients are required to determine whether the degree of abnormality at presentation might predict the likelihood of wound healing and what happens to the abnormalities observed in the wounded legs after the wounds heal.

The novelty of this study lies in three aspects: first, the local blood perfusions were measured on legs with existing venous ulcers so that the microvascular blood flow close to wounded skin was tested. Second, all the loads were applied around the laser Doppler sensors which ensured that changes in blood perfusion measurements were related to loadings. In previous blood perfusion tests involving patients with leg ulcers, the external loads were applied only at the distal thigh with pressure cuffs while the blood perfusions were measured near the ankles (Mlacak et al. 2005; Jochmann et al. 1993). Therefore, the response of blood perfusion to loading of the region near the ulcerated skin was unclear before this study. Finally, the application of shear loads in this study differentiates itself from other studies that have been conducted with respect to venous ulcers. Most research on venous ulcers, even leg ulcers, are only focused on the influence of external normally applied pressures (Holloway Jr. et al. 1976; Bliss & Schofield 1996; Reeder 2013; Milic et al. 2009). Recently, the importance of shear load in pressure ulceration has become more apparent (Olesen et al. 2010), yet few studies of shear have been conducted with regard to venous ulcers (Pascarella et al. 2005).

These results emphasize that it is important to study blood flow responses to loadings in the vicinity of both the perfusion measurements and the wounds if we are to really understand the pathobiology of this common disease. Furthermore, In addition to possibly offering new insights into the pathobiology of venous stasis disease, these findings are of potential clinical significance because they demonstrate that patients with venous stasis disease exhibit abnormal responses to loading that can be readily discerned by a non-invasive measurement. The suggestion that the contralateral unwounded legs of patients with known venous stasis ulcers exhibit intermediate responses is particularly exciting since we know that these patients are at high risk for subsequent venous stasis ulcer development in their previously unwounded legs (Abbade & Lastória 2005; Kunimoto et al. 2001). Clearly, these results require confirmation and extension in a larger data set, as well as longitudinal follow-up to determine how perfusion responses to loading change as patients' ulcers heal. It will also be important to investigate directly the effects of age and body habitus on the hyperemic response to loading, as these are covariates with the presence of venous stasis disease. Finally, repetitive forces are likely to affect the epithelial cells directly as well as modulating their perfusion, and this may also alter wound healing (Kovalenko et al. 2012; Han et al. 1998). Conversely, patients at high risk who are not candidates for intervention, either because of anatomy or socioeconomic factors, may be more effectively counselled about preventive strategies such as compression stocking use, intermittent leg elevation, and intermittent ambulation, if they can be told that they are at particularly high risk.

The goal of this research was to study the changes in the arterial and venous blood flow in the forearm through the use of MRA phase-contrast imaging with the application of normal and shear loads.

The results of the experiments demonstrated that with the addition of shear loads, blood flow in the AIOA and BV decreased further than with the addition of normal load alone. While the AIOA comparisons produced significant differences, only a marginal significance was observed in the case of BV. However medium to high effect sizes were observed, suggesting that the marginal significance was due to the small sample size and statistical significance could be obtained with a larger sample.

Published research has indicated that when sitting, or lying in an inclined bed, an individual experiences both normal and shear loads on the body (Goossens et al. 1997; Bush & R. Hubbard 2007; Gilsdorf et al. 1990; Hobson 1992; Mimura et al. 2009). A limited number of studies have examined the effects of shear loading on the skin in humans. Those studies reported that the transcutaneous blood flow decreased with the addition of shear applied to the skin (Manorama et al. 2010; L Bennett et al. 1979; Zhang & Roberts 1993; Zhang & Roberts 1994). However, until now, it was not clear what effect an external shear load had on deeper vessel blood flow. The work presented here confirms that external loads of combined normal and shear forces decrease the internal blood flow, more so than normal load alone.

This research was novel on two levels. First, the methods were unique in that shear and normal loading were applied while in an MRI scanner. An apparatus was developed to consistently apply both normal and shear loads to the forearm while meeting all the requirements for use in the MRI scanner. Secondly, the use of MRA phase-contrast imaging in

combination with *in vivo* shear loading on humans to document changes in blood flow is novel. Scientific literature reporting such results is not available elsewhere.

Results also indicated that a variation in normal force occurred across the subject pool. This was due to the anatomical build of the individual, and how the pressure cuff interacted with the individual's forearm. However, in the data analysis, each data set was compared to the individual's own baseline data, so analyses were conducted on the change in blood flow from the baseline values per each individual. A limitation of this study was that the shear loads at the site of the study (MRI suite) could not be measured. So, it is possible that some variation in shear loading occurred across participants. Additionally, another limitation is that this study involved only male participants, whereas women are also prone to pressure ulcers. Future work will include female participants.

Based on the results of this work, shear loads applied at the skin cause a reduction in blood flow in the deeper vessels. From prior work of the authors, (Manorama et al. 2010), it was found that the perfusion at the skin level decreased with the addition of shear loads. The current data in conjuction with this prior study shows that a decrease in blood flow occurs at both the superficial and deep levels when shear loading is applied on the skin. Additionally, research shows that a decrease in blood flow leads to tissue necrosis (Goossens et al. 1994; Kosiak et al. 1958; Bouten et al. 2003; Bansal et al. 2005). Thus, based on this information, both scenarios of pressure ulcer formation are possible, i.e. pressure ulcers could be initiated superficially, or at a deep level. Future research will combine the understanding of the effects of shear load on superficial perfusion and on deeper vessel blood flow through a porous media model to obtain a better understanding of where a pressure ulcer is likely to be initiated.

The findings from this work indicate that shear force is an important factor to consider when studying the changes in blood flow. Additionally because of the relationship between decreased blood flow and tissue damage, understanding the effects of shear in the formation, prevention, and treatment of pressure ulcers should also be considered.

3.4.1 Limitations

One limitation of this pilot study is that the study patients with wounds tended to be older than our healthy volunteers. This reflects our recruitment of the healthy volunteers on a university campus while patients with leg wounds tend to be older. Future work may benefit from stratification by age or deliberate recruitment of an older healthy comparative group. Additionally, we will increase our sample size in future work. Due to the change in the medical management system used at the clinic, not all medical data were available to the researchers. Additional testing will include a form where the number of reoccurring wounds, time to heal, and time in treatment will be gathered at the time of testing directly from the patient and nurse. This study conducted a single test session, to assess test-retest reliability, it would be beneficial to conduct multiple tests one each participant on the same day; however the time commitment for each participant would be significantly increased.

3.5 Conclusion

Legs with venous stasis ulcers exhibited highest blood perfusion values of post occlusive reactive hyperemia, and largest decrease in perfusion values under normal and combined normal and shear loadings. Statistical evaluation indicated that the wounded legs and healthy legs were significantly different in comparisons of both reactive hyperemia and blood perfusion

changes due to load application. Effect sizes indicate that additional significant differences might be observed between non-wounded legs and healthy legs with higher sample sizes.

These findings indicate the need to study both normal and shear loadings, the need to look at the effects of loading near the wound, and evaluation of both the wounded and non-wounded limbs. These data support the possibility that changes in force-perfusion responses could be a possible indicator of underlying disease that might predispose to ulcerogenesis or interfere with ulcer healing, and raise the possibility of using these data for a predictor of when conditions change and ulcers are on the verge of formation. Additionally, they have the potential to be used for subgroup identification where alternative treatment approaches may be more effective than standard treatment.

Acknowledgements

The authors would like to thank Renee Chabon, Jessica Buschman and Deven Patel for their assistance in data collection. The authors would also like to thank the physicians, nurses and staff at Sparrow Health System's Wound and Hyperbaric Clinic for their support during this project. Finally, we would like to acknowledge funding support from Michigan State University.

4 A POTENTIAL TOOL FOR THE STUDY OF VENOUS ULCERS: BLOOD FLOW RESPONSES TO LOAD

(Wu Pan, Joshua P Drost, Sara Roccabianca, Seungik Baek, Tamara Reid Bush., A potential tool for the study of venous ulcers: blood flow responses to load. Journal of Biomechanical Engineering: *under review*)

4.1 Introduction

Venous ulcers, or stasis ulcers are severe skin ulcers that comprise almost 90% of all lower extremity ulcers (Cleveland Clinic 2015; Snyder 2005). Venous ulcers are chronic, painful, and have recurrence rates up to 78% (Kolluri 2014). Most individuals who develop these ulcers are 65 years and older, with a compromised vascular system (Lamel & Kirsner 2013). Further, treatment and associated care of these ulcers claim more than 25 billion dollars in US annually (Lazarus et al. 2014). Venous ulcers are not limited to the US; they are also a global problem with staggering cost. In Europe, the annual cost of treatment for venous ulcers is £300~600 million in the UK (Johnson 2002), 128 million dollars in France (Simka & Majewski 2003), and 25 million dollars in Sweden (Valencia et al. 2001).

In venous ulcer patients, the calf muscle pump does not work efficiently, leading to a reduction in the blood flow that returns to the heart. This decrease in efficiency, results in blood pooling in the lower leg (Milic et al. 2009). Researchers have shown that this pooling of blood triggers several biological events that lead to tissue necrosis and eventually wound formation (Collins & Seraj 2010; Ontario 2010). Pooling of blood causes edema, resulting in an increased internal pressure, and a change in vessel resistance.

Additionally, throughout the day, the skin is loaded and unloaded. This occurs from contact with a chair, couch, ottoman or crossing one's legs. Physiologically, the application of a load results in increased pressure on the leg, this external pressure causes a reduction in the local skin microcirculation (Herrman et al. 1999), which in turn causes a subsequent reactive hyperemia that correlates with ischemia (Jan et al. 2013). The hyperemia response is a physiological defense to the external pressure (Rendell & Wells 1998), and is achieved by

venous dilation (Mollison et al. 2006). Such cyclic loading, over a long period of time can lead to tissue damage, cell death and can eventually result in the formation of a venous ulcer (Langemo 1999; Mlacak et al. 2005).

Patients who are likely to develop an ulcer are prescribed a compression stocking and asked to wear them daily as a means to reduce the blood pooling. However, these stockings are thick, elastic bands that are hot, and uncomfortable, so most individuals choose not to use the stockings in a preventative fashion. Rather, the status quo is to wait until an ulcer forms, and then treat it using these stockings (Kolluri 2014). There is lack of quantifiable measures in a patient specific format to identify when an individual is at a higher risk of developing an ulcer. Thus, there is no approach to identify physiological changes and apply a "just-in-time" preventive measure (Heit et al. 2001).

Therefore, a critical need exits to develop a model that can be used to monitor patient-specific responses related to physiological changes that can be linked to ulcer formation. The work presented here looks at parameters that are related to changes in blood perfusion as a response to loading. Loads are applied and released on the skin throughout the day. This results in a cycle where the following process occurs: 1) the blood perfusion is at steady state, 2) loads are applied which results in a decrease in blood perfusion, 3) the load is released, then a spike in the blood perfusion occurs immediately after the load release (reactive hyperemia), and 4) the blood perfusion recovers and reaches a value near that of the pre-loaded condition. This cycle introduces several events that lead to tissue damage and wound development.

Background

To better understand the blood flow characteristics, the Windkessel model was first proposed by Otto Frank in 1988 (Sagawa et al. 1990). It is a classical model that was used to study the hemodynamic characteristics of overall cardiovascular blood flow via a compartmental electrical circuit system, in which, the voltage represented the blood pressure; the current represented the blood flow; and resistors and capacitors represented the blood resistance and vessel compliance respectively (Westerhof et al. 2009; Zheng & Mayhew 2009). Such a model was successfully developed for use as a clinical index for aortic pressure and artery stiffness measurements, however, it has not been applied in venous ulcer research (Abdolrazaghi et al. 2010; Segers et al. 1997).

Several other Windkessel-based models have been developed to study the hemodynamics of smaller veins and capillaries, but these models had complex circuit compartments/blocks, in which multiple resistors and capacitors were used to represent a single event and were computationally expensive (Vo et al. 2007; de Mul et al. 2005; de Mul et al. 2009; Humeau et al. 2000; Solovyev et al. 2013; Smye & Bloor 1990). Several models also addressed the component of reactive hyperemia i.e., the temporary spike in blood flow after vascular occlusion (Wilkin 1987). Reactive hyperemia is important because when the ischemic tissue or vessels experience a spike in reperfusion, it results in vessel injury and cell damage (Grace 1994; Mak et al. 2010). Furthermore, the recovery of blood perfusion in the reperfusion period is also a key indicator for the functionality of tissue metabolism and vasoconstriction (Hagisawa et al. 1994). Using experimentally measured perfusion data obtained from laser Doppler flowmetry, De Mul established a sophisticated compartmental model that was able to replicate the reactive hyperemia spike and the recovery of the perfusion. His model used one

resistor with one capacitor to represent the arterial system and three resistors with one capacitor to present the capillary system (de Mul et al. 2009; de Mul et al. 2005). Meanwhile, Vo introduced a model with a voltage diode to account for the venous occlusion induced by an external pressure cuff and compared the model output with tissue oxygenation data from healthy subjects (Vo et al. 2007). Even though these models have addressed components of the occlusion and reperfusion process, no models represent the changes in perfusion for the entire loading and unloading process. Further, none have applied this approach to study venous ulcers.

Therefore, the goal of this work was to develop a Widnkessel-based model that could be used to identify parameters that changed between healthy individuals and those with wounds. This model replicated: a) decrease in blood flow due to locally-induced loading, b) spike in blood flow following load release due to reactive hyperemia, and c) recovery of blood flow. Prior experimental research by the authors showed that blood perfusion behaviors in the skin were different between three samples: patients with venous ulcers, the non-wounded legs of those same patients, and legs from a healthy population (Pan et al. 2015). The model presented here used these experimental data to identify specific parameters associated with changes in the physiology that are related to ulcer formation.

4.2 Methods

4.2.1 Experimental data collection

Prior work used experimental techniques to determine the changes in perfusion on the lower leg during a loading and unloading scenario (Pan et al. 2015). The data collected from this

prior work were used for model development. Eighteen patients with venous ulcers on one or both of their legs and twenty healthy participants were tested. During the perfusion test, normal (perpendicular to skin) and combined normal and shear (parallel to skin) loading was applied on the lateral side of the participant's lower leg via a customized load applicator while blood perfusion data were simultaneously gathered (Figure 4-1). The load applicator allowed the load to be applied to the area surrounding the perfusion sensor. The magnitudes and directions of the loads were measured with a six-axis load cell (MC3A, AMTI, USA).

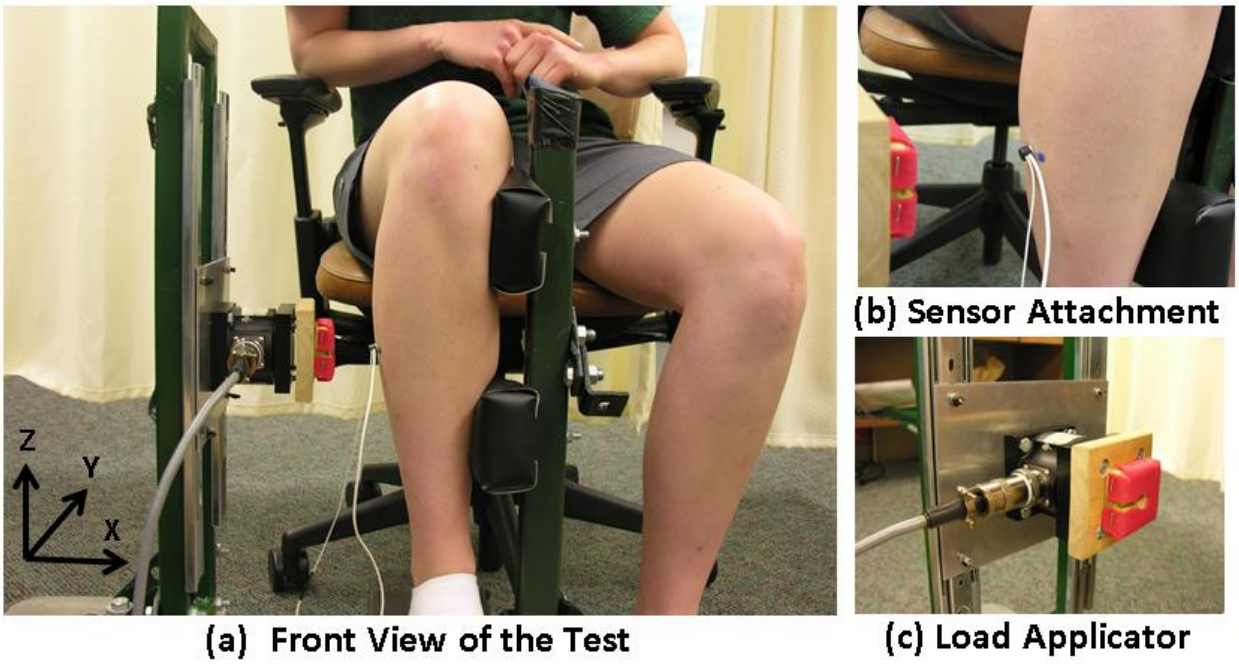

Figure 4-1: Leg perfusion test set up a) Front view of the test set up with perfusion sensor attached to the participant's lateral lower calf, the customized load applicator can slide in the medial/lateral and vertical directions to apply normal and shear loadings respectively b) Non-invasive perfusion sensor attached to the skin, and c) Load applicator with the contact platform (Pan et al. 2015)

The perfusion data were continuously recorded by a Laser Doppler Perfusion Monitor (PF 5010 LDPM Unit, Perimed, Sweden). Each leg of each participant was tested under two

loading conditions 1) normal loading, 2) combined normal and shear loading. Each data plot was sectioned into five phases: 1) baseline (no load), 2) the perfusion decrease under the first loading, 3) the hyperemia spike and perfusion recovery after the first loading, 4) the perfusion decrease under the second loading, and 5) the perfusion recovery after the second loading. A typical LDPM signal output plot for one loading condition is shown in Figure 4-2, the output of the LDPM was the then imported into MATLAB and used as a comparator for the model output.

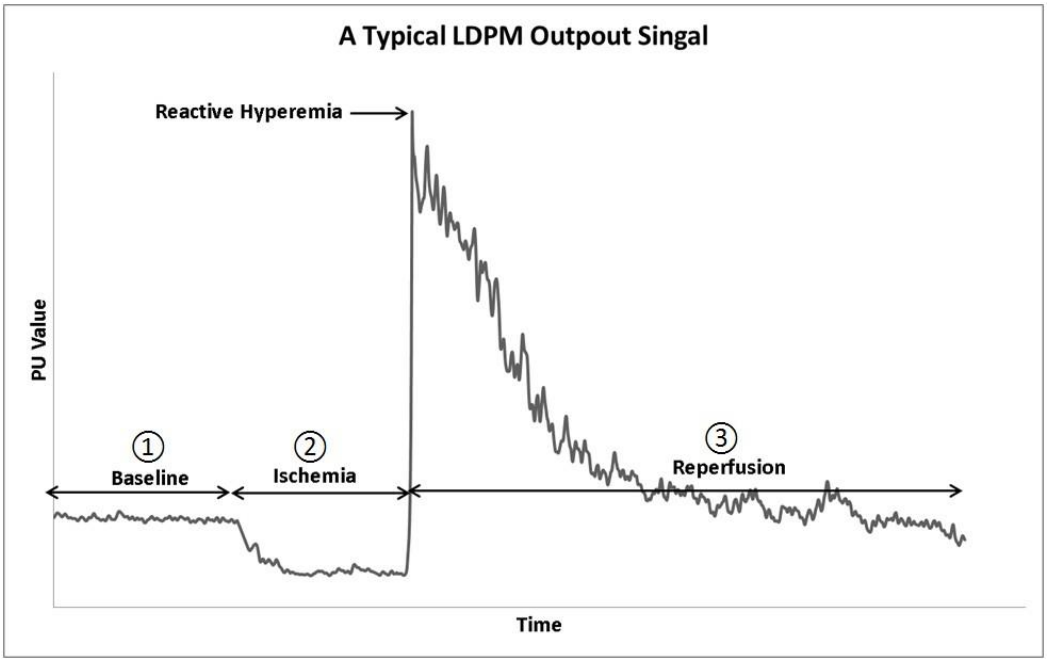

Figure 4-2 A typical Last Doppler output of perfusion during testing in which the 1) baseline period is prior to loading, 2) the ischemia period is under loading, and, 3) the reperfusion is the blood flow recovery after loading. Two loading conditions occurred during one testing with similar LDPM output. This figure represents one loading scenario. The reactive hyperemia is the spike in the blood flow upon the release of the loading. PU refers to Perfusion Unit, which is defined as the relative number and velocity of blood cells in the tissue (Perimed, 2001)

The test participants' legs were divided into three categories: 1) "wounded legs", legs with existing stasis ulcers; 2) "non-wounded legs", the legs from patients that did not have open wounds or ulcerations on that leg but had venous ulcers on the other leg; 3) "healthy legs", legs from healthy participants. This categorization resulted in 20 wounded leg datasets,

15 non-wounded leg datasets(some participants had ulcers on both legs), and 40 healthy leg datasets (Pan et al. 2015).

4.2.2 Model development and simulation

4.2.2.1 Model

In the Windkessel approach, the vascular compartmental circuit model uses the analogy of an electrical circuit; Ohm's law (Eq. (4-1a)) for electricity is equalized with Poiseuille's law (Eq. (4-1b)) for fluid dynamics of the blood vessel.

$$R = \frac{U}{I} \; ; \qquad VF = \frac{\pi \, (\Delta P) \, (R_V)^4}{8 \, (\eta_{blood}) \, (L_V)} \tag{4-1a,b}$$

Where R represents the resistance, U represents the voltage and I represents the current. VF is the volumetric flowrate, ΔP is the pressure difference between the two ends of a vessel, R_V is the vessel radius and L_V is the vessel length and η_{blood} is the blood viscosity.

One circuit model was created with two resistors, one capacitor, and two voltage sources (V_{ext} as external pressure induced by load and V_0 as hydrostatic pressure). The voltage sources were in mmHg which were consistent with literature (Vo et al. 2007). In our model (Figure 4-3), the first resistor (R_1) represented the global vascular resistance in the leg, while the second resistor (R_2) represented the local vascular resistance of the loaded region. The capacitor (C) represented the local vascular compliance of the leg. By adapting an approach similar to Vo's model, the voltage source V_{ext} was placed in series with R_2 and represented the external pressure locally applied by loading on the legs of the participants. The pressure was calculated as the applied force over the contact area between the leg and load applicator (Eq. (4-2)),

$$V_{ext} = K\frac{F}{S} \tag{4-2}$$

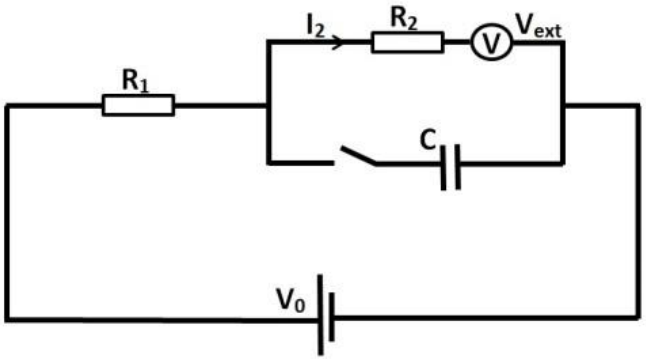

Figure 4-3: Model to simulate the blood flow of the lower leg under external loadings. R_1 and R_2 are global and local vessel resistances, respectively, C is the local vessel compliance, V_0 is the hydrostatic pressure at the testing site and V_{ext} is the pressure induced by locally applied external loadings

Where V_{ext} is the external pressure induced by external loads, F is the external normal load that was applied during the experimental testing, S is the contact surface between the load applicator and the participant's leg and K is the ratio factor to account for both normal and combined normal and shear loads.

The factor K was introduced to account for the change in blood flow due to shear loading. As indicated by other studies when shear loading was applied in addition to normal loading, and the magnitude of the shear loading was 50% of the normal loading, the blood flow was further decreased by 25% (Manorama et al. 2013; Zhang & Roberts 1993; Leon Bennett et al. 1979). Therefore, when only normal loading was applied, K was equal to 1; when combined normal and shear loading was applied, K was equal to 1.25.

The voltage source V_0 represented the hydrostatic pressure at the testing site on the lower leg. According to Burton's theory (Burton 1972), the arterial pressure at the heart is

documented as 100 mmHg, and decreases as a function of distance away from the heart. Using Burton's theory, the hydrostatic pressure at the testing site was calculated as Eq. (4-3)

$$V_0 = V_{art} + \rho g \times dh = 142.7\ mmHg \quad (4\text{-}3)$$

Where V_{art} is the arterial pressure at the heart, ρ is the blood density (1056kg/m^3) (Cooney 1973), g is gravity (9.81 N/kg) and dh is the vertical distance between the heart and where the measurement was taken on the lower leg when the participant was seated, which was on average 0.55m.

As part of the model, a switch feature was added in series with the capacitor so that the effect of the capacitor could be controlled and implemented only in the reperfusion period. The capacitor was pre-charged by assigning an initial voltage; this allowed the model to mimic a hyperemia spike. The magnitude of this initial voltage was required to be higher than the voltage over R_2, which was the distributed voltage of V_0 between R_1 and R_2. The capacitor was pre-charged, and the capacitor's most important time-history characteristics were the exponential decay in the discharging period, this represented the change after hyperemia. The capacitor's effect in the "charging" (occlusion) period could be neglected by controlling the switch. Hence, the switch was open during the baseline and loading period, and when the external loading was removed the switch was then closed and connected the capacitor as part of the circuit.

4.2.2.2 Simulation procedure

Based on Ohm's law, the governing equation of the circuit model of the localized lower extremity was constructed as:

$$(R_1 + R_2)I_2 + CR_1R_2\frac{dI_2}{dt} = V_0 - V_{ext} - CR_1\frac{dV_{ext}}{dt} \quad (4\text{-}4)$$

The model was built in Simulink (MATLAB R2013a, MathWorks, Inc, USA) in which V_{ext} was a rectangular wave function that corresponded to the external loading period (Figure 4-4), I_2 was the output of the Simulink model and was then read into MATLAB for comparison with the experimental data.

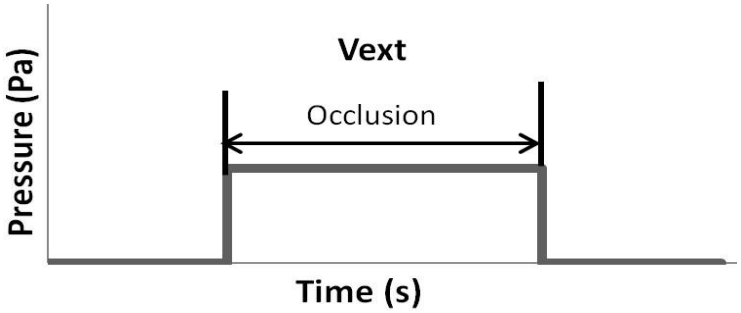

Figure 4-4: V_{ext} as a rectangular wave function

Based on de Mul's data (de Mul et al. 2005), the initial values of R_1, R_2 and C were chosen to be R_1=1, R_2=10 and C=1. Next, the output of the model was compared to the experimental data of a specific participant. Several iteration steps were conducted adjusting the parameters of each element until the model output matched a given experimental data set. The R_1 value was first adjusted to match the baseline period and then the R_2 together with R_1 values were adjusted to maintain the baseline period while matching the loading period. The C value was adjusted last to fit the exponentially decaying trend in the recovery period after the reactive hyperemia spike. The model parameters (resistance and capacitance) were iterated on until the model output matched each experimental dataset to identify patient specific parameter values. Two individuals ran the model and iterated on the RCR values until the model output matched the experimental data. This process was conducted on all 75 datasets.

The subject-specific R_1, R_2 and C values were obtained and compared. One-way ANOVA and post-hoc Tukey statistical tests were conducted to compare the differences of each RCR

value between the three groups: wounded legs, non-wounded legs and healthy legs. Significant difference was identified by using a 95% confidence level ($p<0.05$ yielded significance).

4.3 Results

4.3.1 Simulation results

Figure 4-5 shows an example of the comparison between the simulation output and experimental data for a single participant, as generated by the two operators. The RCR values from all the simulations are reported in Table 4-1. The results indicate that the healthy and non-wounded legs had higher average global resistance (R_1) values than wounded legs (R_1= 9.21, 9.25 and 8.85 (Operator 1); and R_1= 6.36, 6.91 and 5.02(Operator 2) for healthy, non-wounded and wounded groups, respectively). The healthy legs also had higher localized resistance (R_2) values than both wounded and non-wounded legs (R_2= 3.64, 2.61 and 2.05 (Operator 1); and R_2= 6.24, 4.14 and 4.97 (Operator 2) for healthy, non-wounded and wounded groups, respectively). The wounded legs had higher localized C values than both non-wounded and healthy legs (C=7.30, 6.86 and 26.76 (Operator 1); and C=4.28, 5.49 and 11.65 (Operator 2) for healthy, non-wounded and wounded groups). The same trends were identified across operators although the magnitudes differed.

4.3.2 Comparison of model fit between operators

Error calculation was conducted to compare the goodness of fit of the model with the experimental data. The goodness of fit was assessed for both operators. The Normalized Root Mean Square Error (NRMSE) and Mean Square Error (MSE) were used to compute the error between experimental data and model output. Despite the different iteration process of each

operator, the average NRMSE for Operator 1 and 2 both yielded 11% error (with the standard deviation of NRMSE for Operator 1 at 5.5% and Operator 2 at 6.3%) between the experimental data and model output. T-tests between the two operators for both NRMSE and MSE also indicated no significant differences (for NRMSE: p=0.50 and for MSE: p=0.35).

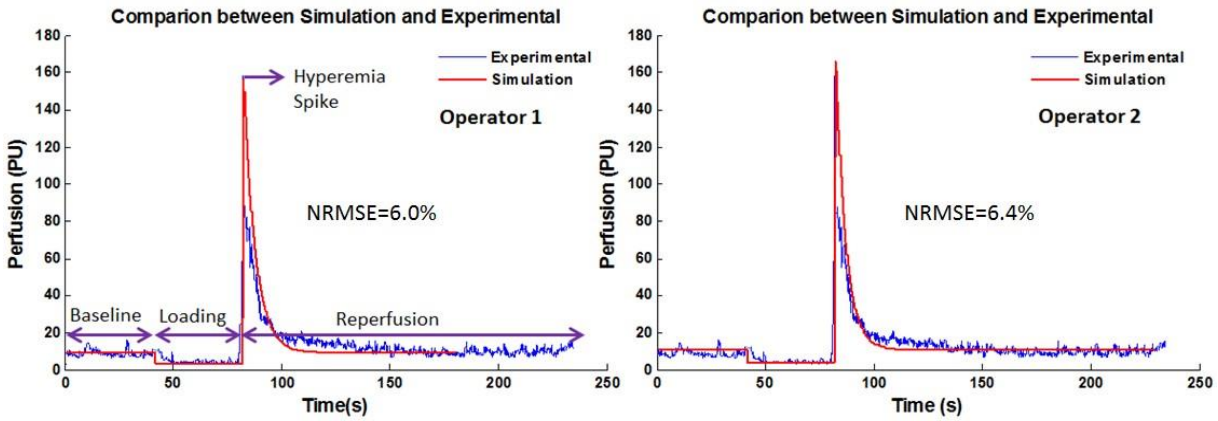

Figure 4-5: Comparison between the model output (red) and experimental data (blue). Left (a): Operator 1, R_1=12, R_2=2.5, C=2, NRMSE=6.0%; Right (b): Operator 2, R_1=10, R_2=3, C=2, NRMSE=6.4%

Table 4-1: Parameter comparisons between groups and Operators

	Operator 1		**Operator 2**	
R_1	Average	SD	Average	SD
Wounded	8.85	4.56	5.02	3.46
Non-Wounded	9.25	4.93	6.91	4.65
Healthy	9.21	4.36	6.36	3.93
R_2	Average	SD	Average	SD
Wounded	2.05	3.21	4.97	3.61
Non-Wounded	2.61	3.25	4.14	3.70
Healthy	3.64	1.58	6.24	2.59
C	Average	SD	Average	SD
Wounded	26.76	46.59	11.65	27.51
Non-Wounded	6.86	8.15	5.49	9.70
Healthy	7.30	9.62	4.28	4.85

4.3.3 Statistical results

A statistical analysis was conducted to compare each of the parameters (R_1, C, R_2) between the three groups. A significant difference in the localized resistance (R_2) was found between all three groups for both operators (p=0.0033 for Operator 1 and p=0.0044 for Operator 2). The localized compliance (C) between the three groups for both operators was also significantly different (p=0.00027 for Operator 1 and p=0.044 for Operator 2). For Operator 1's data, a post-hoc Tukey's test indicated that for the localized resistance, wounded legs were significantly different than healthy legs; for the localized compliance, wounded legs were significantly different from both non-wounded legs and healthy legs (Figure 4-6). For Operator 2's data, the wounded legs were significantly different than healthy legs with regard to compliance. Due to the conservativeness of Tukey's test and the unbalanced group size (Kutner et al. 2013), a difference in R_2 values were not found from Tukey's test . However, the small to medium effect sizes (0.23 between wounded and non-wounded legs, and 0.41 between wounded and healthy legs) indicated that statistically significant differences in R_2 could be expected between pairwise wounded and non-wounded legs, as well as between wounded and healthy legs with a larger sample size (Cohen 1992; Nakagawa & Cuthill 2007).

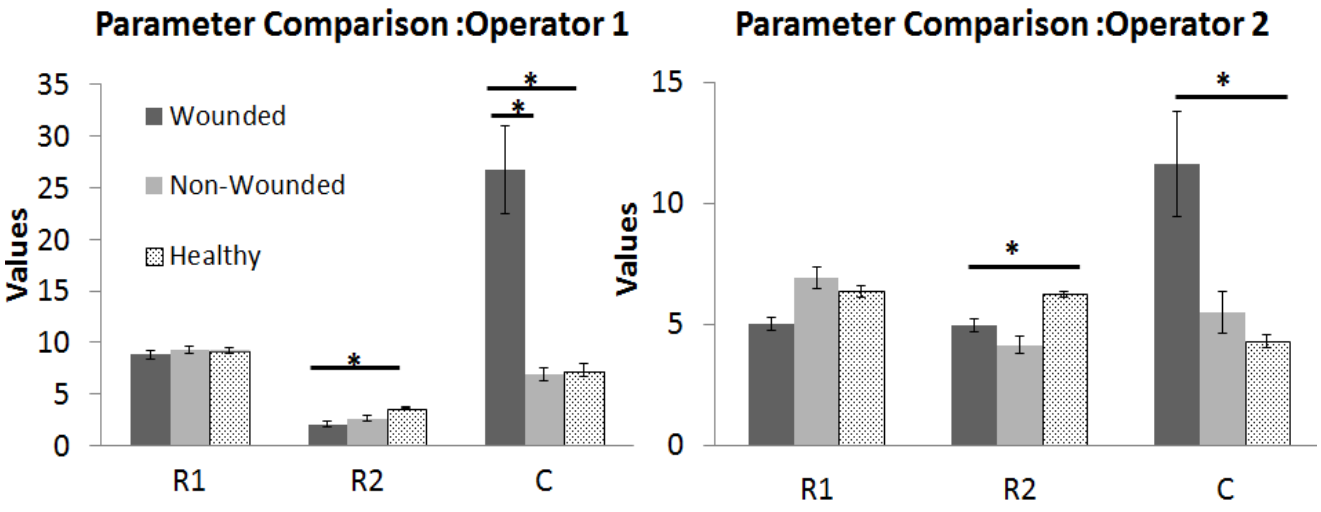

Figure 4-6: Comparison R_1, R_2, C between wounded, non-wounded and healthy legs from Operator 1 (left) and Operator 2 (right) (* indicates statistical significant difference, $p<0.05$)

4.4 Conclusion and Discussion

4.4.1 Model innovation

With regard to model development, most existing models have focused on the process of wound *healing* (Sherratt & Dallon 2002) rather than wound formation. Some models treat wound healing as a bio-chemically and bio-mechanically driven process, including inflammation, growth factors, and wound ischemia (Sherratt & Dallon 2002; Geris et al. 2010; Gefen 2009; Bennett et al. 2003). Few models have addressed the relation of blood perfusion and wound *formation*.

Our model is novel in that it was able to successfully replicate the complete blood flow profile of our experimental data including blood perfusion during baseline, the decrease in perfusion during locally applied loading, the reactive hyperemia spike and the recovery phases after the load was released. Furthermore, we were able to obtain patient-specific RCR

parameters for individuals and show differences in these parameters between a population with venous ulcers and healthy individuals.

A unique switch feature was placed in series with the capacitor to reduce the simulation and iteration time cost, which distinguished this model from all other Windkessel-based models. In other Windkessel-based models, the researchers indicated that the capacitor would only affect the reactive hyperemia period when the external pressure was high enough to complete the venous occlusion (Vo et al. 2007). In our experimental setup, the vessel was fully occluded by external loadings (higher than critical pressure 30~45 mmHg (Casavola et al. 2000)).

4.4.2 Clinical application

In this work, the localized venous resistance was significantly different between wounded and healthy legs, and the contralateral non-wounded leg showed an intermediate trend between the wounded legs and healthy legs. The global resistance did not differ between wounded, non-wounded or healthy legs. The difference in the capacitance was due to the slower recovery of the wounded legs after the load was removed as compared to the healthy legs. This phenomenon is likely a result of the impaired blood circulation of the ulcerated leg, particularly due to the inflammation near the ulcerated skin and the increased tissue edema (Pan et al. 2015; Suehiro et al. 2014; Kolluri 2014). Also, the local compliance measure from the "non-wounded" legs (i.e., legs from patients with wounds on the other leg) demonstrated values near those of the healthy legs; thus when this parameter changes it may be an early indicator that internal conditions have changed and a wound is likely to form.

Our model results indicate that differences exist between groups and can be quantified through Windkessel models of blood flow. Once a larger data set is collected, further clinical strategies could be established for “just-in-time” prevention. By combining the blood perfusion measurement and the model output, it is possible to identify the abnormalities in blood flow and vascular behavior in the area of interest before visible symptoms such as edema or an ulcer occur. This would be an improvement from the current approach where treatment occurs after the wound is present.

The potential of this work is significant; our modeling approach has the capability of determining patient specific parameters that could eventually change the care of patients with vascular disease. In the future, we could use this model to determine the ranges of values for vascular resistance and compliance, which in turn could be used for identifying when patient-specific parameters deviate outside the normative range. This deviation would indicate an internal change in the system, meaning conditions have reached a point where an ulcer is likely to form and the patient’s response to loading is compromised, preventive measures can be applied “just in time”.

The model, comprising of the bones, muscle, skin, and ground surface, was meshed in Autodesk Simulation Multiphysics (Autodesk Inc., CA), using a mix of 157144 brick and tetrahedral elements.

4.4.3 Limitations

Our model was developed to represent phenomenological local blood flow changes due to external loading. Physiologically, the static external pressure reduces the local skin microcirculation (Herrman et al. 1999), causing a subsequent reactive hyperemia which

correlates with skin ischemia (Jan et al. 2013). The hyperemia response is a physiological defense to the external pressure (Rendell & Wells 1998), and is achieved by venous dilation (Mollison et al. 2006). However, the specific mechanism of how external pressure affects the internal pressure in the vessels and tissue needs to be further explored.

Another limitation is different iterations by different operators resulted in different mean values for RCR parameters. This indicates that multiple combinations of RCR values exist to accomplish same results, however, even with these different approaches, the trends seen in the RCR values remained the same across operators for the three groups. Future work is necessary to develop an optimization function to find the best RCR values and identify the thresholds of each parameter for healthy, non-wounded and wounded populations. Once that occurs, the model could be used as a predictive tool for screening patients with venous insufficiencies. The results of this initial study are promising from a clinical perspective.

Acknowledgement

The authors would like to thank Sheng Chen, Amy Lenz , Yifan Men and Kelly Patterson in their assistance with this work.

5 LITERATURE STUDY ON WOUND AND SKIN MODELING

5.1 Introduction

In Chapter 2, a brief introduction was provided on wound and skin modeling. To better understand the fundamentals of skin wounds for the preparation of the Finite Element (FE) model in this study, a more detailed literature study was conducted and is discussed in this chapter.

5.2 Modeling for wound healing

Several mathematical and numerical modeling approaches have been investigated with regard to wound modeling, particularly in the area of the wound healing process. As wounds heal, complex bio-chemical and bio-mechanical changes occur (Buganza Tepole & Kuhl 2013). In most of the modeling studies, rather than modeling the entire process, a single aspect of the process is addressed such as: epidermal healing, dermal Extracellular Matrix (ECM) repair, wound contraction, or wound angiogenesis (Sherratt & Dallon 2002; Geris et al. 2010; Buganza Tepole & Kuhl 2013).

5.2.1 Epidermal healing models

Epidermal healing involves cell migration and is affected by growth factors (such as keratinocyte growth factor: KGF) and bio-chemical regulations (Sherratt & Dallon 2002). The first mathematical model to describe epidermal wound healing was proposed by Sherratt and Murray, in which the conservation of cell density and conservation of chemical concentration were applied to investigate the normal healing of circular wounds (Sherratt & Murray 1991). Later, Vermolen et al. simulated the relation between cell density and an epidermal growth

factor; Vermolen's group proved that the healing of the epidermis progressed from the undamaged region of the wound towards the center of the wound (Vermolen & Javierre 2012).

5.2.2 Dermal ECM repair models

Dermal ECM repair, also known as ECM remodeling, contributes to tissue repair and scar formation (Xue et al. 2009). In Xue's model, the ECM was modeled as a growing viscoelastic material with a pressure function. This was necessary as wound healing occurs under mechanical pressure. Maini et al. also modeled the ECM as viscoelastic material with material property changes due to cell growth and remodeling to simulate dermal wound healing (Maini et al. 2010). The newly grown dermal ECM turns into scar tissue which results in the changes of mechanical properties of the tissue (Sherratt & Dallon 2002). In venous ulcer formation, ECM is also changing due to the fibrin deposition (Falanga et al. 1987), therefore, understanding ECM remodeling under mechanical forces and how the ECM remodeling would cause tissue mechanical property change can be beneficial in understanding wound formation.

5.2.3 Wound contraction models

Wound contraction modeling was first proposed by Murray et al., in which they suggested that tissue patterning and shape was primarily guided by a mechanical force (Murray et al. 1988). Later Olsen et al. developed a subsequent model indicating that the driving force for wound contraction was provided by the change in cell and collagen concentrations (Olsen et al. 1995). Javierre et al. further improved and modified Olsen's model, incorporating growth factors, mechanical stress, and ECM into the model (Javierre et al. 2009). Wound contraction correlates cell-driven mechanical force with the tissue configuration change, a similar concept can be applied to wound *formation* to address tissue stress and strain under mechanical force,

either externally or internally applied, as a function of edema through the inclusion of cells such as Glucosaminoglycans (GAGs), or the consideration of growth factors, mechanical force, and ECM changes.

5.2.4 Wound angiogenesis models

Wound angiogenesis is a process where the new capillaries grow in the structure provided by the fibroblasts (Rijn 2010). Pettet et al. developed a continuum model which described a series of events, from the production of capillary-tip endothelial cells to the constitution of new capillary vessels, that developed during the soft tissue healing (Pettet et al. 1996). Pettet's model was the first to model dermal wound healing (Sherratt & Dallon 2002). Later, Schugart et al. expanded Pettet's model into a more comprehensive system, they treated wound angiogenesis as a function of oxygen, and studied the optimal wound treatment with regard to an oxygen therapy regimen (Schugart et al. 2008). Recently, Vermolen and his coworkers have developed a comprehensive mathematical model that simulated the combined process of wound contraction, angiogenesis and epidermal healing all together. Their model was based on continuum mechanics and provided a qualitative description for cutaneous wound healing (such as burns and skin ulcers) (Vermolen & Javierre 2012; Vermolen & Rijn 2012; Vermolen & Javierre 2010).

5.3 Modeling for venous ulcer formation

Even though models for the wound healing process have been widely studied, there is a lack of modeling research conducted with regard to *wound formation*, especially for venous ulcers. However, from the existing wound healing models, some aspects and key parameters

such as inflammation and edema can also be applied to better understand the wound formation process. Similar to the reported wound healing models, the wound formation models presented in this study also consider both bio-chemical and bio-mechanical driven changes within the skin tissue during ulcer formation.

5.3.1 Blood pooling, inflammation and edema

Blood pooling in the lower leg first leads to inflammation and edema, which is then followed by venous ulcer formation (Collins & Seraj 2010; Ontario 2010). The blood pooling first occurs in the hypodermis layer of the skin, which increases the blood pressure (venous hypertension) and causes the blood vessel wall to leak fluid into the dermis. Also, large molecules such as fibrinogen and blood cells leak into surrounding tissue (Burnand, Whimster, et al. 1982; Fahey 1998). The leakage increases the interstitial fluid and results in a palpable swelling, also known as edema (Ely et al. 2006). Meanwhile, fibrinogens create a layer of fibrin in the peri-capillary space which becomes a barrier to the oxygen transportation, leading to ischemia, tissue necrosis and eventually ulceration (Valencia et al. 2001; Burnand, Whimster, et al. 1982). When fibrin deposits and forms fibrotic tissue, it will cause inflammation, slow down wound repair and lead to tissue damage, increasing the risk for leg ulcers (Falanga et al. 1987; Falanga 1993; Wahl 1997; Coleridge Smith 2001). Therefore, it is important to identify the cell environmental changes under inflammation and determine the identifiers for further modeling the edema.

5.3.2 Glycosaminoglycans accumulation

In the inflammatory process, GAGs are released to regulate the inflammation (Lever et al. 2001). GAGs have been reported to have key roles in maintaining the growth factors

gradient concentration, inflammation, and are also responsible for causing internal swelling which leads to skin edema (Wiig & Swartz 2012; Lotti et al. 1990). Because GAGs have been shown to be a key factor in the inflammation process, GAGs were chosen as one of the identifiers for inflammation in the study presented here. The GAGs are linear polymers which possess negative charges that attract water into tissue (House et al. 2009), causing an osmotic swelling pressure and contributing the change of mechanical properties in the tissue (House et al. 2009). Such osmotic swelling caused by the accumulations of GAGs has been studied by cardiovascular researchers (Humphrey 2012) and several models have been developed to simulate the swelling in cardiovascular vessel tissues (Lanir 2012). Azeloglu et al. studied GAGs distribution and residual stress relations based on the osmotic swelling theory in an aorta ring FE model (Azeloglu et al. 2008a). Also Sorrentino et al. compared different degrees of swelling in central arteries (Sorrentino et al. 2015). Roccabianca et al. proved that pooled GAGs induced stress concentrations and increased osmotic swelling pressure within the aortic wall. Additionally, they found that GAGs pooling perturbed smooth muscle, disrupted ECM homeostasis, and sometimes caused tearing or rupture of the thoracic aorta wall (Roccabianca et al. 2014). All these models have successfully correlated GAGs pooling and tissue swelling in the aortic tissue, however, this process has not been investigated for the wound formation, specifically for venous ulcers.

5.3.3 Sodium increase and tissue osmolarity change

In addition to GAGs accumulation, an increased sodium content was also observed within the cell during the inflammation process (Schwartz et al. 2009; Titze 2009), which led to the decrease in extracellular osmolarity (Cooney 1976). When the extracellular osmolarity was

below the normal physiological level it was defined as “hypotonic”, and resulted in drawing water into the cell and leading to significant swelling of the tissues and cells (Elkin et al. 2010; Waseem et al. 2007). Azeloglu et al. studied the influences of the external bath osmolarity on the swelling and residual stresses in the aorta (Azeloglu et al. 2008a). They reported that the tissue exhibited higher swelling and residual stress when the external bath osmolarity value was low (higher osmolarity *within* the tissue). The effects of osmolarity also contributes to the treatment of lower limb ulcers (Satishkumar et al. 2013; Yaghoobi et al. 2013). Hence, in study presented here, the influences of osmolarity were also explored through model simulation.

5.4 Computational modeling for skin tissue

Skin modeling has been widely studied in many areas such as biomechanics, medicine and cosmetology (Flynn & McCormack 2010). Different researchers have successfully used different multi-layer skin models for various simulation applications. Sopher and Flynn developed three-layer skin models to study wrinkling of the skin (Flynn & McCormack 2010; Sopher & Gefen 2011). Hendricks et al. and Groves used two-layer skin models to determine the skin mechanical properties in comparison with experimental tests (Groves 2011; Hendriks et al. 2003). Vermolen investigated wound contraction and closure also via a skin model with two layers: the epidermis and dermis (Vermolen & Javierre 2010). Flynn et al. presented a two-layer human face model to study the *in vivo* tension that facial skin experienced during different facial expressions (Flynn et al. 2013).

Skin models have also been applied in skin growth and expansion for reconstructive surgery area. Socci et al. used a two-layer skin Finite Element (FE) model to simulate the increase in skin due to an expander. The model was then validated using experimental testing

with pig skin (Socci et al. 2007). Buganza Tepole and Zöllner both used four different shaped tissue expanders and studied the skin stress distribution during expander inflation. They not only investigated the stress during the expander inflation, but also looked into the residual stress during expander deflation (Buganza Tepole et al. 2011; Zöllner et al. 2013).

The most popular skin material models used by the studies mentioned above were Neo-Hookean and Mooney-Rivilin. Other nonlinear elastic material and viscoelastic materials such as the Ogden material and orthotropic Bischoff material were also applied in skin FE modeling studies. A list of the skin FE models and their layer thickness as well as material types are reported in Table 5-1.

Table 5-1: Skin Finite Element models overview of literature

Literature	Skin Layers	Thickness	Material	Simulation
Hendriks et al., 2003	Dermis	Subject-specific	Extended Monney-Rivlin	Compare with experimental suction test and characterize the subject-specific material parameters
	Subcutaneous fat			
Groves, 2011	Epidermis	0.07 mm	Ogden	Small deformations of skin under spherical indenter
	Dermis	0.84 mm		
	Hypodermis	3 mm		
Sopher & Gefen, 2011	Stratum Corneum	0.0.15 mm	Neo-Hookean	Maximal shear stress and strain under the effects of skin wrinkles, age and wetness
	Epidermis+ upper Dermis	0.05 mm (young); 0.2 mm (aged)		
	Deep Dermis	1.235 mm (young); 1.085 mm (aged)		
Flynn & McCormac, 2010	Stratum Corneum	20 µm	Neo-Hookean	Skin wrinkle deformation under different water content and collagen fiber density
	Dermis	1.2 mm	Orthotropic-viscoelastic	
	Hypodermis	1.5 mm	Fung's Quasi-Linear Viscoelastic (QLV) model	

Table 5-1 (Cont'd)

Literature	Skin Layers	Thickness	Material	Simulation
Vermolen & Javierre, 2010	Epidermis	0.05-1.5 mm	Visco-Elastic	Qualitative describe the wound contraction and closure process with different parameters of fibroblasts, ECM, capillaries and epidermal cells
	Dermis	0.3-3 mm		
Flynn et al., 2013	Epidermis+ Dermis	1.5 mm	Variation of Fung's constitutive equation	Facial skin stress analysis on different facial expression and simulate skin of different ages
	Hypodermis	4-11 mm	Mooney-Rivlin	
Socci et al., 2007	Epidermis+ Dermis	2 mm	5th order Neo-Hookean-like material	Skin expansion under expander inflation and evaluate skin mass gain
	Hypodermis	20 mm		
Zöllner et al., 2013	Epidermis	0.1-1 mm	Neo-Hookean	Area growth of skin under tissue expansion with different fillings in the expander
	Dermis	1.0-4.0 mm		
Buganza Tepole et al., 2011	Epidermis	0.06-1 mm	Neo-Hookean	Skin area growth under expander inflation and residual stress during expander deflation
	Dermis	1-4 mm		

5.5 Conclusion

The literature reviewed here provided a comprehensive understanding of the current state of skin modeling with regard to wound healing, inflammation and tissue edema. By adopting this information, a multi-layer skin FE model was established and parametric studies were performed to investigate the influences of GAGs accumulation and sodium increase (osmolarity change) during the inflammation on tissue edema, and venous ulcer formation.

6 INFLUENCES OF SODIUM AND GLYCOSAMINOGLYCANS IN SKIN EDEMA AND ULCERATION: A FINITE ELEMENT APPROACH

6.1 Introduction

The pathology of venous ulcers has been widely studied and many theories regarding ulcer formation have been proposed, yet, a generally agreed upon mechanism of ulcer formation does not exist (Abbade & Lastória 2005). A common understanding of venous ulcers is that they are related to calf muscle pump failure and chronic venous insufficiency (Kolluri 2014; Langemo 1999). These conditions result in reduced venous function, so blood in the lower leg cannot efficiently be returned to the heart. When blood pools in the lower leg, it causes inflammation (i.e. a reaction to the molecules being leaked through the vessel wall as a result of blood pooling and being trapped in the micro-circulation space (Bergan et al. 2006)), which leads to skin edema (skin swelling due to the excess fluid in the interstitial volume (Ely et al. 2006)). This process of inflammation followed by edema results in tissue necrosis and eventually ulceration (Bergan et al. 2006). To better understand the pathology of venous ulcers, it is important to understand how skin tissue reacts to blood pooling and the inflammation process; this understanding can be established through the creation of models that characterize the changes within the skin tissue. The overall goal of this study is to develop a model that simulates the inflammation, determines the internal stresses and pressure of the skin tissue; and provides a better understanding of the mechanism associated with venous ulcer formation.

When studying the models associated with skin wounds, recent focuses have been on the wound healing processes, specifically for epidermal healing, dermal extracellular matrix (ECM) repair, wound contraction and angiogenesis (new blood vessel growth and formation) (Sherratt & Dallon 2002; Geris et al. 2010; Buganza Tepole & Kuhl 2013). In epidermal healing models, growth factors are introduced to simulate the growth of the epidermis under bio-

chemical regulations (Sherratt & Murray 1991; Vermolen & Javierre 2012). In dermal ECM repair models, the bio-mechanical property changes in the skin tissue are investigated during scar tissue formation (Xue et al. 2009; Maini et al. 2010; Sherratt & Dallon 2002). In wound contraction models, cell and collagen-driven mechanical forces are studied. Results of these models indicate that mechanical forces are the primary driving forces in this process (Murray et al. 1988; Javierre et al. 2009; Olsen et al. 1995). Lastly, studies have reported that Glycosaminoglycans (GAGs) play a significant role in inflammation (Lotti et al. 1990; Wiig & Swartz 2012). In several wound angiogenesis models, inflammation and wound ischemia are modeled with GAGs and growth factors (Geris et al. 2010; Gefen 2009; Bennett et al. 2003; Schugart et al. 2008) and results indicate that chronic inflammation results in wound ischemia (Schugart et al. 2008). Hence, the wound angiogenesis model successfully linked GAGs with inflammation and tissue ischemia. Overall, these reported models have treated wound healing as a biochemically and biomechanically driven process.

Although several wound healing models have been developed, there is still a lack of information on *wound formation*. However, wound healing models guided our study on both the bio-chemical and bio-mechanical driven changes that occur during tissue inflammation, which leads to edema, then tissue ischemia, and eventually result in the formation of venous ulcers.

As indicated by literature, venous ulcers are caused by blood pooling in the lower legs (Collins & Seraj 2010; Ontario 2010). It is believed that such pooling first occurs in the hypodermis (subcutaneous) layer of the skin, leads to an increased blood pressure, and then a leakage of blood through the vessel wall (Burnand, Clemenson, et al. 1982; Fahey 1998). Such

leakage causes an increase of interstitial fluid volume and results in a palpable swelling, known as edema (Ely et al. 2006). In the context of our study, swelling and edema are used interchangeably. The large molecules such as fibrinogens that leak into surrounding tissue create a layer of fibrin in the peri-capillary space which have two major impacts in the wound formation processes: 1) this fibrin layer creates an oxygen transportation barrier, which results in the decreased oxygen, leading to tissue ischemia and necrosis (Valencia et al. 2001; Burnand, Clemenson, et al. 1982); 2) during fibrin deposition, inflammation occurs and slows down wound repair, increasing the risks for ulcerations (Falanga 1993; Wahl 1997; Coleridge Smith 2001). In the study presented here, the impact of blood pooling leading to inflammation is investigated via a modeling approach to further analyze their roles in the wound formation. A schematic drawing of blood pooling and skin edema can be seen in Figure 6-1.

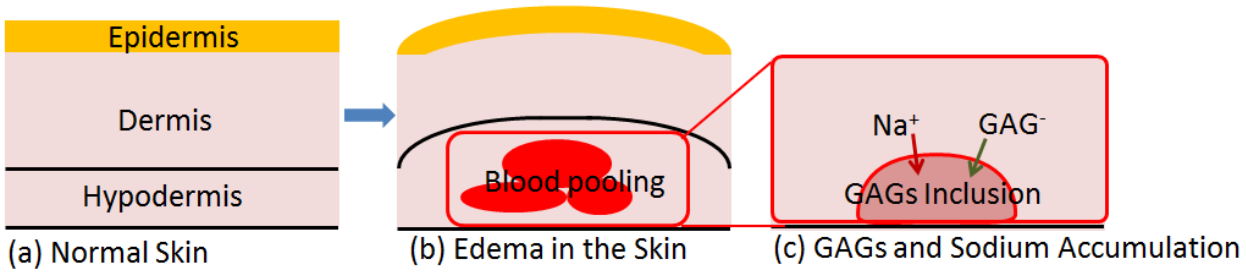

Figure 6-1: The comparisons between (a) normal skin and (b) edema in skin due to the blood pooling. In the skin with edema, Glucosaminoglycans (GAGs) and sodium accumulate due to the blood pooling and inflammation (c)

During inflammation, two bio-chemical agents, known as Glucosaminoglycans (GAGs) and sodium are increased (Figure 6-1 c) as biological responses to the inflammation process (Lever et al. 2001; Schwartz et al. 2009; Reed & Rubin 2010). The GAGs that carry negative charges will attract water into the tissue, induce an osmotic swelling pressure, lead to tissue swelling, and change tissue mechanical properties (House et al. 2009). The swelling caused by GAGs accumulation has been studied in multiple cardiovascular studies and the results have

shown with more GAGs in the tissue, it causes more swelling. The increased swelling was a result of increased negative charges carried by the GAGs (Humphrey 2012; Lanir 2012; Azeloglu et al. 2008a; Sorrentino et al. 2015; Roccabianca et al. 2014). Further, higher negative charges in GAGs accumulation also increase tissue stress and osmotic swelling pressure, leading to the tearing or rupture of the soft tissue (Roccabianca et al. 2014; Roccabianca et al. 2014).

The increase of sodium, at the same time, has also been reported in the inflammation process (Schwartz et al. 2009; Titze et al. 2004). With more sodium accumulated within a GAGs inclusion, this causes the extracellular tissue osmolarity to decrease below the normal physiological level (Cooney 1976). Osmolarity is defined as the concentration of the sodium in the water within the tissue (Lai et al. 1991). The differences between the decreased external osmolarity and normal internal osmolarity leads to tissue swelling (Bhave & Neilson 2011a; Elkin et al. 2010; Waseem et al. 2007). Azeloglu et al. investigated the influences of osmolarity in aorta tissue swelling both experimentally and numerically and found that with decreased osmolarity, the tissue exhibited higher swelling and more residual stresses (Azeloglu et al. 2008a). Similar to studies by Azeloglu et al. and Lai et al., the osmolarity values in our study refer to the extracellular osmolarity or “external bath” osmolarity. During inflammation, the osmolarity in the extracellular space decreases as the sodium is drawn into the GAGs inclusion.

Therefore, by combining the influences of both GAGs accumulation and the sodium increase under inflammation, our hypothesized physiological pathway from blood pooling to ulcer formation is proposed in Figure 6-2.

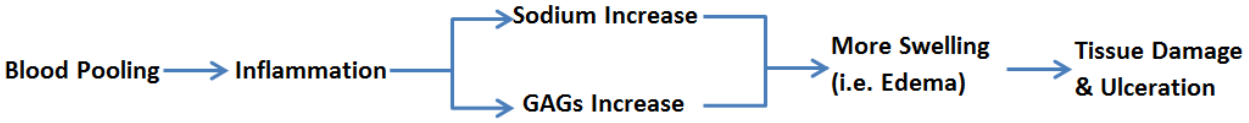

Figure 6-2: Hypothesized physiological pathway from blood pooling to ulcer formation with inflammation and skin edema caused by changes in GAGs and sodium content within the GAGs inclusion

In order to validate this pathway and characterize mechanical changes in the skin tissue, a computational model for the skin is required.

Skin computational models have been widely used in medicine and cosmetology applications (Flynn & McCormack 2010). In the existing models, skin is usually treated as a multi-layer system with a different mechanical behavior in each layer. For different skin layers, some studies separate the stratum corneum (the hardest superficial layer of the epidermis) from the dermis layer (Sopher & Gefen 2011; Flynn & McCormack 2010; Geerligs et al. 2011), whereas some treat the epidermis and dermis as a single compound layer (Buganza Tepole et al. 2011; Zöllner et al. 2012; Zöllner et al. 2013). The hypodermis is usually treated as a separate layer from the epidermis and dermis since it is much softer (Hendriks et al. 2003). Different material models and parameters have also been reported in the literature. The commonly used material models are Neo-Hookean (Sopher & Gefen 2011; Flynn & McCormack 2010; Socci et al. 2007; Zöllner et al. 2013; Buganza Tepole et al. 2011). Other hyperelastic models such as Mooney-Rivilin, Ogden, and some viscoelastic models have also been utilized in skin models (Hendriks et al. 2003; Groves 2011; Vermolen & Javierre 2010). It is worth noting that the material properties vary at different body sites (Hendriks 2005) and can be affected by age and skin hydration (Sopher & Gefen 2011). A detailed listing of the properties selected for the model in our study is provided in the methods section.

For the study presented here, a multi-layer skin computational model was developed in order to identify the bio-chemical and bio-mechanical changes in the skin tissue when it is undergoing inflammation and edema. Our model specifically investigated the roles of the increased GAGs and sodium in the process leading towards tissue rupture and ulcer formation.

The specific goals of this study are to: 1) compare different GAGs inclusion geometries and GAGs distributions within the skin to understand their effects on skin edema; 2) compare the effects of different GAGs negative charge levels on skin fluid pressure and elastic stress; 3) compare the effect of different GAGs inclusion osmolarity levels (i.e. sodium content) in skin fluid pressure and elastic stress.

6.2 Methods

6.2.1 Model establishment

A three-layer skin model (epidermis, dermis and hypodermis) was developed. The thicknesses of the epidermis, dermis and hypodermis were chosen as 1 mm, 2 mm and 2 mm respectively, those values were based on the reported literature data (Hendriks et al. 2003; Groves 2011; Flynn et al. 2013; Zöllner et al. 2012; Socci et al. 2007). We adopted a similar approach developed by Roccabianca et al. for the thoracic aorta, where a quarter-symmetric FE model was used to mimic a portion of the aorta and a GAGs inclusion was centrally placed (Roccabianca et al. 2014). The model in this study created a half-symmetric skin portion with a quarter-symmetric inclusion of GAGs located in the bottom-center of the hypodermis layer (Figure 6-3). In this way, the pooled GAGs were exposed for parametric study and analyses. The geometric model was then meshed and preprocessed in Hypermesh (Hyperworks 12.0, Altair,

USA), and later imported into FEBio (Version 2.4.0, University of Utah) for computing and postprocessing.

Boundary conditions were applied to all surfaces except the top surface. Zero displacement was used as the constraints in defining the boundary conditions to the model.

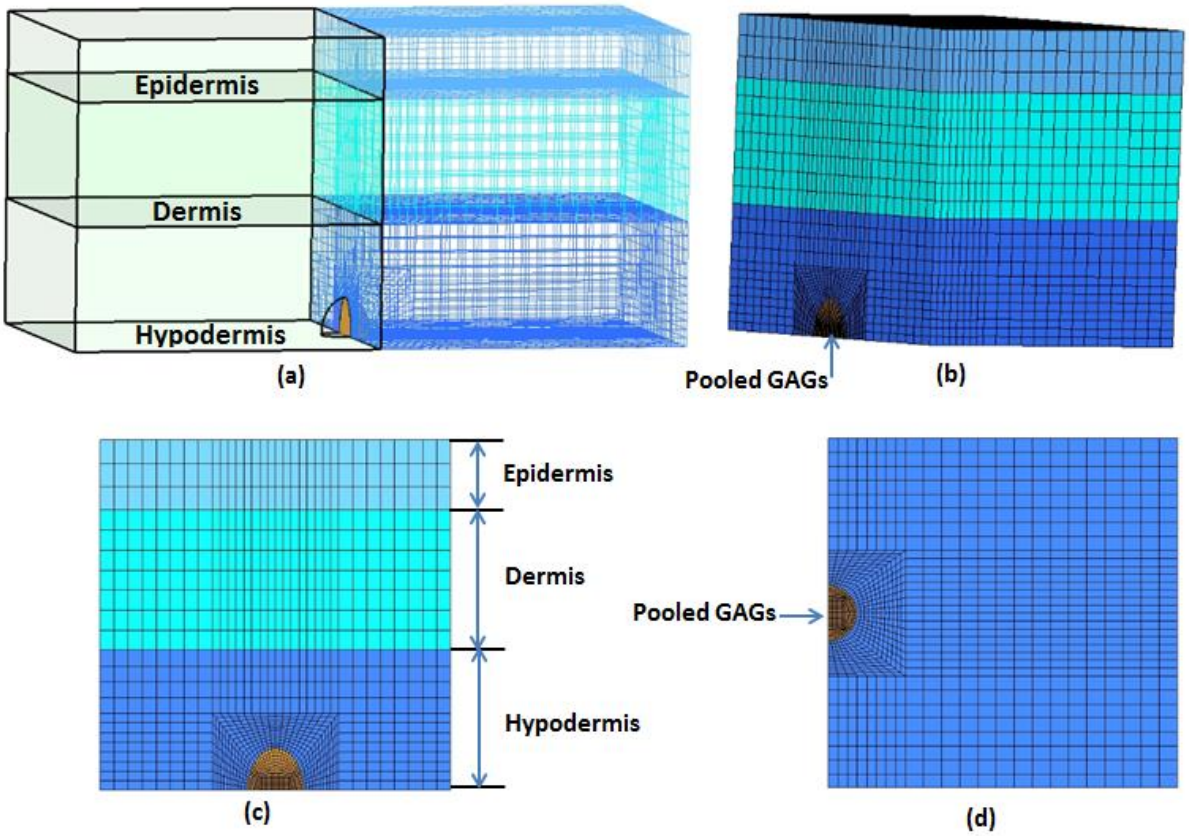

Figure 6-3: The skin and GAGs pooling FE model (a) the skin is half symmetric to allow the exposure of GAGs while the GAGs is quarter symmetric and centrally placed in the hypodermis (b) front view of model with pooled GAGs in the central bottom (c) left view of the

6.2.2 Model material parameters

Since the inflammation and the resulting skin edema consist of both bio-mechanical and bio-chemical processes, a mixed model coupling materials that represent both mechanical and chemical behaviors was used in this study. Details are provided in the following sections.

6.2.2.1 Solid material

Skin as a soft biological tissue exhibits large deformation when under small loads (Smalls et al. 2006), therefore, in accordance with other skin models in the literature, our model used a nonlinear, hyperelastic, Neo-Hookean material to simulate the skin tissue (Socci et al. 2007; Zöllner et al. 2013). Because the epidermis layer is thin and the majority of the tissue underneath stratum corneum in the epidermis has been reported to share same properties with the tissue in the upper dermis, researchers combined the epidermis and dermis layers into a single compound layer in their models (Sopher & Gefen 2011; Zöllner et al. 2012; Zöllner et al. 2013; Buganza Tepole et al. 2011). Hence, the epidermis and dermis were simulated with the same material properties in the model presented here. The material parameters reported by Buganza Tepole et al. and Zöllner et al. were used for both the epidermis and dermis layers with the Young's modulus at 100 kPa and Poisson's ratio at 0.47 (Buganza Tepole et al. 2011; Zöllner et al. 2012). For the hypodermis layer, literature reported a varied range from 0.12 kPa to over 80 kPa for the Young's modulus (Hendriks et al. 2003; Flynn et al. 2013; Liang 2013; Li et al. 2012; Gennisson et al. 2004). Based on the work by Li et al. and Gennisson et al., in which the Young's modulus was 53.7 kPa and 80.8 kPa respectively, with the Poisson's ratio at 0.48 (Li et al. 2012; Gennisson et al. 2004); the Young's modulus for our work was chosen to be 70 kPa (a number between the values reported by Li et al. and Gennisson et al.) with the Poisson's ratio at 0.48. Table 6-1 lists the solid material parameters assigned for each layer of the skin in our model.

Table 6-1: Skin material properties assigned to the model

	Epidermis	Dermis	Hypodermis
Young's Modulus	110 kPa	110 kPa	70 kPa
Poisson's Ratio	0.47	0.47	0.48

6.2.2.2 Donnan osmotic swelling material

The charges carried by sodium and GAGs lead to an imbalance of the osmolarity between the external and internal of the cell membrane, induce a Donnan potential (Philipse & Vrij 2011). Therefore, several studies have used a swelling material to describe the Donnan effect that GAGs bring into the skin (Chahine et al. 2004; Wiig et al. 2000; Wiig & Swartz 2012). In our model, the Donnan swelling material was assigned to the pooled GAGs inclusion in the hypodermis as well as the distributed GAGs throughout the skin tissue. In the Donnan's material model defined in FEBio (Ateshian & Hung 2006; Lai et al. 1991), three parameters were required to characterize the material behavior: 1) fluid volume fraction; 2) external bath osmolarity, which is the osmolarity in the region outside of the GAGs inclusion (extracellular) (Fig 6-4), and 3) fixed charge density (FCD) which is the negative charges carried by the GAGs. For the fluid volume fraction, a range between 0.70 and 0.85 was reported in the literature (Bhave & Neilson 2011b; Azeloglu et al. 2008b; Bian et al. 2009). In accordance with Bhave and Neilson's work, this value was set to 0.72 for our model (Bhave & Neilson 2011a). The physiological osmolarity for normal skin has been reported to be between 270 milliosmoles/Liter(mOsm/L) and 300 mOsm/L (Sorrentino et al. 2015; Guo et al. 2007; Azeloglu et al. 2008b; Negoro et al. 2008), therefore 280 mOsm/L was chosen as the "normal" osmolarity level for our model based on the work reported by Negoro et al.

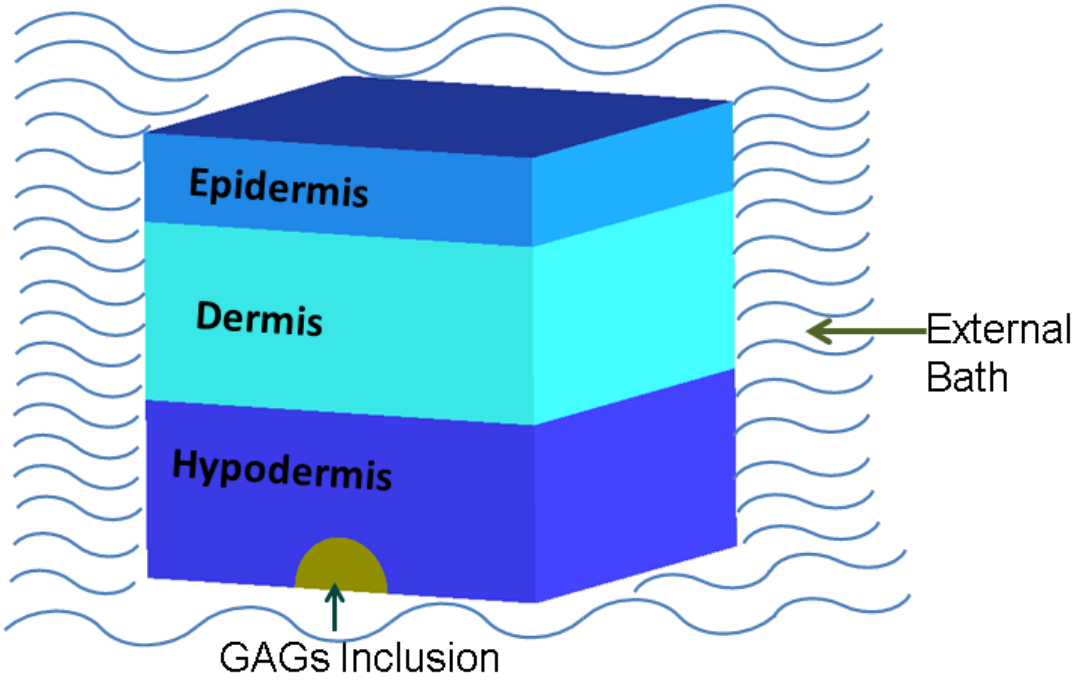

Figure 6-4: External bath of the skin block model where the external bath osmolarity refers to the sodium content within the fluid environment surrounding the skin tissue and GAGs inclusion

The fixed charge density (FCD) is defined as the concentration of negative charges fixed in the wet tissue (Venn & Maroudas 1977a) and is calculated as:

$$C_0^F = \frac{z \cdot c}{M} \tag{6-1}$$

Where C_0^F is the FCD at the original status (i.e., no swelling), z is the number of negative charges carried by the GAGs, M is the molecular weight for GAGs, and c is the milligram of GAGs per milliliter of water in the skin. For z and M, literature reported that GAGs carry two negative charges (2 Equivalents "Eq") per unit and each GAGs unit has a molecular weight of 513 grams (Chahine et al. 2004; Venn & Maroudas 1977a). For c , Wiig et al. reported the GAGs content in the normal skin was 3.7~4.2 mg/g of wet tissue weight and the total tissue water content was 0.6 ml/g of wet tissue weight (Wiig et al. 2000; Wiig & Swartz 2012), therefore the average GAGs content in total tissue water content was calculated as:

$$c = \frac{3.95\ mg/g}{0.6\ ml/g} = 6.58\ mg/ml \quad (6\text{-}2)$$

Hence, based on the above information, the distributed GAGs FCD in skin at normal status was derived to be:

$$C_0^F = \frac{2\ Eq * 6.58\ mg/ml}{513g} = 25.7\ mEq/L \quad (6\text{-}3)$$

6.2.3 Parametric study

A series of parametric studies was conducted in order to compare the stress and pressure differences in the tissue for four cases: different geometric shapes of the GAGs inclusion, different skin GAGs distribution, different GAGs inclusion external bath osmolarity, and different negative charges (i.e. FCD) carried by the accumulated GAGs. A total of 35 simulations were performed in FEBio to investigate the influences of three GAGs distribution types within the skin, two GAGs inclusion geometries, five GAGs inclusion negative charge levels (FCD) and five GAGs inclusion external bath osmolarity levels in the tissue swelling. Each of the simulations is discussed in the following sections.

6.2.3.1 Different GAGs inclusion geometries and distributions

Two GAGs inclusion geometries and three different GAGs distribution types were evaluated (Figure 6-5). The two pooled GAGs inclusion geometries included a spherical GAGs inclusion, which had radius of 0.6mm; and an ellipsoidal GAGs inclusion with a major radius of 0.6mm and a minor radius of 0.4mm (Figure 6-5 a). The three different GAGs distributions were defined as: 1) uniformly distributed through the tissue, “Uniform”; 2) a gradual decrease from the epidermis to the hypodermis, “Linear”; and 3) higher mass fraction in the dermis with a gradual decrease towards the epidermis and the hypodermis, “Parabola” (Figure 6-5 b).

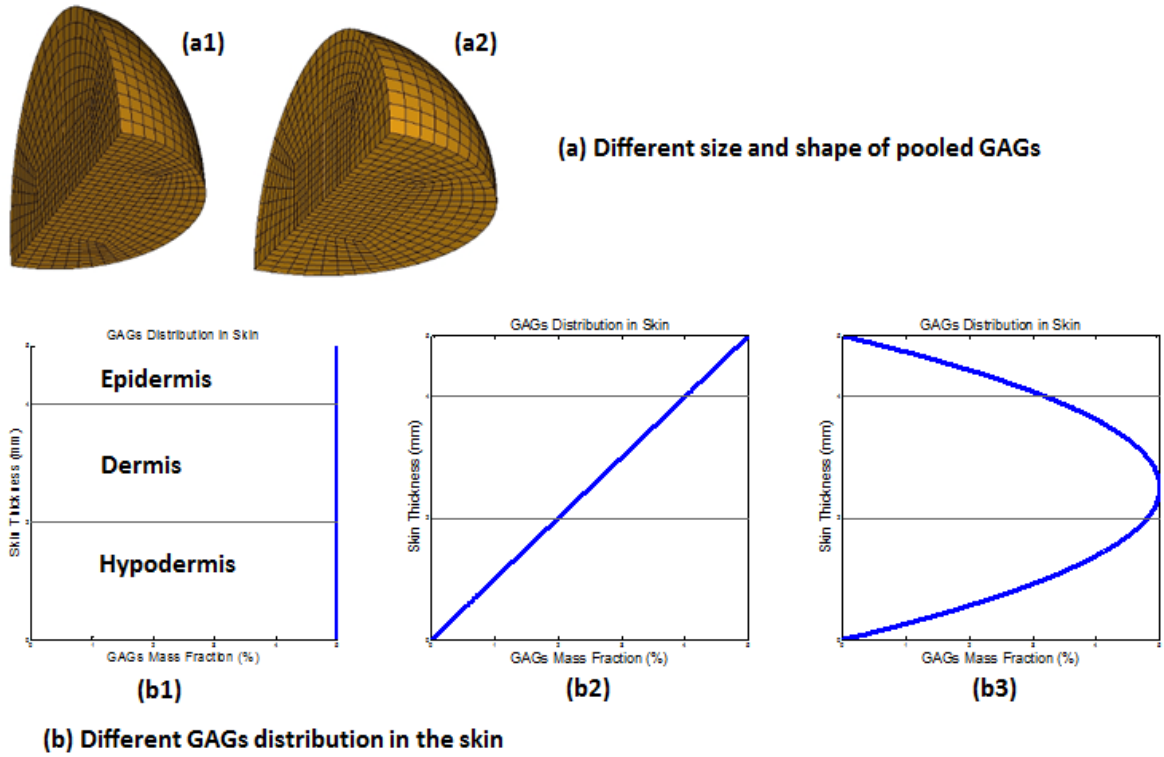

Figure 6-5: Different size and shape of pooled GAGs as well as different distribution of GAGs in the skin. (a) Different size and shape of pooled GAGs: a1) Ellipsoid shaped GAGs inclusion, a2) Sphere shaped GAGs inclusion; (b) Different GAGs distribution in the skin: b1) uniformly distributed throughout the three skin layers, termed "Uniform", b1) a linear decrease in GAGs distribution from the epidermis to the hypodermis termed "Linear", b3) parabolic distribution: a higher distribution in the dermis and gradually decreased as it moves towards the epidermis and hypodermis "Parabola"

6.2.3.2 Different GAGs inclusion external bath osmolarity levels

For the external bath osmolarity, Azeloglu et al. conducted a parametric study on osmolarity ranging from 20 mOsm/L to 2000 mOsm/L, and evaluated the tissue residual stresses in the aorta ring (Azeloglu et al. 2008a). In our model presented here, a series of external bath osmolarity values were chosen: 1) 50 mOsm/L; 2) 100 mOsm/L; 3) 280 mOsm/L; 4) 500 mOsm/L; 5) 1000 mOsm/L. These values fell in the range of the values studied by Azeloglu et al., and also included the normal osmolarity value of 280 mOsm/L (Negoro et al. 2008).

6.2.3.3 Different GAGs inclusion FCD levels

For the FCD in the GAGs inclusion, Roccabianca et al. performed a parametric study for FCD ranged from 20 mEq/L to 160 mEq/L and studied its influences in the aortic tissue stresses (Roccabianca et al. 2014). In our model, five different levels of FCD in the accumulated GAGs inclusion were selected: 1) FCD=25.7 mEq/L, the same as normal GAGs in the skin tissue as calculated above (Eq.6-3) (2) FCD=150 mEq/L, near the upper limit reported in the parametric study from Roccabianca et al. (Roccabianca et al. 2014), 3) FCD=257 mEq/L which is 10 times higher than normal skin GAGs level , 4) FCD=514 mEq/L which is 20 times higher than the normal skin GAGs level, and 5) FCD=771 mEq/L which is 30 times higher than the normal skin GAGs level. These higher FCD values were selected to represent the increased GAGs during inflammation. Since there is a lack of information on the upper limit of GAGs FCD values in the literature, 10, 20, and 30 times higher than the normal skin GAGs values were chosen to parametrically investigate the effects of the GAGs inclusion during inflammation and determine the associated swelling.

6.2.4 Theoretical pressure and stress analysis

Both fluid pressure and elastic stress affect the tissue stresses (Guyton et al. 1971). The fluid pressure has been reported to affect the tissue compliances and permeability (Wiig & Swartz 2012; Venn & Maroudas 1977b) while the elastic stress contributes more to tissue tear and damage (Lai et al. 1991; Roccabianca et al. 2014). Therefore, it is important to identify the different roles of both fluid pressure and elastic stress in the overall tissue stresses associated with the wound formation process. As reported in the literature, the fluid pressure caused by accumulated GAGs swelling is defined as (Ateshian & Hung 2006; Lai et al. 1991):

$$p = RT\sqrt{(C^F)^2 + (\bar{C}^*)^2} - \bar{C}^* \tag{6-4}$$

Where R and T are the universal gas constant and absolute temperature, $\bar{C}^*$ is the external bath osmolarity, C^F is the FCD in the current configuration (defined as the final state after swelling) and is calculated as follows (Azeloglu et al. 2008a; Ateshian & Hung 2006):

$$C^F = \frac{\varphi_0^w C_0^F}{J-1+\varphi_0^w} \tag{6-5}$$

Where φ_0^w is the fluid volume reaction, C_0^F is the FCD at reference configuration (defined as the original state before swelling), $J = \det F$ is the relative volume (derivative of the deformation tensor F) (Azeloglu et al. 2008a; Ateshian & Hung 2006). Based on Eq. (6-4) and Eq. (6-5), the change of fluid pressure in the tissue can be computed and analyzed.

The total stress in this model is a sum of the fluid pressure and elastic stress (Azeloglu et al. 2008a):

$$\sigma = -pI + \sigma^e \tag{6-6}$$

Where σ is the Cauchy stress, and p is the fluid pressure calculated from Eq. (6-4). The negative sign in front of p is because the pressure is generally treated as compression in stress analysis (Ateshian & Hung 2006). I is the identity matrix and σ^e is the elastic stress. The elastic stress endured by the tissue is then calculated as:

$$\begin{bmatrix} \sigma_{xx}^e & & \\ & \sigma_{yy}^e & \\ & & \sigma_{zz}^e \end{bmatrix} = \begin{bmatrix} p & & \\ & p & \\ & & p \end{bmatrix} + \begin{bmatrix} \sigma_{xx} & & \\ & \sigma_{yy} & \\ & & \sigma_{zz} \end{bmatrix} \tag{6-7}$$

From Eq. (6-7), the elastic stress can be computed from the fluid pressure and the total stress state, and further analyzed to evaluate the maximum tensile stress in the model.

6.3 Results

6.3.1 Skin GAGs distribution comparison (Uniform, Linear, Parabola)

Fifteen simulations were performed to study the effects of different skin GAGs distribution types on tissue edema. In this series of parametric studies, the GAGs geometry used the spherical shape. The external bath osmolarity for the GAGs inclusion and skin were maintained at 280 mOsm/L, the FCD for the skin was 25.7 mEq/L for “Uniform” distribution. For “Linear” distribution, the FCD in the skin was 0 mEq/L at the bottom surface of the hypodermis layer and increased to 25.7 mEq/L on the top surface of the epidermis layer. Similarly, for “Parabola” distribution, the FCD in the skin was at 0mEq/L at both bottom and top surfaces of the skin block, and increased towards the center layer until it reached at 25.7 mEq/L in the middle of the dermis. Simulations were conducted for GAGs inclusion FCD at 25.7mEq/L, 150 mEq/L, 257mEq/L, 514 mEq/L and 771 mEq/L for all three different skin GAGs distributions (“Uniform”, “Linear” and “Parabola”). The trend of the differences between the three skin GAGs distributions at different GAGs inclusion FCD levels was similar. Figure 6-6 shows the comparison of total displacement and Von Mises Stress between the different skin GAGs distributions when the GAGs inclusion FCD was set to 25.7 mEq/L as an example.

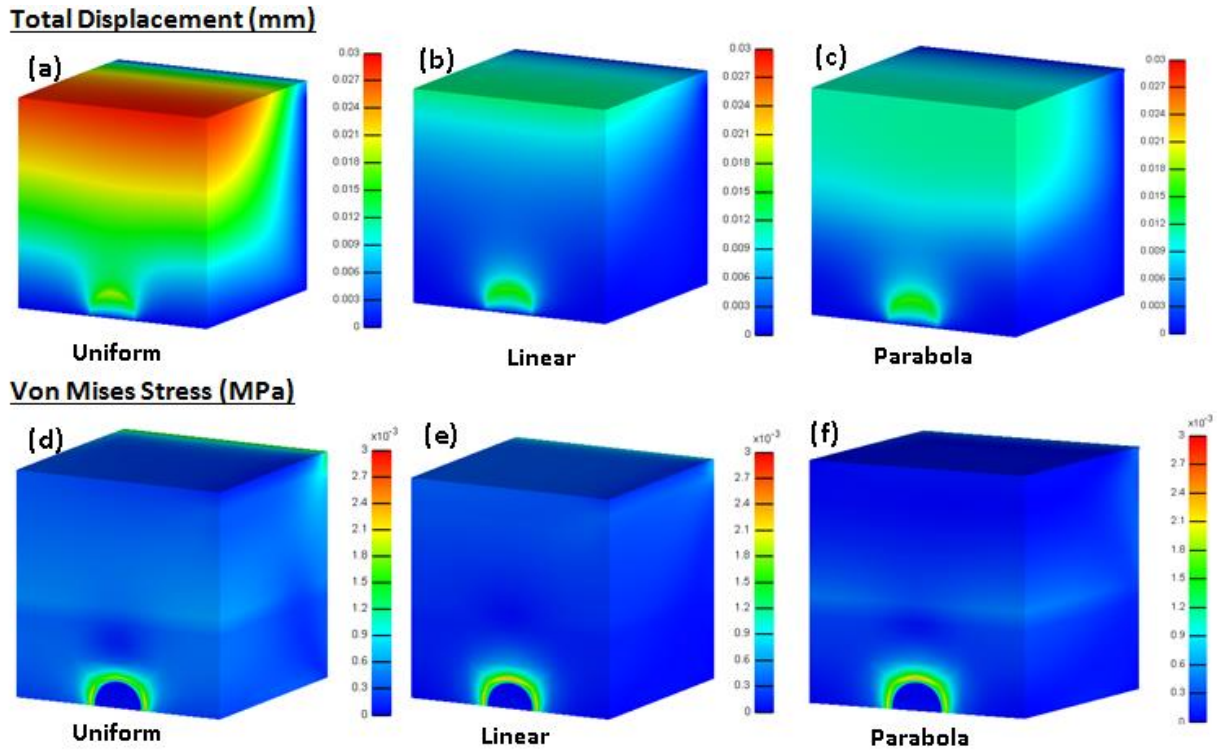

Figure 6-6: Comparison of total displacement and Von Mises stress between three skin GAGs distributions when the osmolarity for both the skin and GAGs was held at 280 mOsm/L, the GAGs inclusion FCD at 25.7 mEq/L and the skin FCD between 0 mEq/L to 25.7 mEq/L at different layers depending on the distribution type. Top row (a)-(c): the total displacement (mm) of the model when skin GAGs distribution is a) Uniform, b) Linear, and c) Parabola. Bottom row (d)-(f): the Von Mises stress (MPa) of the model when skin GAGs distribution is d) Uniform, e) Linear, and f) Parabola

It can be seen that the skin has the highest deformation and stress concentration with a uniformly distribution GAGs (Figure 6-6 a, d). And the skin with linearly distributed GAGs has the lowest deformation and stress. This trend is due to the differences in the total GAGs amount in the three different distribution types. The total amount of GAGs throughout the whole thickness of skin can be treated as the area between the distribution line and the vertical-axis (skin thickness) from Figure 6-3 (b1)-(b3). Since the existence of GAGs causes the skin to swell, the "Uniform" distribution, which has higher total amount of GAGs throughout the skin than other two distribution types, resulted in the highest deformation and stress. Also,

no matter what distribution, the highest stress consistently occurred at the interface between the accumulated GAGs inclusion and the normal skin. This indicates the need for further analysis on the stress localization in the surrounding tissue of the GAGs inclusion, which will be discussed in a later section.

6.3.2 GAGs inclusion geometry comparison (Sphere, Ellipsoid)

Ten simulations were also performed to compare the role of GAGs inclusion geometry in skin deformation and stress distribution. In this set of comparisons, the external bath osmolarity for the accumulated GAGs and the skin were both maintained at 280 mOsm/L. Since the goal for this set of simulations was to compare the different effects of “Spherical” and the “Ellipsoidal” shaped GAGs inclusion on the skin edema, “Uniform” distribution of the GAGs in the skin was maintained across all simulations, i.e. the skin FCD was at 25.7 mEq/L throughout the entire skin block. The GAGs inclusion FCD was simulated at 25.7 mEq/L, 150 mEq/L, 257 mEq/L, 514 mEq/L, 771 mEq/L for both of the two GAGs inclusion geometry models. Results showed the similar trends between the two geometries for all five GAGs FCD levels. As an example, Figure 6-7 shows the comparison of total displacement and Von Mises stress between the “Spherical” and “Ellipsoidal” GAGs inclusion geometries when GAGs inclusion FCD level is at 150 mEq/L.

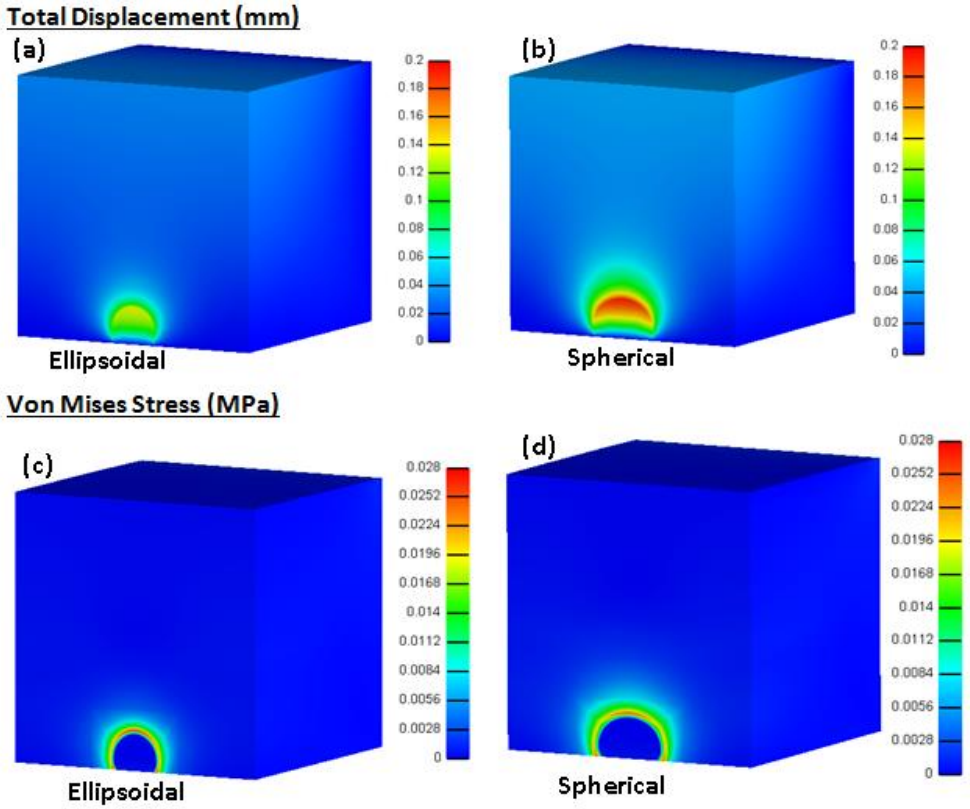

Figure 6-7: Comparison of total displacement and Von Mises stress between two GAGs inclusion geometries when the osmolarity for both the skin and GAGs at 280 mOsm/L, the skin FCD at 25.7 mEq/L and is under uniform distribution, the GAGs inclusion FCD is 150 mEq/L. Top row (a)-(b): the total displacement (mm) of the model when the GAGs inclusion geometry is a) Ellipsoidal, b) Spherical. Bottom row (c)-(d): the Von Mises stress (MPa) of the model when the GAGs inclusion geometry is c) Ellipsoidal, e) Spherical

As can be seen from Figure 6-7, the total displacement and Von Mises Stress are higher when the GAGs inclusion is a spherical geometry. The total volume for the quarter-symmetric GAGs inclusion is 0.23 mm^3 in the "Spherical" shape and 0.10 mm^3 in the "Ellipsoidal" shape. Therefore, the spherical GAGs inclusion has larger porous volume and in turn attracts more water into the tissue, and causes larger deformation and higher stresses. Similar to the comparison of the skin GAGs distribution, in this set of simulations, the higher stress also occurred at the interface between the GAGs inclusion and normal skin tissue in both GAGs inclusion geometries. This also indicates that it is critical to investigate the stress localizations in

this interface area. The following two sections further quantitively illustrate the stress distribution in the surrounding tissue of the GAGs inclusion with respect to different GAGs inclusion FCD and GAGs inclusion extracellular osmolarity.

6.3.3 GAGs inclusion Fixed Charge Density (FCD) comparison

Five simulations were performed to study the effect of different GAGs inclusion FCD levels in the tissue deformation and stress distribution. In this set of studies, the GAGs inclusion geometry was chosen as “Spherical” and the skin GAGs distribution type was “Uniform”. Both the skin and GAGs external bath osmolarity were maintained at 280 mOsm/L and the skin FCD was 25.7 mEq/L. In this way, the only variable was the GAGs inclusion FCD which was simulated at 25.7 mEq/L, 150 mEq/L, 257 mEq/L, 514 mEq/L and 771 mEq/L. The total displacement and Von Mises stress of this model at all five GAGs inclusion FCD levels are displayed in Figure 6-8.

It can be seen that the total displacement and the Von Mises stress both increase for GAGs inclusion and the surrounding tissue when the GAGs inclusion FCD level is increased. The GAGs endure the highest level of swelling when the FCD is at 771 mEq/L, which is 30 times higher than the normal skin GAGs FCD level. At the same time, the surrounding tissue of the GAGs inclusion is compressed due to the osmotic swelling pressure from the accumulated GAGs. High stresses occur at the interface between GAGs inclusion and the surrounding tissue at all GAGs inclusion FCD levels.

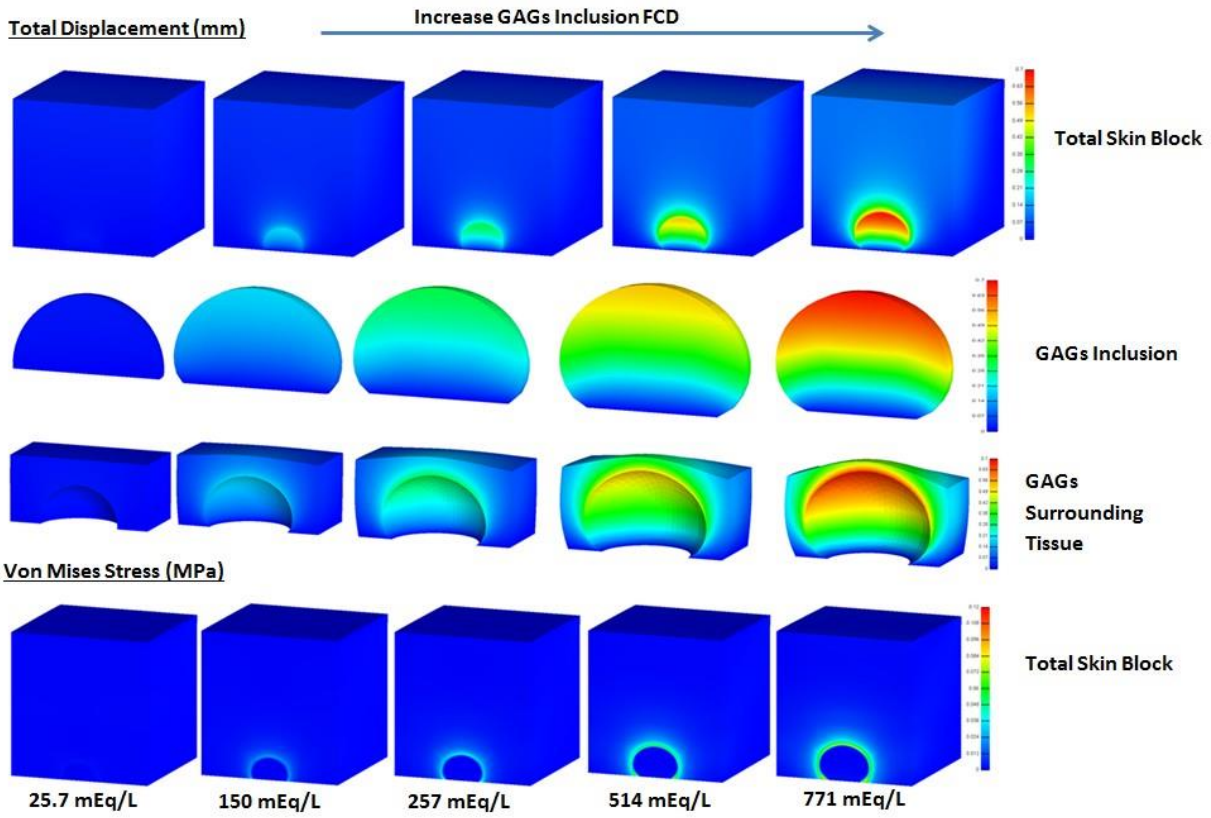

Figure 6-8: Comparison of the influences of GAGs inclusion FCD levels on the total displacement (mm) and Von Mises stress (MPa). From left to right, five simulations were taken when GAGs inclusion FCD at 25.7 mEq/L, 150 mEq/L, 257 mEq/L, 514 mEq/L and 771 mEq/L. The largest deformation and highest stress concentration is at 771 mEq/L. The displacement and stress increase with the increased GAGs inclusion FCD

In order to quantify the stresses localization in the tissue surrounding GAGs inclusion and provide more detailed information about the tissue tensile stress and tissue fluid pressure change under the increased GAGs inclusion FCD influences, four Regions of Interest (ROIs): 1) Left, 2) Right, 3) Top, and 4) Center were chosen to perform stress and pressure analyses (Figure 6-9). These four ROIs represent the regions that exhibit the minimum compressive stress (maximum in magnitude) and maximum tensile stress when the surrounding tissue is subjected to the osmotic swelling pressure from the accumulated GAGs. Four elements from each of the ROI were selected for calculating the elastic tensile stress and fluid pressure. FEBio

formulated all solid elements in a global coordinate system, and the osmotic pressure was considered isotropic (Maas et al. 2015). Therefore, in the elastic stress calculation, the σ_{xx}^{e}, σ_{yy}^{e}, and the σ_{zz}^{e} are all with respect to the global coordinate as identified in Figure 6-9.

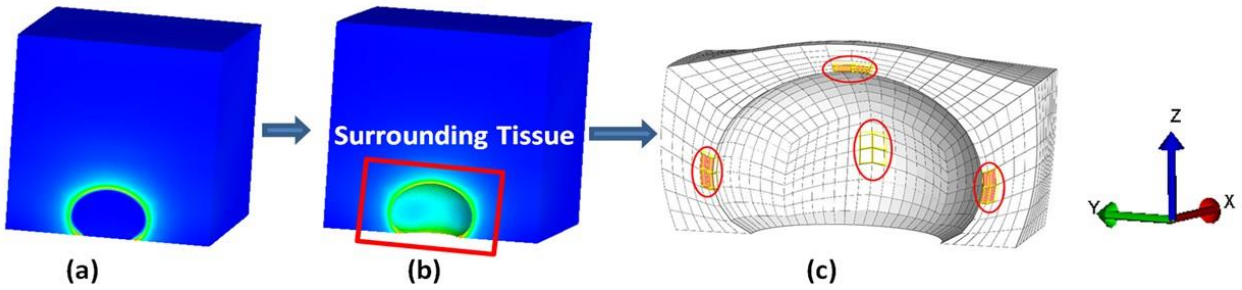

Figure 6-9: The selection of four Regions of Interest (ROIs) under global coordinate system. a) the whole skin block model; b) the skin block model without GAGs inclusion; c) the surrounding tissue with four ROIs and the coordinate system

The maximum elastic stresses σ_{xx}^{e}, σ_{yy}^{e}, and σ_{zz}^{e} for the four ROIs were calculated according to Eq. (6-7) and are reported in Figure 6-10. The Von Mises stresses for the four ROIs are also included in the same figure.

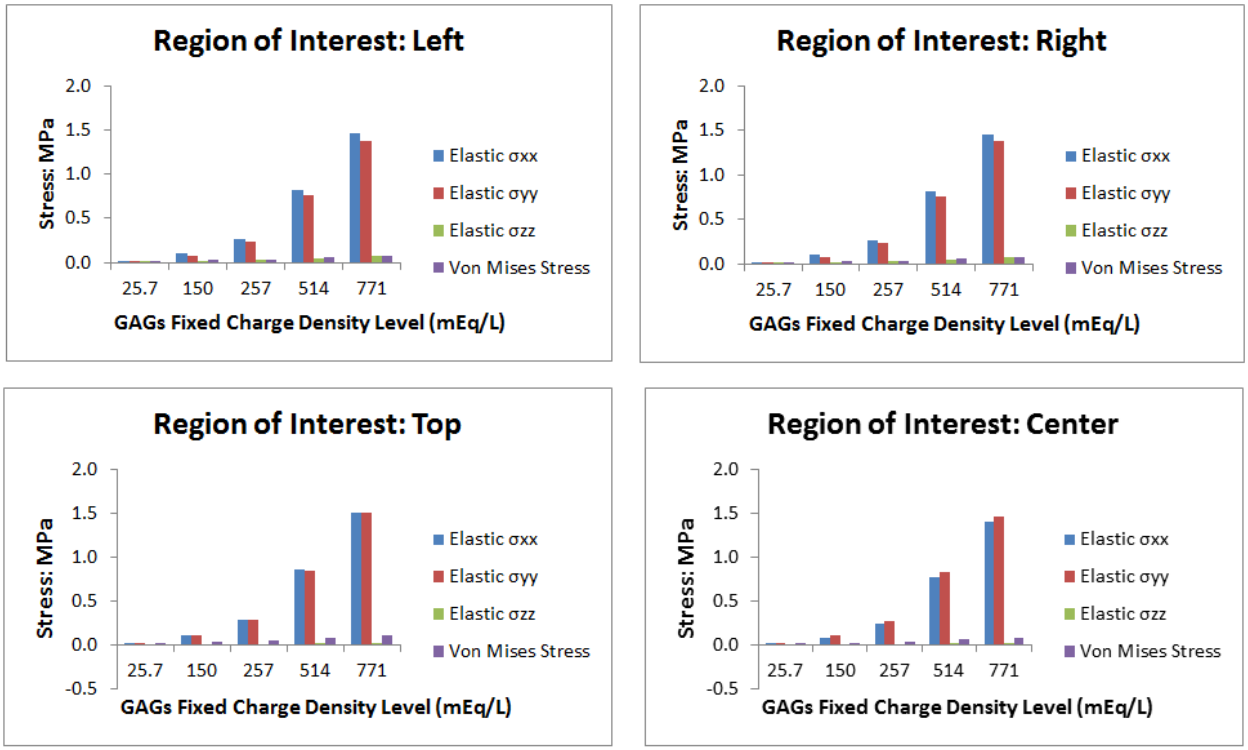

Figure 6-10: Maximum elastic stresses σ^e_{xx}, σ^e_{yy}, and σ^e_{zz} and Von Mises stresses in four Regions of Interest (ROIs) at for GAGs inclusion FCD at 25.7 mEq/L, 150 mEq/l, 257 mEq/L, 514 mEq/L and 771 mEq/L

It can be seen that the maximum tensile stress occurs in either X or Y directions (σ^e_{xx}, σ^e_{yy}) for all four regions at all five GAGs inclusion FCD levels. When the GAGs inclusion FCD is 771 mEq/L. the maximum tensile stress is 1.5 MPa for both σ^e_{xx} and σ^e_{yy} at the top region of the surrounding tissue where it interacts with the GAGs inclusion. As reported in the literature, the Ultimate Tensile Strength (UTS) for skin tissue ranges between 0.1-40 MPa (Gallagher et al. 2012; Flynn et al. 2011; Ní Annaidh et al. 2012). For patients with compromised vascular systems and undergoing inflammation and edema, the skin is weakened to sustain less pressure and stress (Bansal et al. 2005; Meyer & Aviv 1992).Therefore, by comparing with the UTS reported at by Zhou et al., which was 0.25-1.0 MPa (Zhou et al. 2010), it can be predicted that the tissue will tear and damage with higher GAGs inclusion FCD values.

The fluid pressure within the skin tissue consists of the osmotic pressure within the GAGs inclusion, and the interstitial fluid pressure in the surrounding tissue outside of the GAGs inclusion. These two pressures were calculated according to Eq. (6-4) to investigate the change of the skin tissue fluid pressure before and after swelling, and determine the damage on the blood vessels and skin due to the tissue pressure changes. Results of the pressure change during swelling are plotted in Figure 6-11.

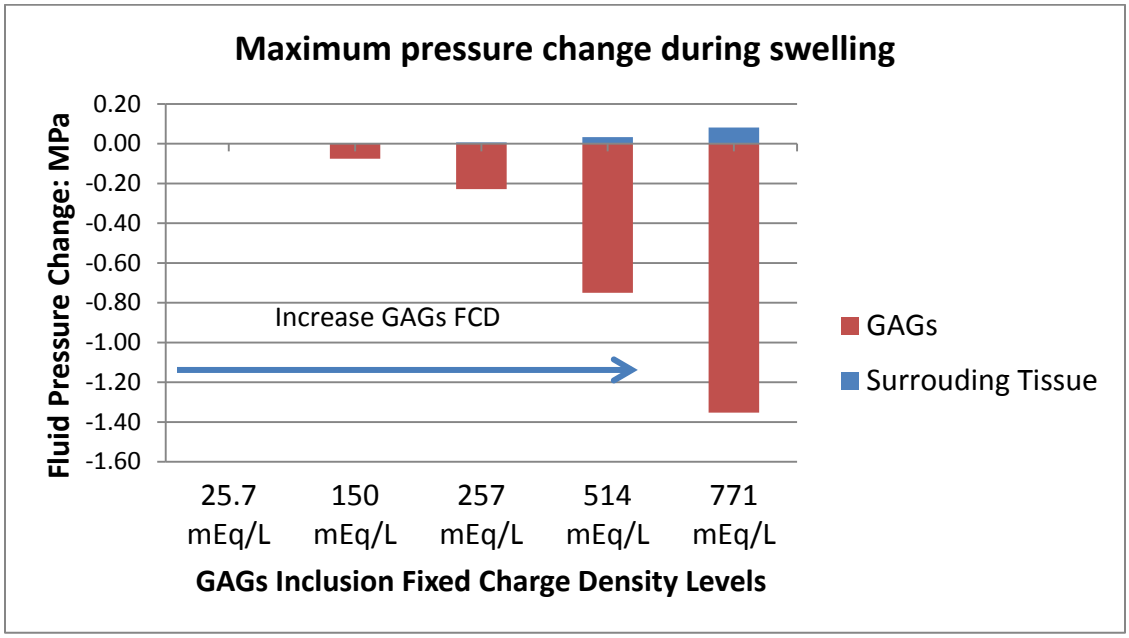

Figure 6-11: Maximum pressure change during swelling at GAGs inclusion FCD levels of 25.7 mEq/L, 150 mEq/L, 257 mEq/L, 514 mEq/L and 771 mEq/L

It can be seen that the osmotic pressure within the GAGs inclusion decreased after swelling (i.e. the pressure change shows negative values) at all GAGs inclusion FCD levels. The definition of osmotic pressure describes the minimum pressure a membrane needs to prevent an influx of water (Cooney 1976). Within the swollen GAGs inclusion, water content is at a higher level and the osmotic pressure needed for further swelling is lowered. This is also reported as a "drop" of osmotic pressure during swelling (Reed & Rubin 2010; Philipse & Vrij

2011). With the increased GAGs inclusion FCD values, the osmotic pressure within the GAGs inclusion decreased further. The increased "drop" of osmotic pressure within the GAGs inclusion at a higher GAGs inclusion FCD level indicates a larger intracellular edema and supports the environment that leads to venous ulcers (Venn & Maroudas 1977a). Specifically, this work indicates an increased interstitial fluid pressure which compresses more on the blood vessel in the surrounding tissue, reduces the blood flow, and leads to tissue ischemia (Hargens et al. 1989). Meanwhile, the surrounding tissue is compressed by the swollen GAGs inclusion, leading to an increased interstitial fluid pressure push on the skin and capillaries (McGee et al. 2009). When GAGs inclusion FCD value increases, this change of the interstitial fluid pressure after swelling also arises. Therefore, it can be predicted that further tissue necrosis and damage will likely occur and tissue wounds will initiate with higher GAGs inclusion FCD levels.

6.3.4 GAGs inclusion extracellular osmolarity comparison

Similar to the GAGs inclusion FCD comparison, another 5 simulations were performed to study the influences of the GAGs inclusion external bath osmolarity on skin edema. In this study, the GAGs inclusion geometry was chosen as spherical and the skin GAGs distribution was uniform. The skin FCD was set to 25.7 mEq/L while the GAGs inclusion FCD was set to 150 mEq/L. Skin external bath osmolarity was maintained at physiological level of 280 mOsm/L (Sorrentino et al. 2015) and the GAGs inclusion external bath osmolarity was varied: 50 mOsm/L, 100 mOsm/L; 280 mOsm/L; 500 mOsm/L, and 1000 mOsm/L levels. The total displacement and Von Mises stress comparison can be seen in Figure 6-12.

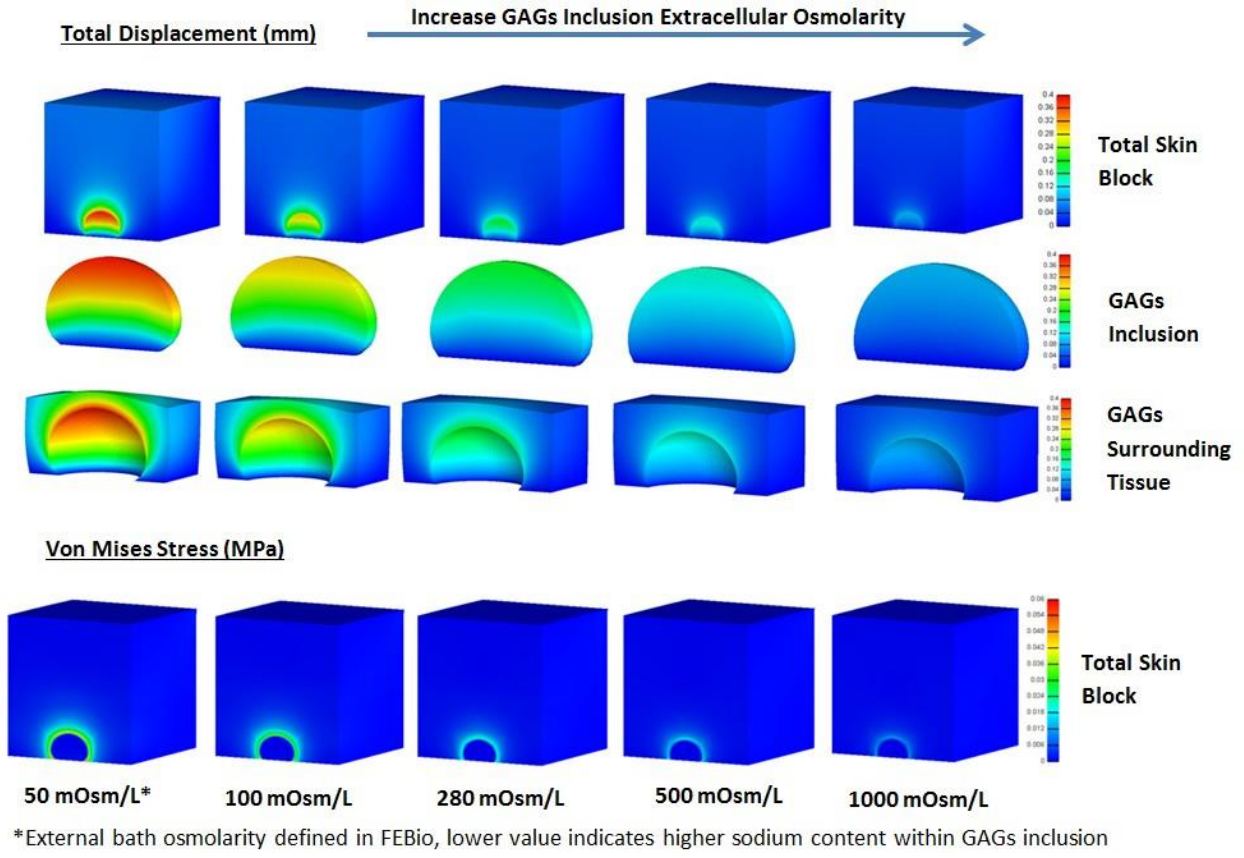

Figure 6-12: Comparison of the influences of GAGs inclusion extracellular osmolarity levels on the total displacement (mm) and Von Mises stress (MPa). From left to right, five simulations were taken when GAGs inclusion extracellular osmolarity was at 50 mOsm/L, 100 mOsm/L, 280 mOsm/L, 500 mOsm/L and 1000 mOsm/L. The largest deformation and highest stress was found when osmolarity was 50mOsm/L. The displacement and stress decreased with the increased GAGs osmolarity

It can be seen that when the GAGs inclusion FCD, skin FCD and skin osmolarity were held constant at 150 mEq/L, 25.7 mEq/L and 280 mOsm/L respectively, the skin swelling displacement and stress decreased when the GAGs inclusion extracellular osmolarity was increased. In other words, the skin swells more with the increased sodium within the GAGs inclusion (lower external bath osmolarity).

Tensile stresses were also analyzed with similar approach as described in Section 6.3.3. Four ROIs were defined and the maximum elastic tensile stresses σ^e_{xx}, σ^e_{yy}, and σ^e_{zz} were

computed. Figure 6-13 showed the maximum elastic stress at different GAGs osmolarity levels for all four ROIs.

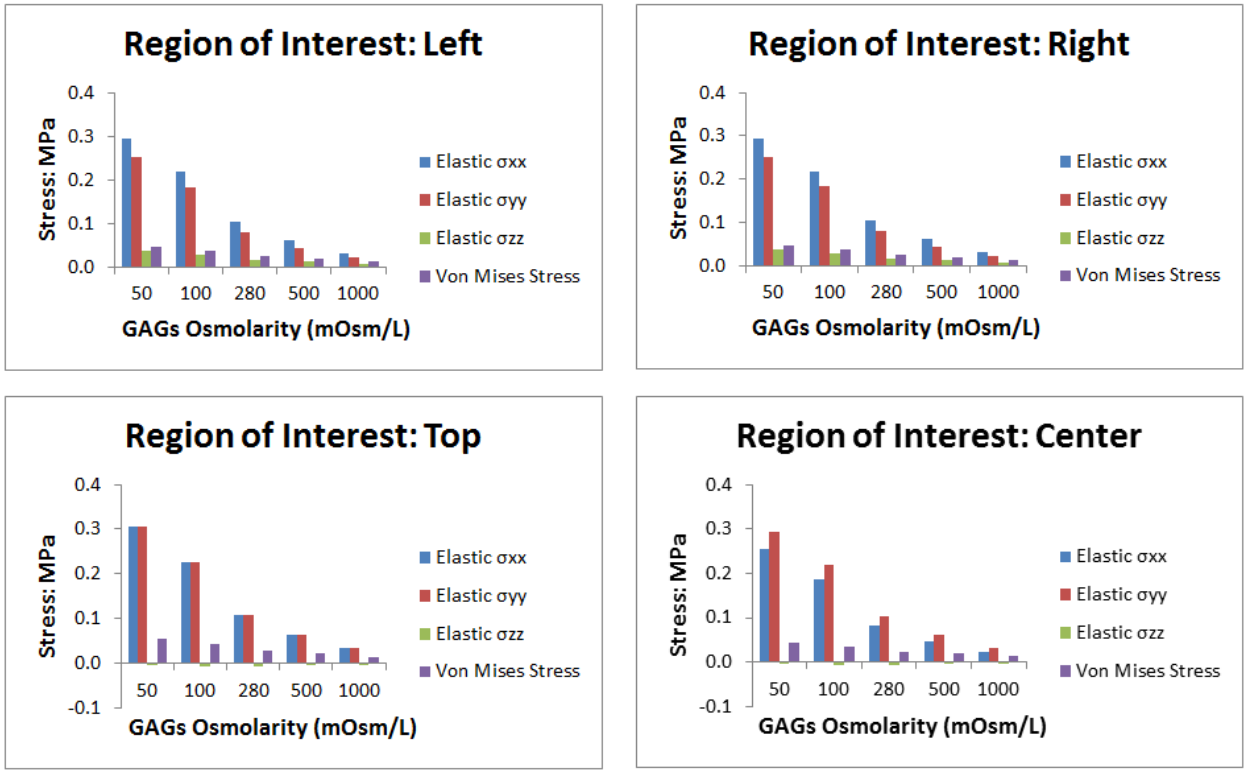

Figure 6-13: Maximum elastic stresses σ^e_{xx}, σ^e_{yy}, and σ^e_{zz} and Von Mises stresses in four Regions of Interest (ROIs) for GAGs inclusion external bath osmolarity at 50 mOsm/L, 100 mOsm/L, 280 mOsm/L, 500 mOsm/L and 1000 mOsm/L

It can be seen that the maximum tensile stress occurred at the top of the surrounding tissue where it interfaced with the GAGs inclusion, and the maximum value was 0.31 MPa for both σ^e_{xx} and σ^e_{yy} when GAGs inclusion external bath osmolarity at 50 mOsm/L. The elastic tensile stresses decreased with the increased extracellular osmolarity values. Comparing with the reported UTS from the literature, which is at 0.25-1.0 MPa (Zhou et al. 2010), further tissue tear and break can be predicted with a lower GAGs inclusion extracellular osmolarity value, i.e. with higher sodium content within the GAGs inclusion.

Osmotic pressure within GAGs inclusion and the interstitial fluid pressure in the surrounding tissue were also calculated with similar approach in section 6.3.3 and the results are displayed in Figure 6-14.

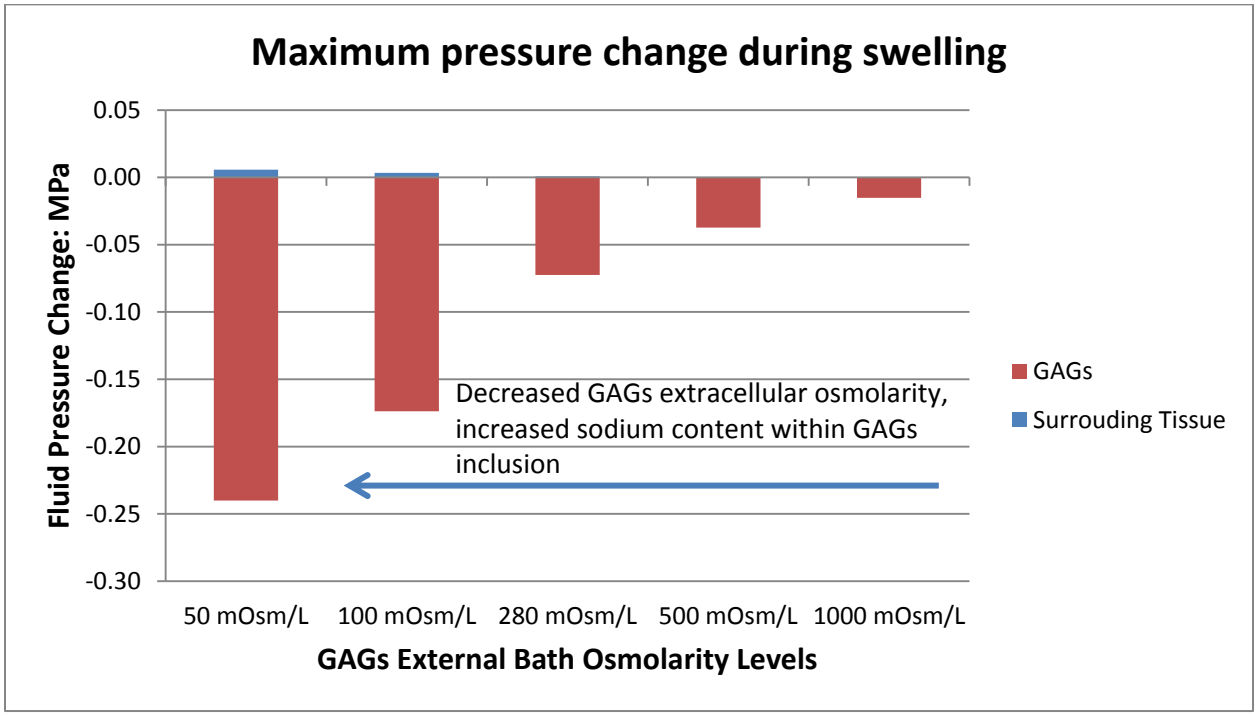

Figure 6-14: Maximum pressure change before and after swelling at different GAGs inclusion external bath osmolarity levels

The osmotic pressure within the GAGs inclusion decreases further during the swelling when the sodium content increases (lower external bath osmolarity). The interstitial fluid pressure in the surrounding tissue increases towards lower osmolarity as well. The further decreased osmotic pressure at a lower GAGs inclusion extracellular osmolarity value indicates larger edema and higher risk for venous ulcers (Maroudas 1976). The interstitial fluid pressure increase in the surrounding tissue leads to the further reduced blood flow and can cause tissue ischemia (Hargens et al. 1989). Therefore, the sodium increase during the inflammation is also a contributor to the initiation of venous ulcers.

6.4 Discussion and Conclusions

6.4.1 Physiology and clinical application

In this study, we explored the effects of GAGs inclusion geometries and skin GAGs distribution types on skin swelling and stress distribution. The results showed that the skin deformed in a similar pattern between the two GAGs inclusion geometries and three GAGs distribution types. The higher stresses found in the Spherical shaped GAGs inclusion, as compared to the Ellipsoidal inclusion, were due to the higher amount of negative charges within the GAGs inclusion because of the larger volume. Similarly, higher stresses were found in the Uniform GAGs distribution as compared to the Linear and Parabolic distributions. This result can be explained by the total amount of negative charges carried by GAGs throughout the skin, a larger number of negative charges are found in the Uniform distribution. However, more interestingly, we found that regardless of the GAGs geometries or skin GAGs distributions, the highest stresses were always localized at the interface between the accumulated GAGs and the surrounding tissue. Since blood pooling and inflammation first affects the subcutaneous area (Burnand et al. 1982), the simulation results indicate that venous ulcers are likely to first happen in the deep tissue and propagate to the superficial level, resulting in open wounds.

The influences of GAGs inclusion negative charges (defined as “Fixed Charge Density” or FCD) and extracellular osmolarity (or external bath osmolarity) levels in the swelling of the skin tissue were also investigated. The elastic tensile stresses in the interface between the GAGs inclusion and surrounding tissue reached the highest stress at 1.5 MPa when the GAGs inclusion FCD was set at 771 mEq/L (30 times higher than normal level), while the skin FCD was at the normal level and both GAGs inclusion and skin tissue had normal osmolarity values. This value

exceeded the range of the ultimate tensile strength reported in literature which was at 0.25-1.0 MPa (Annaidh et al. 2013; Zhou et al. 2010). These data suggest that the stresses are high enough to cause a tissue tear and damage can be expected. It should be noted that a range of UTS was reported in the literature, we used the lower values for our study as our population is known to have compromised tissues (Bansal et al. 2005; Meyer & Aviv 1992).

Meanwhile, the Von Mises stresses within the surrounding tissue also increased with the increased GAGs and sodium accumulation within the GAGs inclusion. Von Mises stress criterions directly relates the shear modulus of the material, which is the ratio of shear stress and shear strain (Beer et al. 2009). In recent skin ulcers studies, shear load and shear stress have been widely considered as significant contributor to skin ulceration (Manorama et al. 2013; Davis et al. 1998; Manorama et al. 2010). Our previous work also emphasized the need to consider both normal and shear loadings when studying venous ulcers (Pan et al. 2015). The work conducted here further supports the fact that shear load is part of the overall process. Even when the loading is internal from edema and increased pressure, shear load is present. Thus, as with the recommendation of other researchers (Gefen 2009; Bergan et al. 2006), shear load and shear stresses should not be neglected in the study of tissue damage and ulcer formation.

Simulation results also show that when the GAGs inclusion FCD was at 150 mEq/L while holding other factors constant, the osmotic pressure change already exceeded the so called “safety factor” for prevention of edema, which is 15mmHg (Guyton et al. 1971). Therefore, we predict that the edema first ensues prior to the FCD level of 150 mEq/L. The results for the GAGs inclusion FCD comparisons show the interstitial fluid pressure in the surrounding tissue

increased 9.75 mmHg (0.0013 MPa) when the GAGs inclusion FCD was at 150 mEq/L and increased 47.25 mmHg (0.0063 MPa) when the GAGs inclusion FCD was at 257 mEq/L. Studies have reported that an increase of 10mmHg in the interstitial fluid pressure would cause up to a 50% capillary blood flow reduction, causing tissue ischemia, and leading to tissue necrosis (Odland et al. 2004; Hargens et al. 1989; Wiese 1993). These indicate that when GAGs inclusion FCD is higher than 150 mEq/L, at least half of the blood flow will be compromised. On the other hand, the results from the GAGs external bath osmolarity comparisons show that when the GAGs extracellular osmolarity is reduced from 280 mOsm/L (physiological level) to 100 mOsm/L, the change of interstitial fluid pressure in the surrounding tissue during GAGs swelling increased from 5.74 mmHg (0.0008 MPa) to 25.09 mmHg (0.0033 MPa). Therefore, it can be hypothesized that the blood flow reduction first occurs when the external bath osmolarity for the GAGs inclusion decreases from 280 mOsm/L to 100 mOsm/L.

By combining the GAGs inclusion FCD and extracellular osmolarity comparative results, a more detailed pathological explanation for venous ulcer formation is obtained (Fig 6-14). Physiologically, when skin is inflamed, the sodium content increases as well as the GAGs content to regulate the inflammation (Schwartz et al. 2009; Lever et al. 2001; Reed & Rubin 2010). The increased sodium content within the GAGs inclusion (lower external bath osmolarity) and the increased GAGs content (higher Fixed Charge Density) leads to increased skin swelling, as supported by the results of this study. For the GAGs inclusion, the further decreased (more negative) osmotic pressure causes increased permeability and larger intracellular edema (Venn & Maroudas 1977b) which is likely to lead to venous ulcers (Collins & Seraj 2010; Kolluri 2014). As for the surrounding tissues, the increased interstitial fluid pressure

results in the increased skin ischemia (Odland et al. 2004; Agrawal & Chauhan 2012) and increased tissue elastic stress (Lai et al. 1991; Han et al. 2011), both ultimately lead to tissue necrosis and tissue damage and the formation of skin ulcers (Falanga 1993). The simulation results provided more details on the possible physiological events happening in the development of venous ulcers, and therefore the Figure 6-2 has been updated to provide a reflection of these findings and predictions.

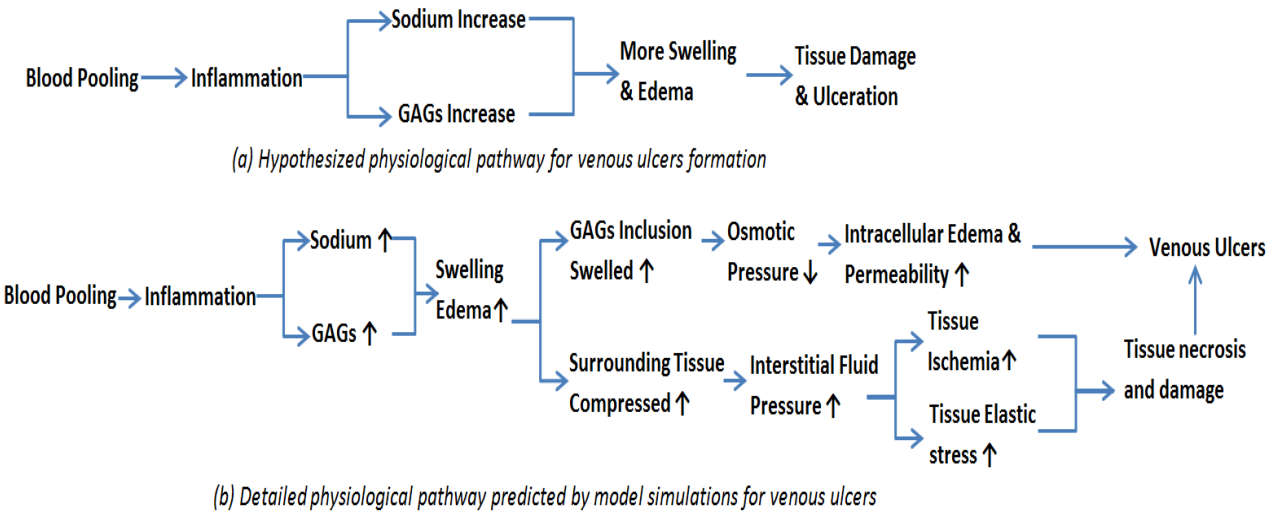

Figure 6-15: The hypothesized and possible detailed physiological pathways predicted by model simulations for the venous ulcers formation. ↑ indicates increase while ↓ refers to decrease

In summary, the model simulated the pathological events that are likely to occur during inflammation and skin edema, and further predicted the damages in the tissue that could potentially lead to venous ulcers.

Comparing to other wound models in the literature; this model was the first to investigate wound formation, specifically the role of GAGs and sodium accumulation in skin edema and ulcer formation. A broader perspective of this research is to correlate the blood pooling and inflammation with skin edema and to provide insights to the formation and

development of venous ulcers. Clinically, this model can predict when the intracellular edema first occurs and when tissue ischemia ensues. The results provided more detailed information to the hypothesis proposed by researchers with regard to the pathology of venous ulcers (Abbade & Lastória 2005). As illustrated in Figure 6-15, the hypothesized pathophysiology for venous ulcer formation began with blood pooling in the lower leg, causing inflammation, leading to skin edema, and resulting skin ulceration. In the model, we observed that when increasing the GAGs and sodium, both reflected the inflammation process within the tissue and caused an increase in deformation and higher fluid pressure, which resulted in a presentation of skin edema. Additionally, the high stress and pressure within the model showed that the edema reached levels that produced stresses that could cause tissue damage and necrosis. Therefore, the model proved that with the blood pooling in the lower leg, the sequential skin edema and inflammation could be illustrated by the proliferation of sodium and GAGs accumulation, and ulcer formation as well as tissue damage could be further explained by the microenvironment.

6.4.2 Limitation and future work

A couple of limitations existed in this study. First, only the role of GAGs and sodium were studied in the process of venous ulcer formation, which is a complex biomechanical and biochemical process. Other contributors to the ulcer formation, such as growth factors activation, and vessel compliance change, still need to be explored. Another limitation was the lack of information in the literature for the boundary values (upper and lower limits) for GAGs inclusion FCD values and the external bath osmolarity values for inflamed skin. In this study a value of 30 times of the normal skin GAGs FCD level was used as the highest upper limit for the

GAGs inclusion FCD. The external bath osmolarity was varied within the range reported by Azeloglu et al (Azeloglu et al. 2008a). Because of these uncertainties, 5 different GAGs inclusion FCD levels and 5 GAGs external bath osmolarity levels were studied. Nevertheless, this model laid a solid foundation for further parametric studies to explore and determine the critical GAGs inclusion FCD and external bath osmolarity values for tissue damage.

During this study, it was observed that the highest stress occurred at the interface between the GAGs inclusion and the surrounding tissue. This finding is interesting and echoes other studies that looked into the balance of FCD between the intra- and extra-cellular permeability and pressurization (Elkin et al. 2010), indicating that this model also has the potential to study the tissue stresses for other diseases that involve swelling, such as lymph node edema or brain edema in the future.

7 CONCLUSIONS

This research was aimed at improving the understanding of the formation and prevention of venous ulcers. By experimentally studying the differences of blood flow responses to loading, numerically investigating the hemodynamic characteristic parameters among different populations; and computationally exploring the pathology of inflammation-induced skin edema and skin ulceration, clearer physiological changes in the skin vascular properties and tissue stresses were identified. These changes were also related to venous ulcer formation.

The first part of this research investigated the local blood flow changes under normal and combined normal and shear loadings for patients with existing venous ulcers and healthy individuals. Results showed that the legs with ulcers had higher reactive hyperemia spikes and a larger decrease in blood flow due to external loading as compared to healthy legs. Such phenomenon indicated the venous ulcer patients experiencing ischemic ulceration exhibited insufficient blood circulation and restoration. The higher hyperemia responses also indicated inflammation. Accompanying inflammation is increased interstitial tissue pressure occurred in the tissue near the venous ulcers. Another important finding was that the “non-wounded” group (the contra-lateral leg (no ulcer) of patients with ulcers) exhibited a trend that was between that of healthy legs and legs with venous ulcers. These results indicated that there is a progression of change that occurs moving from healthy, to “less healthy” but no wound, to a wound formation. Therefore, a possibility exists to use the perfusion tests to identify changes that occur prior to wound formation. Thus, this force-perfusion response has the potential to serve as a predictive measure to identify when internal conditions change and the risk for an ulcer increases.

The second part of this work used a Windkessel-based modeling approach to determine numerical values that represented changes that occur in terms of internal resistance and recovery rates. The model successfully replicated the blood perfusion curve from the experimental data and output patient-specific hemodynamic parameters. By comparing these parameters across test groups, the results indicated there were significant differences between legs with ulcers and healthy legs with regard to local vessel resistance and compliance. The data also suggest that with a larger sample size, significant differences would be likely between all three groups, (i.e., wounded ,non-wounded and healthy). Together with the perfusion test, this modeling approach also has the potential of establishing parameter thresholds to further identify individuals who are at risk of developing venous ulcers.

The last section of the research studied skin edema due to inflammation using a FE model, the roles of glycosaminoglycans (GAGs) and sodium and their influences on skin tissue pressure and stress were evaluated. This parametric study further proved that under inflammation, the accumulated GAGs and sodium led to increased skin swelling. Within the GAGs inclusion, a more negative osmotic pressure indicated a more compromised vessel compliance, increased permeability and intracellular edema. The increased interstitial fluid pressure in the tissue surrounding the GAGs inclusion reached levels that have been shown to produce skin ischemia, tissue necrosis and tissue rupture. Thus, .both GAGs and sodium contributed to the development of venous ulcers. The model simulated the pathological changes that occur under inflammation and skin edema and the cases which would result in skin damage and ulceration. This work fills a gap in existing numerical studies in wounds, no work was available on the modeling of wound formation. The model results echo the findings

obtained from our perfusion testing and Windkessel modeling. This research expands our knowledge on the process of wound formation.

Future work will look into expanding sample size in perfusion testing and Windkessel-based modeling to obtain more complete data and hemodynamic vascular parameters in all demographic aspects. Additionally, if possible, more measurements with regard to tissue fluid pressure and skin vessel compliances to be taken to refine the Finite Element model and also to compare with studies that consider other factors contributing to skin wound formation. Last but not the least, different stages of wound formation and propagation should be further clarified and confirmed with non-invasive measurements, to provide a better strategy for venous ulcers prevention and treatment.

In conclusion, by combining the experimental data and the information gathered from the two different numerical modeling studies, a better understanding of venous ulceration pathology was obtained. Through these analyses, a preventive approach for venous ulcers can be explored which has the potential to identify populations at higher risk of developing ulcers. Thus, instead of waiting and having post-ulcer treatment, an “in-time” treatment can be applied prior to wound formation. This study laid a solid foundation for venous ulcers research and ultimately will contribute to the wound-care community for reducing venous ulcers occurrence.

BIBLIOGRAPHY

BIBLIOGRAPHY

Abbade, L.P.F. & Lastoria, S., 2006. Management of patients with venous leg ulcer. *Continuing Medical Education*, 81(6), pp.509–521.

Abbade, L.P.F. & Lastória, S., 2005. Venous ulcer: epidemiology, physiopathology, diagnosis and treatment. *International Journal of Dermatology*, 44(6), pp.449–56.

Abdolrazaghi, M., Navidbakhsh, M. & Hassani, K., 2010. Mathematical modelling and electrical analog equivalent of the human cardiovascular system. *Cardiovascular Engineering*, 10(2), pp.45–51.

Agrawal, K. & Chauhan, N., 2012. Pressure ulcers: Back to the basics. *Indian Journal of Plastic Surgery*, 45(2), pp.244–254.

Ahn, H. et al., 1987. In vivo evaluation of signal processors for laser Doppler tissue flowmeters. *Medical & Biological Engineering & Computing*, 25(March), pp.207–211.

Alvarez, O.M. et al., 1998. A novel treatment for venous leg ulcers. *The Journal of Foot and Ankle Surgery*, 37(4), pp.319–324.

Annaidh, A.N. et al., 2013. Characterising the Anisotropic Mechanical Properties of Excised Human Skin. , pp.1–24.

Arnold, T.E. et al., 1994. Prospective, multicenter study of managing lower extremity venous ulcers. *Annals of Vascular Surgery*, 8(4), pp.356–362.

Ateshian, G.A. & Hung, C.T., 2006. The natural synovial joint: properties of cartilage. *Proceedings of the Institution of Mechanical Engineers Part J Journal of Engineering Tribology*, 220(8), pp.657–670.

Azeloglu, E.U. et al., 2008a. Heterogeneous transmural proteoglycan distribution provides a mechanism for regulating residual stress in the aorta. *American Journal of Physiology - Heart and Circulatory Physiology*, 294(3), pp.1197–1205.

Azeloglu, E.U. et al., 2008b. Heterogeneous transmural proteoglycan distribution provides a mechanism for regulating residual stresses in the aorta. *American Journal of Physiology-Heart and Circulatory Physiology*, 10027, pp.1197–1205.

Bansal, C. et al., 2005. Decubitus ulcers: a review of the literature. *International Journal of Dermatology*, 44(10), pp.805–10.

Bartlett, H.L., Ting, L.H. & Bingham, J.T., 2014. Accuracy of force and center of pressure measures of the Wii Balanced Board. *Gait Posture*, 39(1), pp.997–1003.

Beebe-Dimmer, J.L. et al., 2005. The epidemiology of chronic venous insufficiency and varicose veins. *Annals of Epidemiology*, 15(3), pp.175–84.

Beer, F.P. et al., 2009. Transformation of Stress and Strain. In *Mechanics of Materials*. McGraw Hill Education, pp. 452–453.

Bennett, L. et al., 1979. Shear vs pressure as causative factors in skin blood flow occlusion. *Arch Phys Med Rahbil*, 60, pp.309–314.

Bennett, L. et al., 1979. Shear vs pressure as causative factors in skin blood flow occlusion. *Archives of Physical Medicine and Rehabilitation*, 60(7), pp.309–314.

Bennett, S.P. et al., 2003. Growth factors in the treatment of diabetic foot ulcers. *The British Journal of Surgery*, 90(2), pp.133–46.

Bergan, J.J. et al., 2006. Chronic venous disease. *The New England Journal of Medicine*, 355(5), pp.488–498.

Bhave, G. & Neilson, E.G., 2011a. Body fluid dynamics: back to the future. *Journal of American Society of Nephrology*, 22(12), pp.2166–81.

Bhave, G. & Neilson, E.G., 2011b. Body fluid dynamics: back to the future-Supplemental Materials. *J. Am. Soc. Nephrol.*, 22(12), pp.2166–81.

Bian, L. et al., 2009. Influence of decreasing nutrient path length on the development of engineered cartilage. *Osteoarthritis and Cartilage*, 17(5), pp.677–685.

Bliss, M. & Schofield, M., 1996. Leg ulcers caused by pressure and oedema. *Journal of Tissue Viability*, 6(1), pp.17–19.

Bouten, C. V et al., 2003. The etiology of pressure ulcers: skin deep or muscle bound? *Archives of Physical Medicine and Rehabilitation*, 84(4), pp.616–619.

Brem, H., Kirsner, R.S. & Falanga, V., 2004. Protocol for the successful treatment of venous ulcers. *The American Journal of Surgery*, 188(1), pp.1–8.

Buganza Tepole, A. et al., 2011. Growing skin: A computational model for skin expansion in reconstructive surgery. *Journal of the Mechanics and Physics of Solids*, 59(10), pp.2177–2190.

Buganza Tepole, A. & Kuhl, E., 2013. Systems-based approaches toward wound healing. *Pediatric Research*, 73(4 Pt 2), pp.553–63.

Burnand, K.G., Whimster, I., et al., 1982. Pericapillary fibrin in the ulcer-bearing skin of the leg: the cause of lipodermatosclerosis and venous ulceration. *British Medical Journal*, 285(6348), pp.1071–2.

Burnand, K.G., Clemenson, G., et al., 1982. The effect of sustained venous hypertension on the skin capillaries of the canine hind limb. *British Journal of Surgery*, 69, pp.41–44.

Burton, A.C., 1972. *Physiology and Biophysics of Circulation*, Chicago, IL: Year Book Medical Publishers.

Burton, S., 1991. Venous Ulceration. *Clinical Materials*, 8, pp.203–208.

Bush, T.R. & Hubbard, R., 2007. Support force measures of midsized men in seated positions. *Journal of Biomechanical Engineering*, 129(1), pp.58–65.

Bush, T.R. & Hubbard, R.P., 2007. Support force measures of midsized men in seated positions. *Journal of Biomechanical Engineering*, 129(1), pp.58–65.

Callam, M.J. et al., 1987. Chronic ulcer of the leg: clinical history. *British Medical Journal*, 294(6584), pp.1389–1391.

Capp, C.L. et al., 2004. Post pressure hyperemia in the rat. *Comparative Biochemistry and Physiology. Part A, Molecular & Integrative Physiology*, 137(3), pp.533–546.

Carden, D.L. & Granger, D.N., 2000. Pathophysiology of ischaemia-reperfusion injury. *The Journal of Pathology*, 190(3), pp.255–66.

Carman, T., 2009. Chapter 13 Compression Therapy for Venous Disorders and Venous Ulceration. In P. Gloviczki, ed. *Handbook of Venous Disorders : Guidelines of the American Venous Forum*. Hodder Arnold.

Carpentier, P.H. et al., 2004. Prevalence, risk factors, and clinical patterns of chronic venous disorders of lower limbs: a population-based study in France. *Journal of Vascular Surgery*, 40(4), pp.650–9.

de Carvalho, M.R., 2015. Comparison of Outcomes in Patients With Venous Leg Ulcers Treated With Compression Therapy Alone Versus Combination of Surgery and Compression Therapy. *Journal of Wound, Ostomy and Continence Nursing*, 42(1), pp.42–46.

Casavola, C. et al., 2000. Blood flow and oxygen consumption with near-infrared spectroscopy and venous occlusion: spatial maps and the effect of time and pressure of inflation. *J Biomed Opt*, 5(3), pp.269–276.

Chaffin, D.B. & Andersson, G.B.J., 1991. *Occupational Biomechanics* 2nd ed., Wiley-Interscience.

Chahine, N.O. et al., 2004. Anisotropic strain-dependent material properties of bovine articular cartilage in the transitional range from tension to compression. *Journal of Biomechanics*, 37(8), pp.1251–1261.

Chen, B. & Bates, B.T., 2000. Comparison of F-Scan in-sole and AMTI forceplate system in

measuring vertical ground reaction force during gait. *Physiotherapy Theory and Practice*, 16, pp.43–53.

Cleveland Clinic, 2015. Lower Extremity Ulcers. Available at: http://my.clevelandclinic.org/services/heart/disorders/pad/legfootulcer.

Cohen, J., 1992. A power primer. *Psychological Bulletin*, 112(1), pp.155–159.

Cohen, J., 1988. *Statistical power analysis for the behavioral sciences* 2nd ed., Lawrence Earlbaum Associates.

Coleridge Smith, P.D., 2001. Update on chronic-venous-insufficiency-induced inflammatory processes. *Angiology*, 52 Suppl 1, pp.S35-42.

Collins, L. & Seraj, S., 2010. Diagnosis and treatment of venous ulcers. *American Family Physician*, 81(8), pp.989–96.

Cooney, D.O., 1973. *Biomedical engineering principles: an introduction to fluid, heat, and mass transport processes*, M. Dekker.

Cooney, D.O., 1976. Chapter 7 Transport through cell memberane. In G. A. Bekey & D. D. Reneau, eds. *Biomedical Engineering Principles: An Introduction to Fluid, Heat, and Mass Transportation Processes*. New York, New York, USA: Marcel Dekker, INC., pp. 229–268.

Craig, D.H., Shiratsuchi, H. & Basson, M.D., 2009. Increased extracellular pressure provides a novel adjuvant stimulus for enhancement of conventional dendritic cell maturation strategies. *Biochemical and Biophysical Research Communications*, 387(1), pp.174–9.

Crane, J.S. & Cheshire, N.J.W., 2008. Chronic ulceration of the leg. *Surgery (Oxford)*.

Davies, A.H. et al., 2009. Chapter 16 Surgical Therapy for Chronic Venous Insufficiency. In P. Gloviczki, ed. *Handbook of Venous Disorders : Guidelines of the American Venous Forum*. Hodder Arnold.

Davis, B.L. et al., 1998. A device for simultaneous measurement of pressure and shear force distribution on the plantar surface of the foot. *Journal of Applied Biomechanics*, 14(1), pp.93–104.

Douglas, W.. & Simpson, N.., 1995. Guidelines for the management of chronic venous leg ulceration. Report of a multidisciplinary workshop. *British Journal of Dermatology*, 132(3), pp.446–452.

Elkin, B.S., Shaik, M.A. & Morrison, B., 2010. Fixed negative charge and the Donnan effect: a description of the driving forces associated with brain tissue swelling and oedema. *Philosophical transactions. Series A, Mathematical, physical, and engineering sciences*, 368(1912), pp.585–603.

Ely, J.W. et al., 2006. Approach to Leg Edema of Unclear Etiology. *The Journal of the American Board of Family Medicine*, 19(2), pp.148–160.

Erickson, C.A. et al., 1995. Healing of venous ulcers in an ambulatory care program: The roles of chronic venous insufficiency and patient compliance. *Journal of Vascular Surgery*, 22(5), pp.629–636.

Fahey, C., 1998. Experience with a new human skin equivalent for healing venous leg ulcers. *Journal of vascular nursing : official publication of the Society for Peripheral Vascular Nursing*, 16(1), pp.11–5.

Falanga, V., 1993. Chronic Wounds: Pathophysiologic and Experimental Considerations. *Journal of Investigative Dermatology*, 100(5), pp.721–725.

Falanga, V., Moosa, H. & Nemeth, A., 1987. Dermal pericapillary fibrin in venous disease and venous ulceration. *Arch Dermatol*, 123(5), pp.620–623.

Flynn, C. et al., 2013. A finite element model of the face including an orthotropic skin model under in vivo tension. *Computer Methods in Biomechanics and Biomedical Engineering*, 18(6), pp.571–582.

Flynn, C. & McCormack, B.A.O., 2010. Simulating the wrinkling and aging of skin with a multi-layer finite element model. *Journal of Biomechanics*, 43(3), pp.442–8.

Flynn, C., Taberner, A. & Nielsen, P., 2011. Modeling the mechanical response of in vivo human skin under a rich set of deformations. *Annals of Biomedical Engineering*, 39(7), pp.1935–1946.

Fonder, M.A. et al., 2008. Treating the chronic wound: A practical approach to the care of nonhealing wounds and wound care dressings. *Journal of the American Academy of Dermatology*, 58(2), pp.185–206.

Gallagher, A.J. et al., 2012. Dynamic tensile properties of human skin. *2012 IRCOBI Conference*, pp.494–502.

Geerligs, M. et al., 2011. In vitro indentation to determine the mechanical properties of epidermis. *Journal of Biomechanics*, 44(6), pp.1176–1181.

Gefen, A., 2009. *Bioengineering Research of Chronic Wounds A Multidisciplinary Study Approach* A. Gefen, ed., Berlin, Heidelberg: Springer Berlin Heidelberg.

Gennisson, J.-L. et al., 2004. Assessment of elastic parameters of human skin using dynamic elastography. *IEEE transactions on ultrasonics, ferroelectrics, and frequency control*, 51(8), pp.980–9.

George, R. et al., 2014. The effect of deep venous stenting on healing of lower limb venous

ulcers. *European Journal of Vascular and Endovascular Surgery*, 48(3), pp.330–6.

Geris, L., Gerisch, A. & Schugart, R.C., 2010. Mathematical modeling in wound healing, bone regeneration and tissue engineering. *Acta Biotheoretica*, 58(4), pp.355–67.

Ghatnekar, A. V et al., 2011. Novel wound healing powder formulation for the treatment of venous leg ulcers. *Journal of the American College of Certified Wound Specialists*, 3(2), pp.33–41.

Gilsdorf, P. et al., 1990. Sitting forces and wheelchair mechanics. *Journal of rehabilitation research and development*, 27(3), pp.239–246.

Glantz, S.A., 1997. Alternatives to analysis of variance and the t test based on ranks. In *Premier of Biostatistics*. pp. 346–354.

Gonsalves, C.F., 2003. Venous leg ulcers. *Techniques in Vascular and Interventional Radiology*, 6(3), pp.132–136.

Goossens, R.H. et al., 1994. Influence of shear on skin oxygen tension. *Clinical physiology*, 14(1), pp.111–118.

Goossens, R.H. et al., 1997. Shear stress measured on beds and wheelchairs. *Scandinavian Journal of Rehabilitation Medicine*, 29(3), pp.131–136.

Grace, P.A., 1994. Ischemia-reperfusion injury. *British Journal of Surgery*, 81, pp.637–647.

Groves, R.B., 2011. *Quantifying the mechanical properties of skin in vivo and ex vivo to optimise microneedle device design*. Cardiff University.

Guo, X., Lanir, Y. & Kassab, G.S., 2007. Effect of osmolarity on the zero-stress state and mechanical properties of aorta. *American journal of physiology. Heart and circulatory physiology*, 293(4), pp.H2328–H2334.

Guyton, A.C., Granger, H.J. & E, T.A., 1971. Interstitial Fluid Pressure. *Physiological Reviews*, 51(3), pp.527–563.

Hagisawa, S. et al., 1994. Assessment of skin blood content and oxygenation in spinal cord injured subjects during reactive hyperemia. *Journal of Rehabilitation Research and Development*, 31(1), pp.1–14.

Han, E. et al., 2011. Contribution of proteoglycan osmotic swelling pressure to the compressive properties of articular cartilage. *Biophysical Journal*, 101(4), pp.916–924.

Han, O., Li, G. Di & Basson, M.D., 1998. Strain induces Caco-2 intestinal epithelial proliferation and differentiation via PKC and tyrosine kinase signals. *American Journal of Physiology*, 275(3), pp.534–541.

Hargens, A.R. et al., 1989. Kappa Delta Award paper. Tissue fluid pressures: from basic research tools to clinical applications. *Journal of Orthopaedic Research*, 7(6), pp.902–909.

Heit, J.A. et al., 2001. Trends in the incidence of venous stasis syndrome and venous ulcer: A 25-year population-based study. *Journal of Vascular Surgery*, 33(5), pp.1022–1027.

Hendriks, F., 2005. *Mechanical behaviour of human epidermal and dermal layers in vivo*,

Hendriks, F.M. et al., 2003. A numerical-experimental method to characterize the non-linear mechanical behaviour of human skin. *Skin Research and Technology*, 9(3), pp.274–283.

Herrman, E.C. et al., 1999. Skin perfusion responses to surface pressure-induced ischemia: implication for the developing pressure ulcer. *Journal of rehabilitation research and development*, 36(2), pp.109–20.

Hobson, D.A., 1992. Comparative effects of posture on pressure and shear at the body-seat interface. *Journal of rehabilitation research and development*, 29(4), pp.21–31.

Holloway Jr., G.A. et al., 1976. Effects of external pressure loading on human skin blood flow measured by 133Xe clearance. *Journal of Applied Physiology*, 40(4), pp.597–600.

House, M., Kaplan, D.L. & Socrate, S., 2009. Relationships Between Mechanical Properties and Extracellular Matrix Constituents of the Cervical Stroma During Pregnancy. *Seminars in Perinatology*, 33(5), pp.300–307.

Howard, D.P.J. et al., 2008. The role of superficial venous surgery in the management of venous ulcers: a systematic review. *European Journal of Vascular and Endovascular Surgery*, 36(4), pp.458–65.

Humeau, M., Saumet, J. & L'huillier, J., 2000. Simplified model of laser Doppler signals during reactive hyperaemia. *Medical and Biological Engineering and Computing*, 38(1), pp.80–87.

Humphrey, J.D., 2012. Possible mechanical roles of glycosaminoglycans in thoracic aortic dissection and associations with dysregulated transforming growth factor-β. *Journal of Vascular Research*, 50(1), pp.1–10.

Jakobsson, A. & Nilsson, G.E., 1993. Prediction of sampling depth and photon pathlength in laser Doppler flowmetry. *Medical & biological engineering & computing*, 31(3), pp.301–307.

Jan, Y.K. et al., 2013. Using reactive hyperemia to assess the efficacy of local cooling on reducing sacral skin ischemia under surface pressure in people with spinal cord injury: A preliminary report. *Archives of Physical Medicine and Rehabilitation*, 94(10), pp.1982–1989.

Javierre, E. et al., 2009. Numerical modeling of a mechano-chemical theory for wound

contraction analysis. *International Journal of Solids and Structures*, 46(20), pp.3597–3606.

Jochmann, W., Mostbeck, a & Partsch, H., 1993. Postocclusive reactive hyperemia and postural vasoconstriction in different kinds of leg ulcers--investigations with laser Doppler. *VASA. Zeitschrift für Gefässkrankheiten*, 22(4), pp.306–15.

Johnson, S., 2002. Compression hosiery in the prevention and treatment of venous leg ulcers. *Journal of Tissue Viability*, 12(2), pp.67–74.

Jor, J.W.Y. et al., 2013. Computational and experimental characterization of skin mechanics: Identifying current challenges and future directions. *Wiley Interdisciplinary Reviews: Systems Biology and Medicine*, 5(5), pp.539–556.

Kohnle, R., 2000. Mattress for minimizing decubitus ulcers. *US Patent 6,052,851*.

Kolluri, R., 2014. Management of Venous Ulcers. *Techniques in Vascular and Interventional Radiology*, 17(2), pp.132–8.

Kosiak, M. et al., 1958. Evaluation of pressure as a factor in the production of ischial ulcers. *Archives of physical medicine and rehabilitation*, 39(10), pp.623–629.

Kovalenko, P.L. et al., 2012. Influence of defunctionalization and mechanical forces on intestinal epithelial wound healing. *American Journal of Physiology. Gastrointestinal and Liver Physiology*, 303(10), pp.G1134-43.

Kramer, S.A., 1999. Compression wraps for venous ulcer healing: A review. *Journal of Vascular Nursing*, 17(4), pp.89–97.

Kunimoto, B. et al., 2001. Best practices for the prevention and treatment of venous leg ulcers. *Ostomy/Wound Management*, 47(2), pp.34–46, 48–50.

Kutner, M.H. et al., 2013. Analysis of Factor Level Means. In *Applied Linear Statistical Models*. McGraw Hill Education, pp. 733–774.

Lai, W.M., Hou, J.S. & Mow, V.C., 1991. A triphasic theory for the swelling and deformation behaviors of articular cartilage. *Journal of biomechanical engineering*, 113(3), pp.245–258.

Lal, B.K., 2015. Venous Ulcers of the Lower Extremity: Definition, Epidemiology, Economic and Social Burden. *Seminars in Vascular Surgery*.

Lamel, S.A. & Kirsner, R.S., 2013. New approaches to enhanced wound healing: future modalities for chronic venous ulcers. *Drug Discovery Today: Disease Mechanisms*, 10(3–4), pp.71–77.

Langemo, D.K., 1999. Venous ulcers: etiology and care of patients treated with human skin equivalent grafts. *Journal of Vascular Nursing*, 17(1), pp.6–11.

Lanir, Y., 2012. Osmotic swelling and residual stress in cardiovascular tissues. *Journal of Biomechanics*, 45(5), pp.780–789.

Lausten, G.S., Kiaer, T. & Dahl, B., 1993. Laser Doppler flowmetry for estimation of bone blood flow: studies of reproducibility and correlation with microsphere technique. *Journal of Orthopaedic Research*, 11(4), pp.573–580.

Lazarus, G. et al., 2014. Chronic venous leg ulcer treatment: Future research needs. *Wound Repair and Regeneration : official publication of the Wound Healing Society [and] the European Tissue Repair Society*, 22(1), pp.34–42.

Leahy, M.J. et al., 1999. Principles and practice of the laser-Doppler perfusion technique. *Technology and Health Care*, 7, pp.143–162.

Lever, R., Smailbegovic, A. & Page, C., 2001. Role of glycosaminoglycans in inflammation. *Inflammopharmacology*, 9(1), pp.165–169.

Lewis, B. & Towne, J., 2011. Negative pressure dressings in venous ulcers. *Venous Ulcers*, pp.105–112.

Li, C. et al., 2012. Determining elastic properties of skin by measuring surface waves from an impulse mechanical stimulus using phase-sensitive optical coherence tomography. *Journal of The Royal Society Interface*, 9(70), pp.831–841.

Liang, X., 2013. Biomechanical Properties of In Vivo Human Skin From Dynamic Optical Coherence Elastography. *IEEE Trans Biomed Eng.*, 57(4), pp.953–959.

Liao, F., Burns, S. & Jan, Y.-K., 2013. Skin blood flow dynamics and its role in pressure ulcers. *Journal of Tissue Viability*, 22(2), pp.25–36.

Loerakker, S. et al., 2011. Ischemia-reperfusion injury in rat skeletal muscle assessed with T2-weighted and dynamic contrast-enhanced MRI. *Magnetic Resonance in Medicine*, 66(2), pp.528–537.

Lotti, T. et al., 1990. Proteoglycans in so-called cellulite. *International Journal of Dermatology*, 29(4), pp.272–274.

Ma, H. et al., 2014. The real cost of treating venous ulcers in a contemporary vascular practice. *Journal of Vascular Surgery: Venous and Lymphatic Disorders*, 2(4), pp.355–361.

Maas, S. et al., 2015. Chap 4 Element Libaray, Chap 5 Constitutive Model. In *FEBio 2.4 Theory Manual*. p. 71,88-89.

Maini, P.K., Olsen, L. & Sherratt, J.A., 2010. Mathematical models for cell-matrix interactions during dermal wound healing. *International Journal of Bifurcation and Chaos*, 12(9), pp.2021–2029.

Mak, A.F.T., Zhang, M. & Tam, E.W.C., 2010. Biomechanics of pressure ulcer in body tissues interacting with external forces during locomotion. *Annual review of biomedical engineering*, 12, pp.29–53.

Manorama, A. et al., 2013. Quantifying the effects of external shear loads on arterial and venous blood flow: implications for pressure ulcer development. *Clinical Biomechanics*, 28(5), pp.574–8.

Manorama, A.A. et al., 2010. Blood perfusion and transcutaneous oxygen level characterizations in human skin with changes in normal and shear loads--implications for pressure ulcer formation. *Clinical Biomechanics*, 25(8), pp.823–8.

Margolis, D.J. et al., 2002. Venous leg ulcer: Incidence and prevalence in the elderly. *Journal of the American Academy of Dermatology*, 46(3), pp.381–386.

Markova, A. & Mostow, E.N., 2012. US skin disease assessment: ulcer and wound care. *Dermatologic Clinics*, 30(1), p.107–11, ix.

Maroudas, A., 1976. Balance between swelling pressure and collagen tension in nromal anddegnerate cartilage. *Nature*, 260, pp.643–645.

Mayrovitz, H.N. & Larsen, P.B., 1994. Periwound skin microcirculation of venous leg ulcers. *Microvascular Research*, 48(1), pp.114–123.

McGee, M.P. et al., 2009. Swelling and pressure-volume relationships in the dermis measured by osmotic-stress technique. *American journal of physiology. Regulatory, integrative and comparative physiology*, 296(6), pp.R1907–R1913.

Meyer, F.A. & Aviv, T., 1992. Interstitial macromoleculus and the swelling pressure of loose connective tissue. *Mechanics of Swelling*, 64, pp.527–543.

Milic, D.J. et al., 2009. Risk factors related to the failure of venous leg ulcers to heal with compression treatment. *Journal of Vascular Surgery*, 49(5), pp.1242–7.

Miller-Keane & O'Toole, M.T., 2003. Perfusion. *Encyclopedia and Dictionary of Medicine, Nursing, and Allied Health*.

Mimura, M. et al., 2009. Mechanism leading to the development of pressure ulcers based on shear force and pressures during a bed operation: influence of body types, body positions, and knee positions. *Wound Repair and Regeneration*, 17(6), pp.789–796.

Mlacak, B. et al., 2005. Microcirculation disturbances in patients with venous ulcer before and after healing as assessed by laser doppler flux-metry. *Archives of Medical Research*, 36(5), pp.480–4.

Mollison, H.L. et al., 2006. Reactive hyperemia increases forearm vein area. *Canadian journal of*

anaesthesia = Journal canadien d'anesthésie, 53(8), pp.759–63.

Morales, F. et al., 2005a. How to assess post-occlusive reactive hyperaemia by means of laser Doppler perfusion monitoring: Application of a standardised protocol to patients with peripheral arterial obstructive disease. *Microvascular Research*, 69(1–2), pp.17–23.

Morales, F. et al., 2005b. How to assess post-occlusive reactive hyperaemia by means of laser Doppler perfusion monitoring: Application of a standardised protocol to patients with peripheral arterial obstructive disease. *Microvascular Research*, 69(1–2), pp.17–23.

de Mul, F.F.M. et al., 2005. A model for post-occlusive reactive hyperemia as measured with laser-Doppler perfusion monitoring. *IEEE Transactions on Biomedical Engineering*, 52(2), pp.184–190.

de Mul, F.F.M. et al., 2009. Time development models for perfusion provocations studied with laser-Doppler flowmetry, applied to iontophoresis and PORH. *Microcirculation*, 16(7), pp.559–571.

Murray, J.D., Maini, P.K. & Tranquillo, R.T., 1988. Mechanochemical models for generating biological pattern and form in development. *Physics Reports*, 2(2), pp.59–84.

Nakagawa, S. & Cuthill, I.C., 2007. Effect size, confidence interval and statistical significance: a practical guide for biologists. *Biological Reviews of the Cambridge Philosophical Society*, 82(4), pp.591–605.

Negoro, K. et al., 2008. Effect of osmolarity on glycosaminoglycan production and cell metabolism of articular chondrocyte under three-dimensional culture system. *Clinical and Experimental Rheumatology*, 26(4), pp.534–541.

Ní Annaidh, A. et al., 2012. Characterization of the anisotropic mechanical properties of excised human skin. *Journal of the Mechanical Behavior of Biomedical Materials*, 5(1), pp.139–148.

Nilsson, G.E., 1984. Signal Processor for lasaer Doppler tissue flowmeters. *Medical & Biological Engineering & Computing*, 2(July), pp.343–348.

Nole, K.L.B. et al., 2015. Educational interventions in venous leg ulcer patients. *Wound Repair and Regeneration*, 23, pp.137–140.

Odland, R.M. et al., 2004. Effect of tissue ultrafiltration on skin flap survival. *Otolaryngology - Head and Neck Surgery*, 131(3), pp.296–299.

Olesen, C.G., de Zee, M. & Rasmussen, J., 2010. Missing links in pressure ulcer research--An interdisciplinary overview. *Journal of Applied Physiology*, 108(6), pp.1458–1464.

Olsen, L., Sherratt, J. a & Maini, P.K., 1995. A mechanochemical model for adult dermal wound contraction and the permanence of the contracted tissue displacement profile. *Journal of*

theoretical biology, 177, pp.113–128.

Omar, A.A. et al., 2004. Treatment of venous leg ulcers with Dermagraft. *European Journal of Vascular and Endovascular Surgery*, 27(6), pp.666–72.

Ontario, H.Q., 2010. Endovascular laser therapy for varicose veins an evidence-based analysis. *Ontario Health Technology Assessment Series*, 10(6), pp.1–92.

Ontario, H.Q., 2011. Endovascular radiofrequency ablation for varicose veins: An evidence-based analysis. *Ontario Health Technology Assessment Series*, 11(1), pp.1–93.

Palfreyman, S.J. & Stone, P.W., 2014. A systematic review of economic evaluations assessing interventions aimed at preventing or treating pressure ulcers. *International Journal of Nursing Studies*, pp.1–20.

Pan, W. et al., 2015. Skin perfusion responses under normal and combined loadings: Comparisons between legs with venous stasis ulcers and healthy legs. *Clinical Biomechanics*, 30(10), pp.1218–1224.

Park, C.J. et al., 2009. Accelerated wound closure of pressure ulcers in aged mice by chitosan scaffolds with and without bFGF. *Acta Biomaterialia*, 5(6), pp.1926–1936.

Partsch, H., 2013. Compression therapy in leg ulcers. *Reviews in Vascular Medicine*, 1(1), pp.9–14.

Pascarella, L., Schönbein, G.W.S. & Bergan, J.J., 2005. Microcirculation and venous ulcers: A review. *Annals of Vascular Surgery*, 19(6), pp.921–7.

Pascarella, L. & Shortell, C.K., 2015. Medical Management of Venous Ulcers. *Seminars in Vascular Surgery*, (March).

Peirce, S.M., Skalak, T.C. & Rodeheaver, G.T., 2000. Ischemia-reperfusion injury in chronic pressure ulcer formation: A skin model in the rat. *Wound Repair and Regeneration*, 8(1), pp.68–76.

Perimed, 2001. PeriFlux System 5000 - Extended User Manual. , (44), p.23.

PERIMED, 2001. PeriFlux System 5000 Laser Doppler Perfusion Monitor. Available at: http://www.perimed-instruments.com/products/periflux-system-5000-ldpm#.

Pettet, G.J. et al., 1996. A model of wound-healing angiogenesis in soft tissue. *Mathematical Biosciences*, 136(1), pp.35–63.

Philipse, A. & Vrij, A., 2011. The Donnan equilibrium: I. On the thermodynamic foundation of the Donnan equation of state. *J. Phys.: Condens. Matter*, 23(23), pp.194106–11.

Poblete, H. & Elias, S., 2009. Venous ulcers: new options in treatment: minimally invasive vein surgery. *Journal of the American College of Certified Wound Specialists*, 1(1), pp.12–9.

Reed, R.K. & Rubin, K., 2010. Transcapillary exchange: Role and importance of the interstitial fluid pressure and the extracellular matrix. *Cardiovascular Research*, 87(2), pp.211–217.

Reeder, S., 2013. *Chronic Venous Disease under Pressure*. Erasmus MC: University Medical Center Rotterdam.Erasmus Universiteit Rotterdam.

Rendell, M.S. & Wells, J.M., 1998. Ischemic and pressure-induced hyperemia: a comparison. *Archives of Physical Medicine and Rehabilitation*, 79(11), pp.1451–5.

Rijn, O. Van, 2010. *Mathematical modeling of angiogenesis and contraction occuring during wound healing in soft tissues*. Delft University of Technology.

Roccabianca, S., Ateshian, G.A. & Humphrey, J.D., 2014. Biomechanical roles of medial pooling of glycosaminoglycans in thoracic aortic dissection. *Biomechanics and Modeling in Mechanobiology*, 13(1), pp.13–25.

Roccabianca, S., Bellini, C. & Humphrey, J.D., 2014. Computational modelling suggests good, bad and ugly roles of glycosaminoglycans in arterial wall mechanics and mechanobiology. *Journal of the Royal Society, Interface / the Royal Society*, 11(97), p.20140397.

Roustit, M. & Cracowski, J.L.J., 2012. Non-invasive Assessment of Skin Microvascular Function in Humans: An Insight Into Methods. *Microcirculation*, 19(1), pp.47–64.

Roy, S. et al., 2009. Characterization of a preclinical model of chronic ischemic wound. *Physiological Genomics*, 37(3), pp.211–24.

Sagawa, K., Lie, R.K. & Schaefer, J., 1990. Translation of Otto Frank's Paper "Die Grundform des Arteriellen Pulses" Zeitschrift fur Biologie 37: 483-526 (1899). *Journal of Molecular and Cellular Cardiology*, 22(3), pp.253–277.

Salomé, G.M. & Ferreira, L.M., 2013. Impact of skin grafting of venous leg ulcers on functional status and pain. *World Journal of Surgery*, 37(6), pp.1438–45.

Satishkumar, R. et al., 2013. Superoxidised solution in the management of lower limb ulcers: Our experience. *Journal of Evolution of Medical and Dental Science*, 2(44), pp.8483–8489.

Schugart, R.C. et al., 2008. Wound angiogenesis as a function of tissue oxygen tension: a mathematical model. *Proceedings of the National Academy of Sciences of the United States of America*, 105(7), pp.2628–33.

Schwartz, L. et al., 2009. Is inflammation a consequence of extracellular hyperosmolarity? *Journal of inflammation (London, England)*, 6, p.21.

Segers, P. et al., 1997. Assessment of distributed arterial network models. *Medical & Biological Engineering & Computing*, 35(6), pp.729–736.

Sherratt, J.A. & Dallon, J.C., 2002. Theoretical models of wound healing: past successes and future challenges. *Comptes Rendus Biologies*, 325(5), pp.557–564.

Sherratt, J. & Murray, J., 1991. Mathematical analysis of a basic model for epidermal wound healing. *Journal of Mathematical Biology*, 29, pp.389–404.

Shingler, S. & Robertson, L., 2013. Compression stockings for the initial treatment of varicose veins in patients without venous ulceration. *Cochrane Database of Systematic Reviews*, (11), pp.1–34.

Shiratsuch, H. & Basson, M.D., 2005. Differential regulation of monocyte/macrophage cytokine production by pressure. *American Journal of Surgery*, 190(5), pp.757–62.

Shiratsuchi, H. & Basson, M.D., 2004. Extracellular pressure stimulates macrophage phagocytosis by inhibiting a pathway involving FAK and ERK. *American Journal of Physiology*, 1932, pp.1358–1366.

Sieggreen, M., 2005. Lower extremity arterial and venous ulcers. *The Nursing Clinics of North America*, 40(2), pp.391–410.

Simka, M. & Majewski, E., 2003. The social and economic burden of venous leg ulcers: Focus on the role of micronized purified flavonoid fraction adjuvant therapy. *American Journal of Clinical Dermatology*, 4(8), pp.573–581.

Smalls, L.K., Wickett, R.R. & Visscher, M.O., 2006. Effect of dermal thickness, tissue composition, and body Site on Skin Biomechanical Properties. *Skin Research and Technology*, pp.43–49.

Smye, S. & Bloor, M., 1990. A single-tube mathematical model of reactive hyperaemia. *Physics in Medicine and Biology*, 35(1), pp.103–113.

Snyder, R.J., 2005. Treatment of nonhealing ulcers with allografts. *Clinics in dermatology*, 23(4), pp.388–95.

Socci, L. et al., 2007. An axisymmetric computational model of skin expansion and growth. *Biomechanics and Modeling in Mechanobiology*, 6(3), pp.177–88.

Solovyev, A. et al., 2013. Hybrid Equation/Agent-Based Model of Ischemia-Induced Hyperemia and Pressure Ulcer Formation Predicts Greater Propensity to Ulcerate in Subjects with Spinal Cord Injury. *PLoS Computational Biology*, 9(5).

Sopher, R. & Gefen, A., 2011. Effects of skin wrinkles, age and wetness on mechanical loads in the stratum corneum as related to skin lesions. *Medical & Biological Engineering &*

Computing, 49(1), pp.97–105.

Sorrentino, T.A. et al., 2015. Local Versus Global Mechanical Effects of Intramural Swelling in Carotid Arteries. *Journal of Biomechanical Engineering*, 137(4), pp.041008–041008.

Suehiro, K. et al., 2014. A study of leg edema in immobile patients. *Circulation Journal*, 78, pp.1733–1739.

Thakral, G. et al., 2015. Treatment Options for Venous Leg Ulcers : Effectiveness of Vascular Surgery , Bioengineered Tissue , and Electrical Stimulation. *Advances in Skin & Wound Care*, 28(4).

Thomas, D.R., 2013. Managing venous stasis disease and ulcers. *Clinics in Geriatric Medicine*, 29(2), pp.415–24.

Titze, J. et al., 2004. Glycosaminoglycan polymerization may enable osmotically inactive Na+ storage in the skin. *American journal of physiology. Heart and circulatory physiology*, 287(1), pp.H203–H208.

Titze, J., 2009. Water-free sodium accumulation. *Seminars in Dialysis*, 22(3), pp.253–255.

Tsuji, S. et al., 2005. Analysis of ischemia-reperfusion injury in a microcirculatory model of pressure ulcers. *Wound Repair and Regeneration*, 13(2), pp.209–215.

United Nations, 2015. *World Population Prospect: The 2015 Revision,World Population 2015 Wallchart. ST/ESA/SER.A/378*,

Valencia, I.C. et al., 2001. Chronic venous insufficiency and venous leg ulceration. *Journal of the American Academy of Dermatology*, 44(3), pp.401-21–4.

Venn, M. & Maroudas, A., 1977a. Chemical composition and swelling of normal and osteoarthrotic femoral head cartilage. I. Chemical composition. *Annals of the Rheumatic Diseases*, 36(2), pp.121–9.

Venn, M. & Maroudas, A., 1977b. Chemical composition and swelling of normal and osteoarthrotic femoral head cartilage. I. Chemical composition. *Annals of the rheumatic diseases*, 36(2), pp.121–9.

Vermolen, F. & Rijn, O. Van, 2012. A Mathematical Model forWound Contraction and Angiogenesis. *Tissue Regeneration – From Basic Biology to Clinical Application*, pp.489–512.

Vermolen, F.J., Gefen, A. & Dunlop, J.W.C., 2012. In Vitro “Wound” Healing: Experimentally Based Phenomenological Modeling. *Advanced Engineering Materials*, 14(3), pp.B76–B88.

Vermolen, F.J. & Javierre, E., 2012. A finite-element model for healing of cutaneous wounds

combining contraction, angiogenesis and closure. *Journal of Mathematical Biology*, 65(5), pp.967–996.

Vermolen, F.J. & Javierre, E., 2010. Computer simulations from a finite-element model for wound contraction and closure. *Journal of Tissue Viability*, 19(2), pp.43–53.

Villavicencio, J.L., 2013. Leg ulcers of venous origin: From ancient to modern times. *Journal of Vascular Surgery: Venous and Lymphatic Disorders*, 1(1), pp.96–99.

Vo, T. Van et al., 2007. Mathematical model for the hemodynamic response to venous occlusion measured with near-infrared spectroscopy in the human forearm. *IEEE Transactions on Bio-Medical Engineering*, 54(4), pp.573–84.

Wahl, S.M., 1997. Inflammation and growth factors. *The Journal of Urology*, 157(1), pp.303–5.

Waseem, T. V. et al., 2007. Hypertonic shrinking but not hypotonic swelling increases sodium concentration in rat brain synaptosomes. *Brain Research Bulletin*, 73(1), pp.135–142.

Westerhof, N., Lankhaar, J.W. & Westerhof, B.E., 2009. The arterial windkessel. *Medical and Biological Engineering and Computing*, 47(2), pp.131–141.

Wiese, K.G., 1993. Osmotically induced tissue expansion with hydrogels: a new dimension in tissue expansion? A preliminary report. *Journal of Cranio-Maxillofacial Surgery*, 21(7), pp.309–313.

Wiig, H., Reed, R.K. & Tenstad, O., 2000. Interstitial fluid pressure, composition of interstitium, and interstitial exclusion of albumin in hypothyroid rats. *American journal of physiology. Heart and circulatory physiology*, 278(8), pp.H1627–H1639.

Wiig, H. & Swartz, M.A., 2012. Interstitial Fluid and Lymph Formation and Transport: Physiological Regulation and Roles in Inflammation and Cancer. *Physiological Reviews*, 92(3), pp.1005–1060.

Wilkin, J.K., 1987. Cutaneous reactive hyperemia: viscoelasticity determines response. *Journal of Investigative Dermatology*, 89(2), pp.197–200.

Xue, C., Friedman, A. & Sen, C.K., 2009. A mathematical model of ischemic cutaneous wounds. *Proceedings of the National Academy of Sciences of the United States of America*, 106(39), pp.16782–7.

Yaghoobi, R., Kazerouni, A. & kazerouni, O., 2013. Evidence for clinical use of honey in wound healing as an anti-bacterial, anti-inflammatory anti-oxidant and anti-viral agent: A review. *Jundishapur Journal of Natural Pharmaceutical Products*, 8(3), pp.100–104.

Yavuz, C. et al., 2012. An alternative therapy for recurrent stasis ulcers in chronic venous insufficiency: venocuff. *Case reports in Vascular Medicine*, 2012(Figure 1), p.315147.

Zamboni, P. et al., 2006. The overlapping of local iron overload and HFE mutation in venous leg ulcer pathogenesis. *Free Radical Biology & Medicine*, 40(10), pp.1869–73.

Zar, J.H., 1999. Multisample hypotheses: the analysis of variance. In *Biostatistical Analysis*. pp. 196–200.

Zhang, M. & Roberts, V.C., 1993. The effect of shear forces externally applied to skin surface on underlying tissues. *Journal of biomedical engineering*, 15(6), pp.451–6.

Zhang, M. & Roberts, V.C., 1994. The reaction of skin and soft tissue to shear forces applied externally to the skin surface. *Proceedings of the Institution of Mechanical Engineers, Part H: Journal of Engineering in Medicine*, 208(4), pp.217–222.

Zheng, Y. & Mayhew, J., 2009. A time-invariant visco-elastic windkessel model relating blood flow and blood volume. *NeuroImage*, 47(4), pp.1371–1380.

Zhou, B. et al., 2010. Strain rate sensitivity of skin tissue under thermomechanical loading. *Philosophical Transactions of the Royal Society A: Mathematical, Physical and Engineering Sciences*, 368(1912), pp.679–690.

Zimmet, S.E., 1999. Venous Leg Ulcers: Modern Evaluation and Management. *Dermatologic Surgery*, 25(3), pp.236–241.

Zöllner, A.M. et al., 2013. Growth on demand: Reviewing the mechanobiology of stretched skin. *Journal of the Mechanical Behavior of Biomedical Materials*, 28, pp.495–509.

Zöllner, A.M., Buganza Tepole, A. & Kuhl, E., 2012. On the biomechanics and mechanobiology of growing skin. *Journal of Theoretical Biology*, 297, pp.166–175.